MUTATIONAL ANALYSIS OF KCNQ1 (Kv 7.1) CHANNEL GATING

by

LIJUAN MA

Submitted to Chemistry Department of
University of Hamburg

in partial fulfillment of the requirements
for the degree of

DOCTOR OF CHEMISTRY

Major: Biochemistry and Molecular Biology
Supervisor: Prof. Olaf Pongs,
Prof. Uli Hahn
Centre for Molecular Neurobiology, Hamburg
September, 2007

Content

1 Introduction 1

1.1 Voltage-gated K^+ channels 3

1.1.1 The voltage-sensor of Kv channels 5

1.1.2 The activation gate of Kv channels 7

1.1.3 Coupling of voltage sensing to gating 8

1.2 KCNQ1 channel 9

1.2.1 KCNQ1 channel properties 9

1.2.2 KCNQ1 channel ß-Subunit Regulation 10

1.2.3 KCNQ1 channel regulation 11

1.3 Aim of this study 12

2 Materials 13

2.1 Chemicals, Enzymes and General Reagents 13

2.2 Bacterial strain 13

2.3 Vectors 13

2.4 Kits 14

3 Methods 15

3.1 Molecular biology 15

3.1.1 Solutions 15

3.1.2 Maintenance of bacterial strains 16

3.1.3 Prepare of competent bacteria 16

3.1.4 Transformation of bacteria 16

3.1.5 Isolation and purification DNA 17

3.1.5.1 Pasmid isolation from 2ml cultures (Miniprep) 17

3.1.5.2 Plasmid isolation from 50ml cultures (Midiprep) 17

3.1.5.3 DNA isolation from agarose gel 17

3.1.6 Enzymatic modification of DNA 17

3.1.6.1 Restriction enzyme digestion of DNA 17

3.1.6.2 Dephosphorylation of vector DNA 18

3.1.7 DNA ligation 18

3.1.8 *In vitro* mutagenesis 18

3.1.9 Agarose gel electrophoresis of DNA 18

3.1.10 cRNA synthesis 19

3.1.10.1 cRNA synthesis from in vitro transcription 19
3.1.10.2 RNA quantitation 19
3.2 Cell biology methods 20
3.2.1 Handling of *Xenopus laevis* oocytes 20
3.2.1.1 Solution for oocytes preparation 20
3.2.1.2 Isolation and maintenance of oocytes 21
3.2.1.3 cRNA injection into oocytes 21
3.3 Electrophysiology 22
3.3.1 Two-Electrode Voltage Clamp (TEVC) 22
3.3.1.1 Experimental set-up 24
3.3.1.2 Procedure for recording from oocytes 24
3.3.1.3 Solutions for TEVC recording 25
3.3.2 The patch clamp technique 26
3.3.2.1 The patch clamp configuration 26
3.3.2.2 Inside-out patch clamping of excised membrane 29
3.3.2.3 Solutions for inside-out patch recording 30
3.3.3 Data analysis 31
3.3.3.1 Voltage-dependent activation 31
3.3.3.2 Conductance and inactivation 33
3.3.3.3 Deactivation kinetics 34
3.4 Molecular modeling 35
4 Results 36
4.1 Gating of KCNQ1 channels 36
4.1.1 Expression of KCNQ1 mutants 38
4.1.2 Voltage-dependent activation properties of KCNQ1 mutant channels 41
4.1.2.1 Mutants with intact voltage-dependent activation 41
4.1.2.2 Mutants with macroscopic inactivation 44
4.1.2.3 Mutants with functional inward rectifier currents 44
4.1.2.4 Comparison of mutational effects on the gate KCNQ1 and *Shaker* channels 47
4.1.3 Deactivation kinetics of KCNQ1 mutant channels 51
4.1.4 G_{Rb}/G_K and inactivation properties of KCNQ1 mutant channels 54
4.1.5 Mapping of KCNQ1 mutants phenotypes onto the Kv1.2 crystal structure 61
4.1.5.1 Defects in functional expression 61

4.1.5.2 Perturbation of G_{Rb}/G_K and inactivation properties 65
4.1.5.3 Mutations that induced global structural changes of the pore 69
4.1.5.4 Mutations that did not affect the pore structure 71
4.2 Ca^{2+} regulation of the KCNQ1 channel 73
4.2.1 Ca^{2+} regulation of KCNQ1 and KCNQ1/KCNE1 (I_{Ks}) currents 73
4.2.2 CaM mediated Ca^{2+}-sensitivity of KCNQ1 or I_{Ks} channels 76
4.2.3 Ca^{2+}-sensitivity of KCNQ1 pore mutants 79
4.3 KCNE1 and KCNQ1 82
4.3.1 Temperature-dependent I_{Ks} channels 82
4.3.2 KCNE1 effects on KCNQ1 pore mutants 84
5 Discussion 90
5.1 Gating of KCNQ1 channel 90
5.1.1 Interface between voltage-sensor and the pore region 91
5.1.2 S4-S5 linker and C-terminal of S6 93
5.1.3 The intracellular gate of KCNQ1 94
5.2 G_{Rb}/G_K and inactivation of KCNQ1 97
5.2.1 Conductance of KCNQ1 97
5.2.2 Inactivation of KCNQ1 98
5.3 Ca^{2+} regulation of KCNQ1 101
5.4 How KCNE1 interacts with KCNQ1 104
6 Summary 109
7 References 111
8 Appendix 121
8.1 Abbreviations 121
8.2 Voltage-dependent activation recordings for KCNQ1 mutant channels 122
8.3 Currents recordings to determine G_{Rb}/G_K and inactivation properties of KCNQ1 mutant channels 134
8.4 Voltage-dependent activation current recordings for KCNQ1 mutants coexpressed with KCNE1 146
8.5 Curriculum Vitae 150
8.6 Publications and conference presentations 151
8.7 Acknowledgments 152

Figure list

Figure 1.1: Different transmembrane topologies of K^+ channel subunits. 2

Figure 1.2: Summary of structural components of voltage-gated potassium channels. 4

Figure 1.3: Crystal structure of Kv1.2 channel. 6

Figure 1.4: Comparison of pore domains from three different potassium channels in the open conformation. 7

Figure 3.1: Simplified schematic diagram of the experimental setup for two-electrode voltage clamp. 23

Figure 3.2: The various configurations of the patch-clamp technique. 27

Figure 3.3: Patch clamp circuit. 28

Figure 3.4: Biphasic, double-exponential time course of the tail currents at -120 mV. 34

Figure 4.1: Identification and sequence comparison of residues in the pore domain of KcsA, Kv1.2 and KCNQ1. 37

Figure 4.2: Voltage- activation relations for the KCNQ1 mutant channels with gating properties similar to wild-type channel. 42

Figure 4.3: Voltage-activation relations for the KCNQ1 mutant channels with altered gating properties. 43

Figure 4.4: Macroscopic inactivation of the KCNQ1 mutant channels. 45

Figure 4.5: Inward rectifying properties of the G345W and G348W mutant channels. 46

Figure 4.6: Effects of KCNQ1 pore mutations on $V_{1/2}$ and z gating parameters. 48

Figure 4.7: G_{Rb}/G_K and inactivation properties of KCNQ1 pore mutants. 58

Figure 4.8: Mapping nonfunctional KCNQ1 mutations in S5 and S6 onto the Kv1.2 structure. 62

Figure 4.9: Mapping nonfunctional mutations in the internal half of the pore domain of *Shaker* and KCNQ1 onto the Kv1.2 structure. 64

Figure 4.10: Perturbations in G_{Rb}/G_K mapped onto the Kv1.2 structure. 66

Figure 4.11: Mapping KCNQ1 mutants with no 'hook' inactivation or macroscopic inactivation. 68

Figure 4.12: Perturbations in the pore structure mapped onto the Kv1.2 structure. 69

Figure 4.13: Global structural changes mapped onto the Kv1.2 structure. 70

Figure 4.14: No global structural change mapped onto the Kv1.2 structure. 72

Figure 4.15: Ca^{2+}-sensitivity of KCNQ1 and KCNQ1/KCNE1 channels in inside-out patches. 75

Figure 4.16: CaM-mediated Ca^{2+} regulation of KCNQ1 and KCNQ1/KCNE1 channels. 77

Figure 4.17: Voltage- and Ca^{2+}-regulation of wild-type and mutant KCNQ1 channels 81

Figure 4.18: Temperature dependency of I_{Ks} channels. 83

Figure 4.19: KCNE1 gating modulations on the KCNQ1 pore mutants. 87

Figure 4.20: Defect of KCNE1 modulation by L266W and F279A KCNQ1 mutations. 88

Figure 4.21: Defect of KCNE1 modulation by F275W and Y278A KCNQ1 mutations. 89

Figure 5.1: Mutations in the external half of the interface between voltage-sensor and the pore. 92

Figure 5.2: Gating-sensitive residues in the internal half of the interface between voltage-sensor and the pore 93

Figure 5.3: The intracellular gate region of K^+ channels 95

Figure 5.4: Sequence alignment between KCNQ1, KCNQ2, and KCNQ3 96

Figure 5.5: Cartoon of KCNQ1 inactivation & C-type inactivation of Kv channels 100

Figure 5.6: Allosteric gating model for KCNQ1 channels 102

Figure 5.7: Distribution of mutants which attenuate the Ca^{2+} sensitivity of KCNQ1 103

Figure 5.8: Distribution of residues which are insensitive to global structural changes 105

Figure 5.9: Defect of KCNE1 gating modulation mapped onto the Kv1.2 structure 107

Table list

Table 4.1: Regional functional expressional level for KCNQ1 mutant channels 38

Table 4.2: Regional functional expressional level for KCNQ1 Ala versus Trp mutant channels 38

Table 4.3: Gating properties of the KCNQ1 mutant channels 39

Table 4.4: Gating perturbation pattern of KCNQ1 pore mutants 41

Table 4. 5: Comparison of gating perturbations between *Shaker* and KCNQ1 mutants 49

Table 4.6: Comparison of the mutational effects on gating between *Shaker* and KCNQ1 channels 50

Table 4.7: Deactivation kinetics for the KCNQ1 mutant channels 52

Table 4.8: Relative Rb^+ conductance (G_{Rb}/G_K) and inactivation fraction of KCNQ1 pore mutants 56

Talbe 4.9: Mutational effect on the pore structure of the KCNQ1 channels 60

Talbe 4.10: Non-functional mutations in the internal half of the pore between *Shaker* and KCNQ1 63

Table 4.11: Gating parameters of wild type and mutant KCNQ1 channels at various intracellular [Ca^{2+}] from inside-out patches. 80

Table 4.12: KCNE1 gating modulations on KCNQ1 pore mutants 86

1 Introduction

Ion channels are macromolecular pores in cell membranes. Their known functions include establishing a resting membrane potential, shaping electrical signals, gating the flow of messenger Ca^{2+} ions, controlling cell volume and regulating the net flow of ions and fluids across epithelial cells of secretory and resorptive tissues (Hille 2001). Ion channels are selective for the types of ions they allow to cross. Named according to the selectivity, the most important ion channels include K^+ channels, Na^+ channels, Ca^{2+} channels, and Cl^- channels.

Cloning and genome projects have revealed over 80 related mammalian genes for K^+ channel subunits. All K^+ channels have pore-lining P-loops with a consensus amino acid sequence (TXXTXGYGD) that has been called the K^+ channel ‘’signature sequence’’. The residues TXGYG, repeated in the four principle subunits, line the selectivity filter. Based on their molecular architecture different channel classes are distinguished (Fig. 1.1). The simplest structural plan of potassium channels is visible in the 2TM/1P class, named after their typical composition of two transmembrane helices (TM) and one P-region and represented by the inward rectifier potassium channels. Most channels are referred to as voltage-gated channels (K_V). They are composed of six TM (S1-S6) and one P-region, resulting in the 6TM/1P class. Furthermore, the Ca^{2+}-dependent potassium channels with their additional helix, S0, belong to this class. The class of the so-called ‘background’ or ‘leakage’ channels is made up of two P-regions, hence structurally referred to as 4TM/2P type. Other K^+ channels principle subunits have an eight TM architecture that contains two P-regions per subunit; e. g. the yeast TOK (or DUK1) channels (Hill, 2001).

K^+ channels consist of two main functional domains, a K^+-selective pore with a gate and a sensor that controls whether the pore is open or closed. The ion conduction pores in K^+ channels are well conserved, supporting remarkable ion throughput rates

(10^6-10^7 s^{-1}) with selectivity of 10^4 times preferring K^+ over Na^+. A variety of sensors are coupled to the gate, conferring on different types of K^+ channels the ability to respond to a variety of stimuli, such as a change in membrane potential, binding of intracellular ligands, e. g. Ca^{2+}, cyclic nucleotides or G protein subunits.

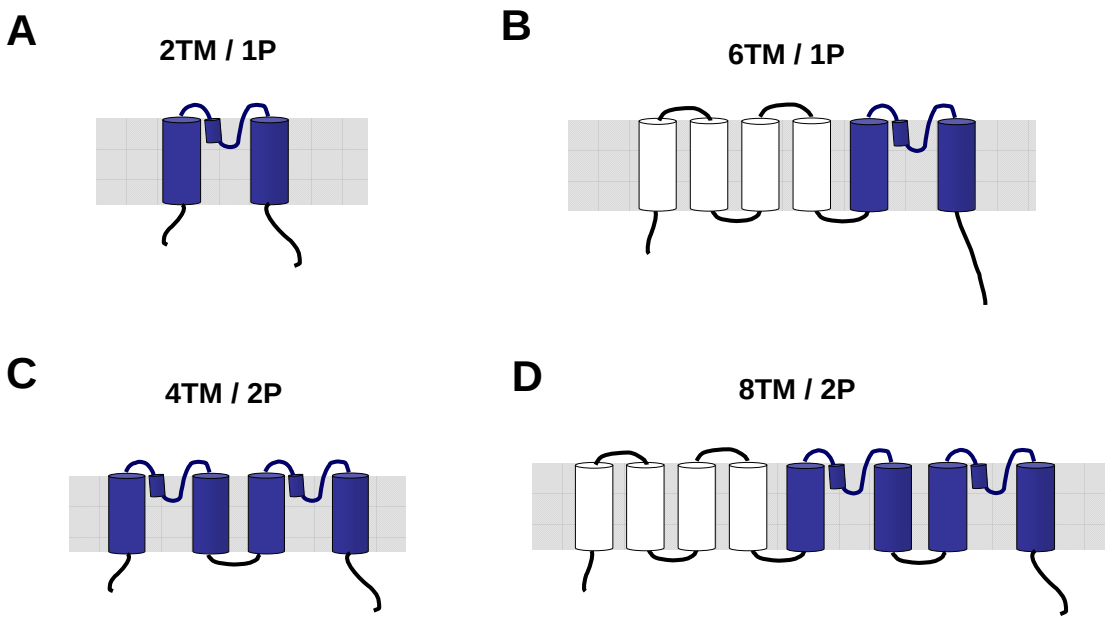

Figure 1.1: Different transmembrane topologies of K^+ channel subunits.
Every K^+ channel has to have enough subunits to bring together four P-loops to line the pore. (A) K^+ channels with two transmembrane (TM) helices and one P-loop, e.g. Kir and KcsA. (B) K^+ channel with six TM helices and one P-loop, e.g. Kv channels, KCNQ, HCN, and TRP channels. (C) K^+ channel with four TM helices and two P-loops, e.g. TWIK. (D) K^+ channel with eight TM helices and two P-loops, e.g. yeast TOK.

1.1 Voltage-gated K^+ channels

Voltage-gated K^+ (Kv) channels ‘’sense’’ voltage differences across the cell membrane and open or close in response to changes in the membrane potential. Kv channels are formed by coassembly of four α-subunits, each containing six α-helical transmembrane segments (S1-S6), with both N- and C-termini usually on the intracellular side of the membrane. Each subunit comprises two membrane-integrated functionally distinct modules; one forms the voltage-sensor (S1-S4) and the other K^+ selective pore with the gate (S5-S6).

The crystal structure of the bacterial potassium channel KcsA (Doyle et al., 1998) is a prototype for the pore forming domain of a K^+ channel in the closed position. KcsA subunits have two transmembrane helices: the outer helix M1 and the inner helix M2. The outer helix is homologous to S5 and the inner helix to S6 of Kv channels. M1 and M2 are connected by an extended loop region in the upper part of the pore, which forms the K^+ selectivity filter. The M2 (S6) helices converge to a ‘bundle-crossing’ to form the activation gate near the cytoplasmic interface of the pore. Between the selectivity filter and bundle crossing is a water-filled cavity.

The N-terminus of *Shaker*-family Kv channels contains a ‘tetramerization domain’ (T1 domain). It determines the specificity of channel subunit assembly and also serves as a platform for binding of Auxiliary Kv β-subunits. The cytoplasmic C terminus of *Shaker* K^+ channels has no obvious domain structure. By contrast, other Kv channels are characterized by the presence of a subunit assembly domain and / or a sensor domain in the C terminus. These include voltage-gated KCNQ and eag/erg channels, as well as channels gated by voltage and intracellular Ca^{2+} (e.g. BK channels) and channels gated exclusively by intracellular ligands like Ca^{2+} (e.g. SK channels). The auxiliary subunits known to be associated with this family (minK, MiRP, BKβ) are transmembrane proteins; they appear to be intimately associated with the pore domain and may displace the voltage-sensor domain or interact with it directly (Fig. 1.2) (Yellen, 2002).

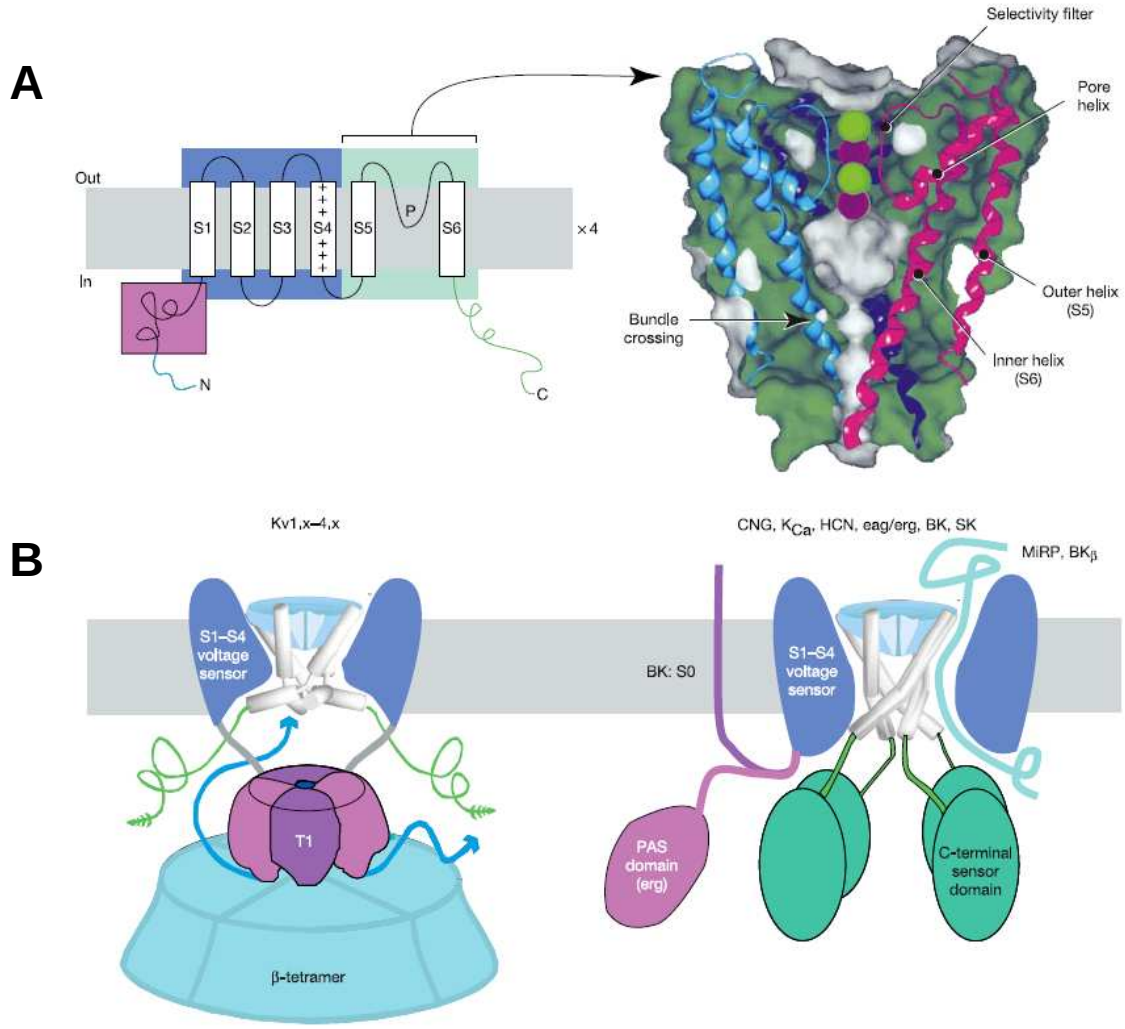

Figure 1.2: Summary of structural components of voltage-gated potassium channels
(A) Simple 2D diagram of voltage-gated potassium channels. Red coloured box shows the tetramerization domain of Kv1-Kv4 channels. The blue box marks the transmembrane domains S1-S4. With the green box are indicated the pore-forming domains S5−P-loop−S6. The 3D crystal structure of KcsA, thought to be a main structural motif for all potassium channels, is shown on the right. The fourth subunit is omitted from the structure for simplicity. (B) Topological diagram of Kv channels with Kvβ subunit, represented at the bottom of transmembrane domains (cyan). The structure of the C-terminus of Kv channels is largely unknown. The C-terminal regions of the channels are represented in green, S1-S4 transmembrane segments in blue. On the right a topological model of other voltage-gated potassium channels (BK, eag/erg, HCN) and their β-subunits is shown (from Yellen, 2002).

1.1.1 The voltage-sensor of Kv channels

Voltage sensitivity of Kv channels arises from the voltage-induced displacement of charges across the membrane electric field, a phenomenon first noted by Hodgkin and Huxley (1952). Biophysical studies of voltage-gated sodium and potassium channels have shown that these channels contain intrinsic voltage sensors, S1–S4 (Hille, 2001; Yellen, 2002; Swartz, 2004). In particular, the highly charged S4 segment is the primary component of the voltage sensor (Sigworth, 1994; Aggarwal and MacKinnon, 1996; Seoh et al., 1996; Marten and Hoshi, 1998; Zei and Aldrich, 1998; Latorre et al., 2003b). Movement of voltage-sensor domains under the influence of the membrane's electric field is associated with gating charge displacement. This most likely brings about a voltage-dependent conformational change that is coupled to opening of the pore (Sigworth, 1994). In the case of *Shaker* Kv channels a total of 12–14 positive elementary charge units cross the membrane electric field during channel activation (Schoppa et al., 1992; Seoh et al., 1996; Aggarwal and MacKinnon, 1996). The large valence of the gating charge contributes to the exquisite voltage-sensitivity of Kv channels, allowing them to gate open in response to small changes in the membrane potential.

The crystal structure of the rat Kv1.2 (Long et al. 2005) shows the four voltage-sensing domains (VSDs) are self-contained domains, quite independent of the pore protein, attached to the gate of the pore domain through S4-S5 linker helices. In addition, the Kv1.2 structure reveals that the VSD from one subunit interacts closely with the pore-forming helices of the adjacent subunit in a clockwise direction when the channel structure is viewed from the extracelluar side of the membrane (Fig. 1.3). Such interactions are believed to play an important role in determining the cooperativity of the voltage-sensor movement during channel opening (Jennifer, 1999; Pathak et al. 2005). The interaction surface between each VSD and the pore domain in Kv1.2 structure is small. However, the exact geometrics of VSD - pore interactions may vary among different Kv channels. A recent study revealed close interactions

between S4 which is part of the voltage sensor and the outer helix of the pore domain in KAT1 (Grabe et al., 2007; Lai et al., 2005).

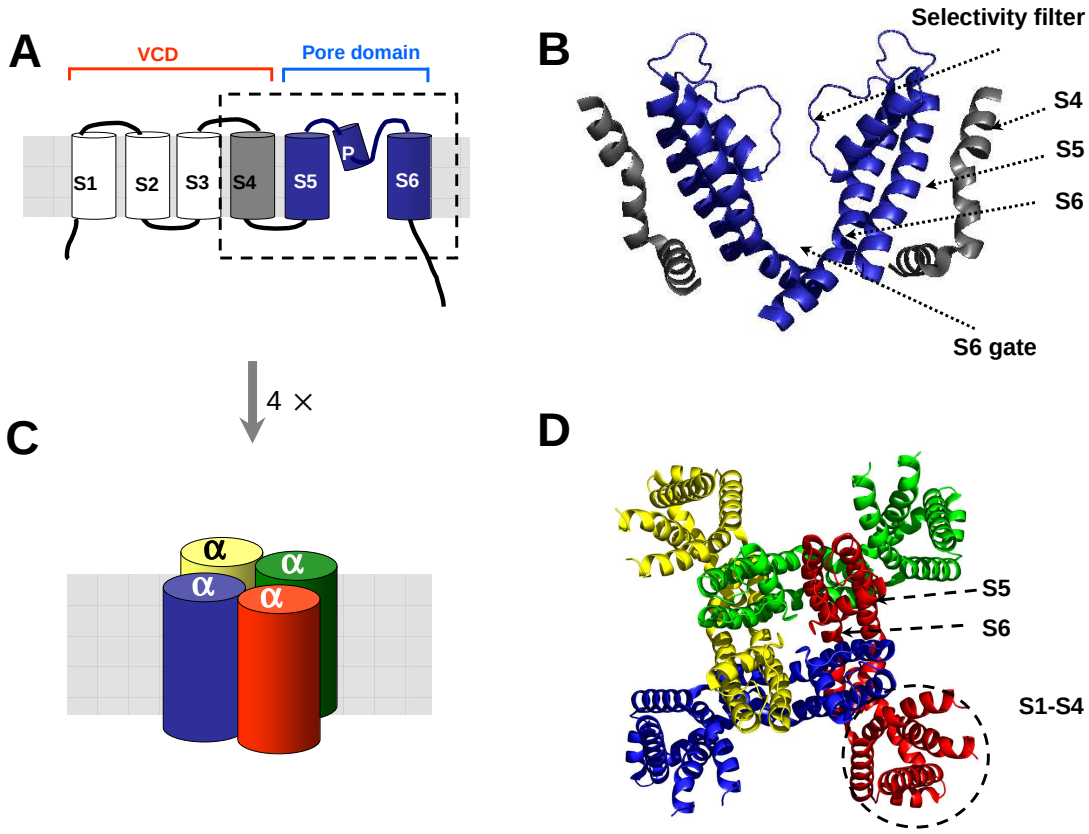

Figure 1.3: Crystal structure of Kv1.2 channel.

(A) The architecture of a Kv channel subunit with six TM helices. (B) Side view of crystal structure of the S4-S6 region of the Kv1.2 structure, showing only the S5-S6 region from two subunits and the nearby S4 helix from two adjacent subunits. (B) Schematic diagram for the Kv channel formed by four α subunits assembly. (D) Top view (extracellular side) of the Kv1.2 tetramer with each subunit shown in a different color. Coordinates from Long et al. (2005), PDB ID 2A79.

1.1.2 The activation gate of Kv channels

The gate region in K^+ channels controls whether K^+ ions can traverse the ion conduction pore. Comparison of the structural data from K^+ channels trapped in the open conformation, MthK, KvAP and Kv1.2 (Jiang et al., 2002, 2003; Zhou et al., 2001; Long et al., 2005), and channels trapped in the closed conformation, KcsA and K_{ir}Bac1.1 (Doyle et al., 1998, Kuo et al., 2003), indicates that gate opening is associated with a conformational change of the S6 helix. Bending of the S6 helix at a glycine hinge may well explain gating in bacterial potassium channels. However, the S6 helix of many eukaryotic Kv channels has a PVP motif. Results of accessibility studies (Liu et al., 1997; Holmgren et al., 1998; del Camino et al., 2000; del Camino & Yellen 2001; Webster et al., 2004) suggest that opening of the S6 bundle takes place at the PVP motif of *Shaker* Kv channels. The crystal structure of the rat Kv1.2 (Long et al., 2005) supports this view and shows that widening of the S6 occurs because of a bend at PVP motif. Apparently, opening of the gate is associated with the bending of inner TM2/S6 helix which can occur at either a glycine or a PVP motif.

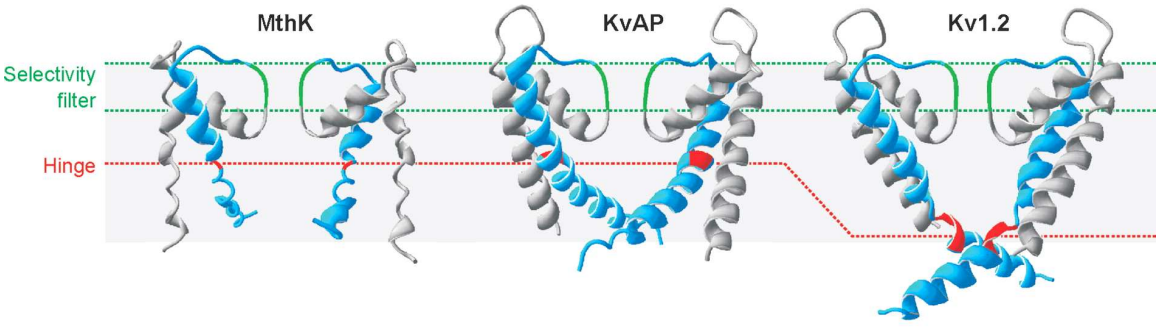

Figure 1.4: Comparison of pore domains from three different potassium channels in the open conformation. Only pore-forming helices from two subunits are shown. S5 (TM1) and the P-helix are shown in gray; the GYG motif in the selectivity filter, in green; and the S6 helix and part of the pore loop, in blue. In the bacterial channels MthK and KvAP, the S6 (TM2) bundle opens at a glycine hinge (*red*). In the eukaryotic Kv1.2, the hinge in S6 corresponds to the PVP motif (*red*). The gray background represents the membrane.

1.1.3 Coupling of voltage sensing to gating

It is not well understood how motion of the voltage sensor couples to the channel opening. Several studies on *Shaker* and related channels suggest the S4-S5 linker is involved in coupling (Isacoff et al., 1991; McCormack et al., 1991; Sanguinetti & Xu 1999; Chen et al., 2001; Decher et al., 2004; Caprini et al., 2005). Previous studies by Lu & colleagues (Lu et al., 2001, 2002) illustrate that both S4-S5 linker and C-terminal end of S6 are required to constitute Kv channels. The crystal structure of Kv1.2 demonstrates this interaction beautifully. The distal end of the S4-S5 linker comes close to the internal end of S5 below the PVP motif, with extensive contacts between side chains of the two regions. This structural picture of the activated conformation suggests that to close the gate, the S4-S5 linker would have to move inward, shutting down the S6 gate (Long et al., 2005).

As discussed above, the S4-S5 linker and C-terminal end of S6 are critical for coupling between voltage sensor movement and channel opening. In addition, studies on a triple mutant of *Shaker* (named ILT) where three positions in S4 were mutated to the corresponding residues in *Shaw* (Smith-Maxwell et al., 1998; Ledwell and Aldrich 1999), revealed that in ILT, the voltage ranges over which the voltage sensor movement and the channel opening occur were quite well separated. It is suggested that S4 itself plays a role in coupling voltage sensing with gating (Pathak et al., 2005). The effect of the ILT mutations was proposed to be due to interactions between a hydrophobic face of S4 and the neighbouring subunit's S5, which is consistent with the crystal structure of Kv1.2 (Long et al., 2005).

1.2 KCNQ1 channel

1.2.1 KCNQ1 channel properties

Members of the Kv7 (KCNQ) channel are expressed in heart, brain, auditory and vestibular organs, and epithelia (Jentsch, 2000; Jespesen et al., 2005). KCNQ channels play a prominent role in human disease and harbour mutations that are linked to cardiac arrhythmias, deafness and benign familial neonatal epilepsy (Jentsch, 2000). KCNQ1 (Kv7.1) channel expression is restricted to the heart and peripheral epithelial and smooth muscle cells. Association of KCNQ1 with the β-subunit KCNE1 constitutes the cardiac I_{Ks} current. Mutations in this channel can cause one form of inherited long QT syndrome, as well as a form of deafness. The other four KCNQ (Kv7.2-7.5) channels are highly expressed in the nervous system. Neuronal M current is mediated by heteromeric channels assembly of KCNQ2 and KCNQ3 subunits (Jentsch, 2000). Mutations in KCNQ2 and KCNQ3 are associated with benign familial neonatal epilepsy. The KCNQ4 gene is thought to encode the molecular correlate of the $I_{K,n}$ in the outer hair cells of the cochlea and $I_{K,L}$ in Type I hair cells of the vestibular apparatus, mutations in which lead to a form of inherited deafness.

Kv7/KCNQ channel subunits probably have a conventional *Shaker*-like K^+ channel topology, with six TM domains (S1–S6), a single P-region that forms the selectivity filter of the pore, a positively-charged fourth transmembrane domain (S4) that is part of the voltage sensor and a long intracellular carboxy-terminal tail. Four such subunits make up a functional Kv7 channel. All five (Kv7.1–Kv7.5) Kv7 channel subunits can form homomeric channels, whereas the formation of heteromers is restricted to certain combinations (Jentsch, 2000). The carboxyl terminus contains a conserved domain (A domain) that determines the subunit specificity of Kv7 channel assembly and deletion of a part of this domain leads to an impaired assembly of channel complexes followed by mistrafficking (Schmitt et al., 2000; Schwake etal., 2000). Moreover, the Kv7 C-termini contains binding sites for several potential regulatory

molecules, such as Calmodulin (CaM), Phosphatidylinositol (4,5)-bisphosphate (PIP2), and A-kinase anchoring protein (AKAP) (Delmas et al., 2005).

1.2.2 KCNQ1 channel ß-Subunit Regulation

The extensive versatility of KCNQ1 channel function is widely due to the channel ability to interact with ancillary subunits from the mink-related peptide (MiRP) family, encoded by KCNE genes. KCNQ1 channels associate with all five members of the KCNE β-subunit family, resulting in β-subunit specific changes of the current characteristics. Coexpression of KCNE1 with KCNQ1 dramatically increases unitary conductance, slows the activation kinetics, shifts voltage-dependent activation to more positive potentials and removes inactivation (Barhanin et al., 1996; Sanguinetti et al., 1996; Sesti and Goldstein, 1998; Yang and Sigworth, 1998). It is well established that KCNQ1 associates with mink (KCNE1) to form the cardiac I_{Ks} channel that contributes to ventricular repolarization (Barhanin et al., 1996; Sanguinetti et al., 1996). In the kidney, KCNQ1 channels expressed together with KCNE1 can be found in the proximal tubule and the distal tubule of the nephron. The function of KCNQ1 channels in the kidney has not been fully established, but KCNE1 knockout mice were found to suffer from hypokalemia, urinary and fecal salt wasting and volume depletion, thereby indicating an important role for the I_{Ks} channel in renal function (Vallon et al., 2001). KCNE2 renders the KCNQ1 channel constitutively open, indicating that in vivo KCNQ1/KCNE2 channels could play an important role in setting the resting membrane potential in organs such as stomach and intestine (Dedek and Waldegger, 2001; Jespersen et al., 2004). KCNE3 greatly reduces the voltage dependence of the KCNQ1 channel leading to largely voltage-independent potassium ‘leak’ current. Channels formed by coassembly of KCNQ1 with MiRP2 (KCNE3) generate potassium currents that may be critical for cAMP-stimulated chloride secretion in the colon and lung (Schroeder et al., 2000; Grahammer et al., 2001).

1.2.3 KCNQ1 channel regulation

It is well known that the cardiac current I_{Ks} is upregulated following sympathetic stimulation (Terrenoire et al., 2005). This upregulation of the KCNQ1/KCNE1 current is mediated by ß-adrenergic receptor activation, leading to an increased level of cAMP and thereby PKA stimulation, which interacts with the I_{Ks} complex through an AKAP protein (Potet et al., 2001). Kass and co-workers (Marx et al., 2002) showed that PKA and protein phosphatase 1 interact with KCNQ1 through the AKAP called yotiao, which binds to the COOH-terminal tail of KCNQ1 via a leucine zipper motif. The cAMP-mediated regulation of KCNQ1 channels in mammalian expression systems is dependent on coexpression of KCNE1, and mutations described in both KCNQ1 and KCNE1 identified in long QT syndrome patients have been found to disrupt this regulation (Kurokawa et al., 2004).

PIP2 is another key intracellular regulator of the KCNQ1/KCNE1 channel activity (Loussouarn et al., 2003; Zhang et al., 2003). The importance of this interaction, occurring primarily with residues in the very proximal COOH terminus, is emphasized by the fact that reduced PIP2 affinity of KCNQ1 mutants isolated from long QT syndrome patients may underlie the syndrome observed in these patients (Park et al., 2005).

Under physiological conditions, such as absorption and secretion, as well as in pathophysiological situations, cell volume and pH may undergo considerable changes. The KCNQ1 current has been shown to be tightly regulated by small cell volume changes. The sensitivity of the KCNQ1 channel to cell volume changes is independent of the presence of the auxiliary KCNE1-3 subunits (Grunnet et al, 2003). In contrast, KCNE subunits determine pH sensitivity of KCNQ1 channels. External pH can modify current amplitude and biophysical properties of KCNQ1. KCNE subunits work as molecular switches by modulating the pH sensitivity of human KCNQ1 (Heitzmann et al., 2007)

1.3 Aim of this study

The objective of this study was to investigate the gating mechanism of the KCNQ1 channel by mutagenesis scanning. For this purpose, each residue in the KCNQ1 pore region (from G245 to V355) was systematically mutated into a small residue (alanine) and/or a bulky residue (tryptophan). cRNAs encoding the mutant channels were injected into *Xenopus* oocytes and the mutational effects on the voltage-dependent activation, conductance and inactivation were evaluated by two-electrode voltage clamp technique. The following topics were addressed:

1. How did the KCNQ1 pore mutants perturb the gating for channel opening? Are the gating behaviors of KCNQ1 pore mutants consistent with that of *Shaker*?

2. Why does the gating of KCNQ1 differ from that of *Shaker* Kv channel? Given that KCNQ1 possesses a large C-terminus where the binding sites of the Ca^{2+} sensor Calmodulin have been identified, it is proposed that the gating of KCNQ1 is dually controlled by voltage and ligand (Ca^{2+}). Inside-out patch clamp technique was used to test this possibility.

3. KCNE1 is an ancillary β subunit with a single transmembrane domain. Assembly of KCNE1 with KCNQ1 leads to a great change in the pore gating properties. To illustrate how KCNE1 modulate the gating through interaction with the pore of KCNQ1, KCNQ1 pore mutants were coexpressed with KCNE1 and effects of the KCNE1 β subunit were tested.

2 Materials

2.1 Chemicals, Enzymes and General Reagents

If it was not mentioned specifically, all the chemicals used in this study were in high quality and purchased from Difco, Fluka, GibcoBRL, Merck, Roth, Sigma&Aldrich. Enzymes, Kits, molecular weight standards were acquired by the companies Ambion, Boehringer Mannheim, Clontech, Invitrogen, New England Biolabs, MBI Fermentas, Stratagene, Agilent Technologies

2.2 Bacterial strain

XL1-Blue	*recA1 endA1 gyrA96 thi-1 hsdR17 supE44 relA1 lac [F'proAB lacI^{q}ZΔM15 Tn10 (tet^{R})]^{C} (Invitrogen life Technologies)*

2.3 Vectors

pCDNA3	Expression vector for mammalian cell line *(Invitrogen)*
pGEM HE Juel	RNA transcription vector

2.4 Kits

GFX *Micro* Plasmid Prep Kit	Plasmid minipreps *(Amersham Biosciences)*
NucleoBond AX® system	Plasmid midipreps *(Macherey and Nagel)*
GFX PCR DNA and Gel Band Purification Kit	DNA fragment Purification *(Amersham Biosciences)*
AMBION cRNA synthesis kit	RNA synthesis *(Ambion)*
Agilent RNA 6000 Nano Assay Kit	Determination of the concentration of RNA samples *(Agilent Technologies)*
Calcium Calibration Buffer Kits	Determination of free [Ca^{2+}] *(Molecular Probes)*

3 Methods

3.1 Molecular biology

3.1.1 Solutions

Ampicillin solution	0.1	g / L	Ampicillin
LB medium	10	g / L	NaCl
	10	g / L	Tryptone
	5	g / L	Yeast extract
LB-Agar	1	L	LB medium
	15	g	Agar, autoclave
LB-Ampicillin medium	1	L	LB medium
	15	g	Agar, autoclave
	1	ml	Ampicillin solution
Diethylpyrocarbonate (DEPC) H_2O	0.01	% (v/v)	DEPC in H2O
Ethidiumbromide solution	10	mg / ml	Ethidiumbromide in H_2O
TAE buffer	40	mM	Tris
	10	mM	Acetate
	1	mM	EDTA, PH7.5
TB buffer	3	g / L	PiPES
	2.2	g / L	$CaCl_2$
	18.6	g / L	KCl
	10.9	g / L	$MnCl_2$
TE (1×)	10	mM	Tris/HCl pH8.0
	1	mM	EDTA

3.1.2 Maintenance of bacterial strains

Strains were stored as glycerol stock (LB-medium, 25% (v/v) glycerol) at -70℃. An aliquote of the stock was streaked on an LB-plate containing the appropriate antibiotic and incubated overnight a 37 ℃ incubator. Plates could be stored up to 6 weeks at 4℃.

3.1.3 Prepare of competent bacteria

A single colony picked from a fresh LB plate, was inoculated into 10 ml LB starter culture and grown at 37℃ shaker overnight. 100 ml LB broth was inoculated with 1 ml overnight grown culture and incubated in a shaker at 37℃ until an OD_{600} reached 0.5. The flask were removed from the shaker and placed on ice for 10min. Cells were centrifuged at 5000 RPM for 10 minutes at 4℃. The bacterial pellet was gently suspended in 80ml of ice-cold TB buffer and put on the ice for 10 minutes. The cell suspension was centrifuged again at 5000 RPM for 10 minutes at 4℃. The bacterial pellet was suspended in 20ml TB buffer and 1.5ml DMSO was added with gentle swirling. With cell suspensions on ice, aliquots of cells in pre-chilled 1.5ml eppendorf tubes were prepared. The cells were frozen immediately by immersion in liquid nitrogen and then stored at -70℃

3.1.4 Transformation of bacteria

The competent cells were thawed on ice. 100µl aliquots of cells were dispensed into pre-chilled eppendorf tubes and placed on the ice. Then the plasmid DNA was added to each tube and the tubes were placed on ice for 30 minutes. The tubes were immersed in the 42℃ water bath for 90 seconds for heat shock, and returned directly to ice for 1 or more minutes. 1 ml LB medium was added to each tube and the cells were incubated for 45-minute recovery. in a shaker at 37 ℃ 100 µl of transformed cells were spread onto the appropriate plates and the plates were placed upside down in a 37℃ incubator overnight.

3.1.5 Isolation and purification DNA

3.1.5.1 Pasmid isolation from 2 ml cultures (Miniprep)

GFX *Micro* Plasmid Prep Kit (Amersham Biosciences) was used for plasmid minipreps. Plasmid DNA was purified according to the manufacturer's protocol and finally dissolved in 30 µl ddH_2O.

3.1.5.2 Plasmid isolation from 50 ml cultures (Midiprep)

NucleoBond AX® system (Macherey and Nagel, Düren, Deutschland) was used for plasmid midipreps. Plasmid DNA was purified as described in the manufacturers protocol. Plasmid DNA was dissolved in 100µl ddH_2O and DNA concentration was determined by UV spectrophotometer (Gene Quant II- Photometer, Pharmacia). Final concentration of plasmid was adjusted to 1µg/µl by adding ddH_2O.

3.1.5.3 DNA isolation from agarose gel

To purify DNA from agarose gel, GFX PCR DNA and gel band purification Kit (Amersham Biosciences) was used. The desired band was excised using a scalpel blade. Then the DNA fragment was purified according to the manufacturer's protocol.

3.1.6 Enzymatic modification of DNA

3.1.6.1 Restriction enzyme digestion of DNA

Plasmid DNA or PCR products were digested by restriction enzymes (Fermentas) that recognized specific sequences of DNA. Digestion reactions were incubated for 90 min at 37℃ and were stopped by adding 20% volume of 5 X concentrated dyes followed by the agarose gel electrophoresis.

3.1.6.2 Dephosphorylation of vector DNA

To avoid self-ligation of linearized vectors with complementary ends, Calf Intestinal Alkaline Phosphatase (CIAP, Fermentas) was used to remove phosphate from protruding ends of dsDNA generated by restriction endonucleases. 1 unit of enzyme was added to the restriction reaction and incubated for 30 min at 37℃, and then reaction was stopped by adding 20% volume of 5 X concentrated dyes followed by the agarose gel electrophoresis.

3.1.7 DNA ligation

The vector DNA was digested with an appropriate restriction enzyme and dephosphorylated using alkaline phosphatase if desired. The treated DNA (0.01 pmol) was ligated with the DNA to be inserted (0.03-0.1 pmol) in a total volume of 10 µl with 1 unit of T4-DNA-Ligase (Fermentas) and T4-ligation buffer. Reaction solution was incubated at 16℃ overnight.

3.1.8 *In vitro* mutagenesis

Human KCNQ1 (Yang et al., 1997, Genebank U86146) point mutations were introduced through site-directed mutagenesis by means of overlapping PCR (Stratagene). Appropriate fragments of PCR products were cloned into corresponding vectors by restriction enzymes and T4-DNA ligase (Fermentas). Mutated channels were sequenced at the sense and anti-sense DNA strains using BigDye terminator cycle sequencing kit (Perkin Elmer) by the ZMNH facilities.

3.1.9 Agarose gel electrophoresis of DNA

Agarose gel electrophoresis was used to analyze or separate DNA fragment. The gel was made of 1% agarose in Tris-acetate-EDTA (TAE) buffer with 1µg/L ethidium bromide, and 15 mV current per cm was applied to the agarose gel using an electrophoresis chamber (LKB GPS 200/400, Pharmacia). The distance DNA

migrated in the gel could be judged by visually monitoring migration of the tracking dyes, bromophenol blue and xylene cyanol. To estimate size and amount of the DNA fragments, a standard DNA marker was used (hyperladder, Bioline). DNA migration was visualized using a UV-transilluminator (BioDoc II, Biometra)

3.1.10 cRNA synthesis

3.1.10.1 cRNA synthesis from in vitro transcription

cRNA synthesis was performed using the AMBION cRNA synthesis kit (Ambion). pcDNA3 and pGEM-He-Juel vectors possess a T7 promoter site, suitable for using the appropriate kit. Double stranded cDNA was linearized by appropriate restriction enzyme and the cRNA synthesis was done following the manufacturer's manual. The cRNA was purified by phenol/chloroform extraction followed by an ammonium acetate/ethanol precipitation and stored at −70℃ in DEPC-H_2O.

3.1.10.2 RNA quantitation

RNA concentrations were determined by RNA-chip method. Agilent RNA 6000 Nano Assay Kit (Agilent technologies) and Agilent 2100 bioananlyzer (Molecular Probes) were used following the manufacturer' s manual protocol.

3.2 Cell biology methods

3.2.1 Handling of *Xenopus laevis* oocytes

The *Xenopus* oocytes expression system is widely used for the electrophysiological characterization of ion channels. It has several advantages over other expression systems. (1) *Xenopus* oocytes could be obtained easily, allowing easy injection with foreign cRNA. (2) *Xenopus* oocytes have only a few endogenous channels, which usually mediate a small fraction of the unspecific currents. (3) They are very stable during recording, making it possible to apply long-lasting protocols.

3.2.1.1 Solution for oocytes preparation

Collagenase-solution	2– 4	mg / ml	Collagenase A (Roche) in OR 2
Gentamycin-solution	75	mM	NaCl
	2	mM	KCl
	2	mM	$CaCl_2$
	1	mM	$MgCl_2$
	5	mM	Na-Pyruvate
	5	mM	HEPES, pH 7.5 (NaOH)
	50	µg / ml	Gentamycin (Sigma)
OR2-solution	82.5	mM	NaCl
	2	mM	KCl
	1	mM	$MgCl_2$
	5	mM	HEPES, pH 7,5 (NaOH)
Tricaine-solution:	1.2	mg / ml	3-Aminobenzoic acid ethyl ester (Sigma) in tap water

3.2.1.2 Isolation and maintenance of oocytes

Xenoupus oocytes were first used to express the membrane receptors and channels almost two decades ago. The oocytes from *Xenopus* frogs are big and viable, suitable for injection of foreign cRNA. South African clawed female frog - *Xenopus laevis*, were purchased from NASCO (Tennessee, USA). Under sterile condition ovarian lobe of one side was surgically removed. The oocytes were washed with OR2 solution and incubated with agitation for 2-3 hours in OR2 solution containing 3mg/ml collagenase (Roche). After collagenase treatment, oocytes were carefully washed several times with OR2 solution. Stage Ⅳ to Ⅶ oocytes were selected and incubated in gentamycin solution overnight at 18℃. cRNAs were microinjecte d the next day.

3.2.1.3 cRNA injection into oocytes

Capillary glass (World Precision Instrument) was used to fabricate cRNA injection pipettes, using a PB-7 puller (Narishige, Japan). The pipette-tips were broken at a diameter of 10-14μm using a MF-900 microforge (Narisshige, Japan). Pipettes were baked at 200℃ for at least 2 hours. A micro-inject or Nanoliter 2000 (World Precision Instrument) was adjusted to the micromanipulator. Pipettes were first back-filled with mineral oil, followed by filling of cRNA up into the glass pipette. Injections were performed in a sterile injection-chamber with grooves cut 90^{o} at one side, and 45^{o} at another side, respectively. The micropipette was adjusted for injection from the 45^{o} side of chamber, and the 90^{o} wall served as mechanical resistance for oocytes. The chamber was filled with OR2 solution during experiment. Injected oocytes were incubated in Gentamycin-solution at 18℃ for 1-7 da ys prior to electrophysiological recording.

3.3 Electrophysiology

3.3.1 Two-Electrode Voltage Clamp (TEVC)

The *Xenopus* oocyte heterologous expression system is widely used for the electrophysiological characterization of ion channels. It has several advantages over other expression systems. *Xenopus* oocytes could be obtained easily and they are viable under appropriate conditions for 2-3 weeks. The cells are big, allowing easy injection with foreign cRNA or cDNA. *Xenopus* oocytes have only a few endogenous channels, which usually mediate a small fraction of the unspecific currents. They are very stable during recording, making it possible to apply long-lasting protocols.

To obtain voltage clamp conditions, two glass-microelectrodes, filled with 3M KCl solution are penetrated into the oocyte. The voltage electrode measures the membrane voltage, transmitting the signal to a feedback amplifier, which injects appropriate amounts of current through the current electrode (second electrode) to keep the membrane potential at a given value. Due to the capacitance of the membrane a transient capacitive current component will flow during the voltage-clamp step charge, which is given by following equation:

$$I_{cap} = C\, dV/dt$$

where I_{cap} is the capacitive current, C is the capacitance of the membrane, V is the membrane potential.)

Two factors are needed to take into consideration when voltage clamps oocytes. Firstly, with apparent surface area on the order of 10^6 μm^2, there is enormous amount of membrane that must be charged in order to clamp the cell. Secondly, one can encounter big current, potentially causing appreciable serious resistance error.

The response time (τ) of a voltage clamp to a step voltage change is

$$\tau = RC / A$$

where R is the resistance of current electrode, C is the capacitance of the membrane, and A is the gain of the amplifier.

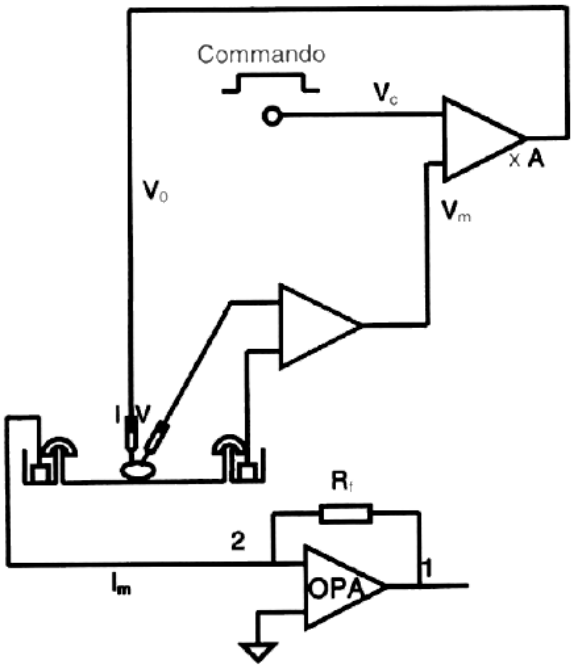

Figure 3.1: Simplified schematic diagram of the experimental setup for two-electrode voltage clamp. The Oocyte was visually inspected by means of a reflected light microscope (400× magnification) in the basin.

3.3.1.1 Experimental set-up

Defolliculated oocyte of *Xenopus laevis* was positioned in a chamber mounted under a binocular and connected to a stopcock for changing the solutions perfusing the chamber. Agar-bridges provided electrical connection between the bath-clamp circuit and the chamber-perfusion solution. The cell was impaled with two microelectrodes. Current-voltage dependencies of the membrane currents of *Xenppus* oocytes are determined by conventional TEVC technique with OOCYTE CLAMP 725 amplifier (Warner Instruments, Inc). The amplifier was synchronized with a Mac G3 computer and the pulse program (HEKA electronics) was used for the control of parameters and application of voltage protocols. For control of the quality of voltage clamp, the time courses of Vc and Vm were monitored on an oscilloscope.

3.3.1.2 Procedure for recording from oocytes

1. Preparation of microelectrodes

Glass micropipettes were pulled from the filament-containing capillaries of borosilicate glass Filament (TW150 F-4, WPI, USA) using a vertical puller PB-7 (NARISHIGE, Japan). The tips of pipettes were broken to get an inner opening diameter of 4-8µm. The pipettes were filled with 3M KCl using a syringe. Such electrodes were ‘leaky’ and could not be used for recording unless the tips were plugged by agar-KCl (3M) solution by a suction syringe. The microelectrodes were inserted into electrode holders mounted to micromanipulators.

2. Offset compensation and electrode resistance measurement

All microelectrodes produce a potential by themselves, the tip potential. This is nonlinear and must be compensated electronically. When the electrodes were immersed into the bath solution of the chamber, the offset was compensated manually by adjusting the offset compensation controls which is available for each electrode.

Then the resistances of the microelectrodes were measured by ohm-meter built-in the amplifier. The resistance was 0.2-0.6 MΩ for voltage electrode, and 0.1-0.4 MΩ for current electrode.

3. Impaling the cell and voltage clamp recording

The electrodes were advanced until they popped through the membrane. The potential across the membrane could be displayed on the *Voltage Electrode* Meter of the amplifier. Then switched to the *clamp mode* and started voltage clamp current recording.

3.3.1.3 Solutions for TEVC recordings

ND96	79.5	mM	NaCl
	2	mM	KCl
	2	mM	$CaCl_2$
	1	mM	$MgCl_2$
	5	mM	HEPES, pH 7.5 (NaOH)
20mM K^+ solution:	97	mM	NaCl
	20	mM	KCl
	1.8	mM	$CaCl_2$
	1	mM	$MgCl_2$
	5	mM	HEPES, pH 7.5 (NaOH)
High K^+ solution:	100	mM	KCl
	0.1	mM	$CaCl_2$
	1.8	mM	$MgCl_2$
	5	mM	HEPES, pH 7.5 (NaOH)
High Rb^+ solution:	96	mM	RbCl
	4	mM	KCl
	0.1	mM	$CaCl_2$
	1.8	mM	$MgCl_2$
	5	mM	HEPES, pH 7.5 (NaOH)

3.3.2 The patch clamp technique

The Patch clamp technique is an electrophysiological method that allows the recording of macroscopic whole cell or microscopic single channel currents flowing across biological membranes through ion channels. Soon after its development by Erwin Neher and Bert Sakmann, it has been adopted by numerous laboratories and subsequently caused a revolutionary advancement of many research areas in both cellular and molecular biology.

3.3.2.1 The patch clamp configuration

The basic approach to measure small ionic currents in the nanoampere range through single channels requires a low noise recording. This is achieved by tightly sealing a glass microelectrode onto the plasma membrane of an intact cell, thereby isolating a small patch. The seal resistance should typically be in excess of 10^9 Ω (“gigaseal”). The currents flowing through ion channels enclosed by the pipette tip within that patch are measured by means of a connected patch clamp amplifier. This so-called “cell-attached” configuration is the precursor to all other variants of the patch clamp technique.

The cell attached configuration may be used to record single channel activity, or one may proceed to isolate the patch from its environment by withdrawing the pipette from the cell. This usually retains the integrity of the gigaseal pipette-patch assembly and allows one to study ion channels in the excised patch configuration. This configuration is called “inside-out” because the cytosolic side of the patch now faces the outside bath solution.

As an alternative to excising the patch, one can simply break the patch by applying a pulse of suction through the patch pipette, thereby creating a hole in the plasma membrane and gaining access to the cell interior. This configuration is characterized by a low-resistance access to the cell interior through the pipette tip, allowing one to voltage-clamp the whole cell (“whole-cell” configuration)

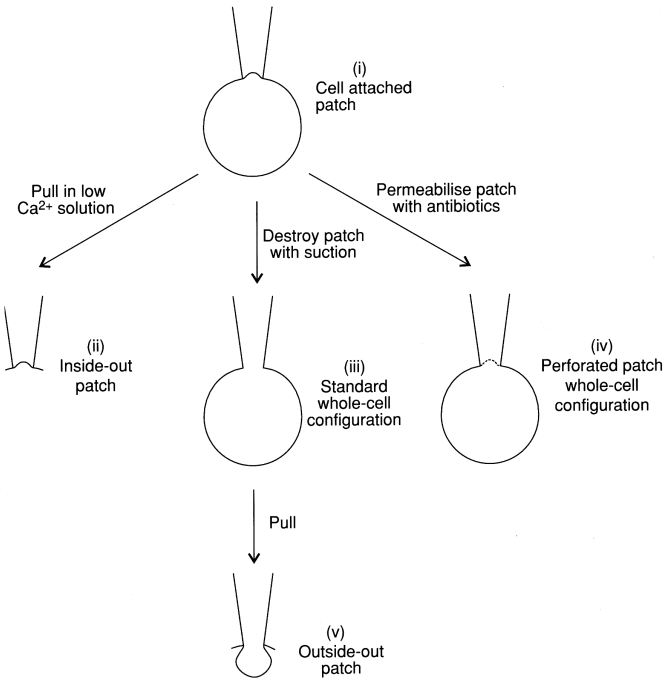

Figure 3.2: The various configurations of the patch-clamp technique.

(i) Forming a seal between the patch pipette and the cell membrane. Withdrawal of the pipette from cell surface produces an inside-out patch (ii) If the patch membrane is destroyed in the cell-attached configuration, the whole-cell configuration is produced. (iii) Permeabilisation with pore-forming antibiotics yields the perforated-patch configuration. Withdrawal of the pipette from the whole-cell configuration produces an outside-out patch.

A typical patch clamp circuit is shown in Fig. 3.3. A key difference between the patch clamp and the two-electrode voltage clamp is that the patch clamp uses a single electrode both to control the membrane potential and to measure current. Another difference is that patch clamp amplifier is sufficiently sensitive to resolve the tiny currents (pA) flowing through ion channels.

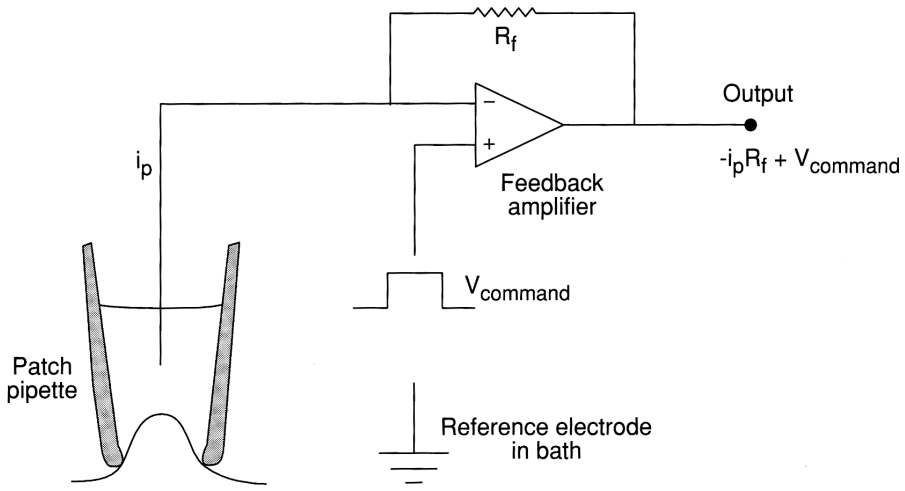

Figure 3.3: Patch clamp circuit.

The patch pipette is connected to the inverting input of a feedback amplifier. Because the input resistance of this amplifier is essentially infinite, all the current recorded by the pipette flows through the feedback resistor (R_f). This has a very high value, typically 10GΩ. Its high resistance enables the tiny sinlg-channel currents (~1 pA) to be measured, since the patch current (I_p) is given by the voltage drop across R_f, i.e., $V=I_pR_f$. The command potential ($V_{command}$) is applied to the other input of the feedback amplifier and the amplifier passes current through the feedback resistor to keep the voltage at the inverting input the same as the command voltage. This means that the desired potential is also applied to the pipette and thus to the patch membrane.

3.3.2.2 Inside-out patch clamping of excised membrane

Oocytes were prepared for study by manually removing the vitelline membrane after shrinking in hypertonic solution (mM): 200 potassium aspartate, 20 KCl, 1 $MgCl_2$, 5 EGTA 10 HEPES, ph7.4. Once removed, the cells were extremely fragile and would easily rupture if mechanically distressed or exposed to air. They should immediately be transferred to the recording chamber. Pipettes were pulled from borosilicate glass (PG10150-4, World Precision Instruments, USA), and polished by micorforge MF900. Inside-out macropatches could be obtained by rapid withdrawal of the pipette from oocyte after getting a seal. Multi-channel application system Valvebank 8 II (AutoMate scientific, Inc) was used for switching between appropriate solutions. At the beginning of the application, the tip of the patch-pipette, which contained the giant membrane patch, was adjusted in close proximity of the application-pipette. Current recordings and data acquisition were controlled by an EPC-9 patch clamp amplifier combined with the Pulse/Pulsefit software package (HEKA Electronic, Germany) running on a Window computer. The patch-clamp recording set-up consiss of: a Faraday cage, a pneumatic vibration isolation table, and a Zeiss Axiovert inverted microscope (Axiovert 405M), and a Patchman micromanipulator (Eppendorf).

To study the Ca^{2+} effect on KCNQ1 channels, Ca^{2+} concentration ($[Ca^{2+}]$) in the buffers was calculated using Winmax software (Stanford University, CA) and was determined regularly by Calcium Calibration Buffer Kits (Molecular Probes). Vanadate and fluoride were added to the internal solutions as lipid phosphatase inhibitors.

3.3.2.3 Solutions for inside-out patch recordings

Internal solution	60	mM	$KMeSO_3$
0 µM $[Ca^{2+}]$	5	mM	KF
	0.1	mM	Na_3VO_4
	10	mM	$K_4P_2O_7$
	10	mM	HEPES
	5	mM	EGTA
	10	mM	HCl
			pH 7.4 (NaOH)
Internal solution	60	mM	$KMeSO_3$
0.025 µM $[Ca^{2+}]$	5	mM	KF
	0.1	mM	Na_3VO_4
	10	mM	$K_4P_2O_7$
	10	mM	HEPES
	5	mM	EGTA
	7.48	mM	HCl
	1.26	mM	$CaCl_2$
			pH 7.4 (NaOH)
Internal solution	60	mM	$KMeSO_3$
0.1µM $[Ca^{2+}]$	5	mM	KF
	0.1	mM	Na_3VO_4
	10	mM	$K_4P_2O_7$
	10	mM	HEPES
	5	mM	EGTA
	4.2	mM	HCl
	2.9	mM	$CaCl_2$
			pH 7.4 (NaOH)
Internal solution	60	mM	$KMeSO_3$
0.2 µM $[Ca^{2+}]$	5	mM	KF
	0.1	mM	Na_3VO_4
	10	mM	$K_4P_2O_7$
	10	mM	HEPES
	5	mM	EGTA
	2.66	mM	HCl
	3.67	mM	$CaCl_2$
			pH 7.4 (NaOH)

External solution for I_{Ks}	2	mM	KCl
(Pippet solution)	6	mM	NaCl
	1	mM	$MgCl_2$
	85	mM	$NaMeS0_3$
	5	mM	NaOH
	5	mM	HEPES pH 7.4 (NaOH)
External solution for KCNQ1	104	mM	$KMeS0_3$
(Pippet solution)	6	mM	KCl
	2	mM	$MgCl_2$
	10	mM	HEPES pH7.4 (NaOH)

3.3.3 Data analysis

All data analysis and calculations were performed by using Igor Pro (version 5.0, WaveMetrics, USA), Kaleidagraph (version 4.0, Synergy software, USA) and Excel (Microsoft software, USA). Current traces were downloaded by using Igor Pro (version 5.0, WaveMetrics, USA). If not otherwise stated, data are expressed as mean ± SE and number of observations (*n*). Statistically significant differences were assessed by unpaired student T-test with the use of Kaleidagraph software (version 4.0, Synergy software, USA).

3.3.3.1 Voltage-dependent activation

For KCNQ1 wild-type and KCNQ1 mutant channels, ionic currents were elicited with pulses between -100 and +60 mV in 10 mV or 20 mV increment followed by a tail recording at -120 mV (holding potential: -100 or -120 mV) in 20 mM K^+ solutions.

Because the activation kinetics among the mutants differed by orders of magnitude, both pulse and interpulse duration were appropriately adapted to the activation time course with the criterion that the ionic currents were fully activated.

The voltage dependence of activation of the wild-type and mutant KCNQ1 channels was determined from tail current analysis. A double exponential fit was applied to the tail currents and the slow exponential component was extrapolated to the beginning of the repolarizing step. Extrapolated tail current amplitudes were plotted *versus* test potential and were fitted using the program Kaleidagraph (version4.0. Synergy software, USA) to single Boltzmann equation:

$$I/I_{max} = (1+e^{-zF(V-V_{1/2})/RT})^{-1}$$

where I/I_{max} is the normalized tail current amplitude, z is the equivalent charge, $V_{1/2}$ is the half activation voltage, F is Farady's constant, R is the molar gas constant, and T is the absolute temperature in Kelvin (K), T=295K.

Free energy difference ΔG_0 (in kcal/mol) for the channel opening at 0 mV was calculated by the following equation:

$$\Delta G_0 = 0.2389\ zFV_{1/2}$$

The differences in $V_{1/2}$ between wild-type and mutant channels were calculated according to the following equation:

$$\Delta V_{1/2} = V_{1/2}^{mut} - V_{1/2}^{wt}$$

As to KCNQ1/KCNE1 channels, the voltage-dependent activation relations were determined at 32℃ in ND96 solutions. The currents were evoked by voltage steps from -80 mV to + 80 mV in 20 mV increments for 3-second followed by a 1-second step to -40 mV, and holding potential is -80 mV or -100 mV.

The voltage-activation relations for KCNQ1/KCNE1 were determined from tail current analysis. Tail currents were normalized to the maximal currents at high potentials and fitted to single Boltzmann function:

$$I/I_{max} = (1+e^{-zF(V-V_{1/2})/RT})^{-1}$$

where $V_{1/2}$ is the half activation voltage, z is the equivalent charge (proportional to the slope), F is Farady's constant, R is the molar gas constant, and T is the absolute temperature in Kelvin (K), T=305K.

Free energy difference ΔG_0 (in kcal/mol) for the KCNQ1/KCNE1 channel opening at 0 mV was calculated by the following equation:

$$\Delta G_0 = 0.2389\ zFV_{1/2}$$

3.3.3.2 Conductance and inactivation

The relative Rb^+/K^+ conductance (G_{Rb}/G_K) and inactivation fraction were measured according to the method from previous studies (Seebohm et al., 2003). G_{Rb}/G_K was determined as the ratio of the peak inward tail current at -120 mV after a 3 seconds pulse stimulation of +40 mV measured from the same oocyte bathed in the high Rb^+ followed by the high K^+ solution.

As shown in Fig. 3.4, the degree of KCNQ1 channel inactivation for oocytes bathed in the high-K^+ solution was assessed by analysis of tail currents that were fitted to a bi-exponential equation of the form:

$$I = A_s \exp(-t/\tau_s) - A_f \exp(-t/\tau_f) - A_0$$

where a fast time constant τ_f reflects the recovery from inactivation at the tail potential and slow time constant τ_s describes the deactivation process and A_0 is a steady-state current. The ratio A_f/A_s is a parameter that depends strongly on the degree of inactivation (Pusch *et al.* 1998). The degree of steady-state inactivation was calculated by the following equation (Seebohm et al., 2003):

$$F_{inac}(\%) = (A_f/ A_s - \tau_f/ \tau_s) / (1- \tau_f/ \tau_s)$$

3.3.3.3 Deactivation kinetics

Tail currents recorded at -120 mV or -100 mV in high K^+ solution were fitted to a triple exponential function of the form:

$$I = A_{s1} \exp(-t/\tau_{s1}) + A_{s2} \exp(-t/\tau_{s2}) - A_f \exp(-t/\tau_f) - A_0$$

where a fast time constant τ_f reflects the recovery from inactivation at the tail potential and two slow time constants τ_{s1} and τ_{s2} describe the deactivation process.

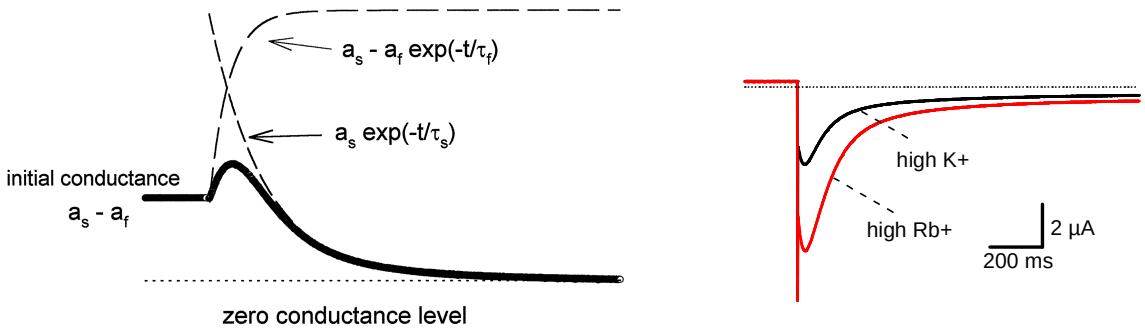

Figure 3.4: Biphasic, double-exponential time course of the tail currents at -120 mV.

A voltage-clamp tail current recorded at -120 mV after depolarization voltage step to +40 mV for 3 seconds, is shown superimposed with a double exponential fit. The two exponential components of the fit are shown as dashed lines. On the right side is the typical tail currents recorded at -120 mV after 3 seconds pulse stimulation to +40 mV in 100 mM Rb^+ solution (red) and 100 mM K^+ solution (black).

3.4 Molecular modeling

The crystal structure of Kv1.2 (Long et al., 2005a) was retrieved from the NCBI Protein Data Bank (2A79). Molecular modeling figures in previous study were made by Pymol software (http://pymol.sourceforge.net/).

4 Results

4.1 Gating of KCNQ1 channels

In Kv channels, each of the four subunits contains six membrane-spanning segments: S1-S4 comprise the voltage sensor and S5-S6 the pore (Fig. 4.1A). Sequence alignment of the pore region of KCNQ1 subunit, which comprises the outer helix (S5), the pore (P) helix, and the inner helix (S6) (Fig. 4.1), with the ones of Kv1.2 and KcsA is in agreement with the notion that K^+ channels have highly conserved pore domains.
Their role in forming a cradle for the selectivity filter toward the extracellular end of the membrane and an activation gate at the intracellular end is well established. To investigate the gating mechanism for KCNQ1 channels, each individual residue in the KCNQ1 pore region and the adjacent S4-S5 linker was mutated into a small residue (alanine) and/or a bulky residue (tryptophan). cRNAs encoding the mutant channels were injected into *Xenopus* oocytes and two-electrode voltage-clamp recording techniques were used to evaluate the functional properties of each mutant including expression, voltage-dependent activation, conductance and inactivation kinetics. It was expected that that an analysis of the resulting mutational perturbations of KCNQ1 channel gating would provide valuable information about energetics and mechanism of KCNQ1 pore opening.

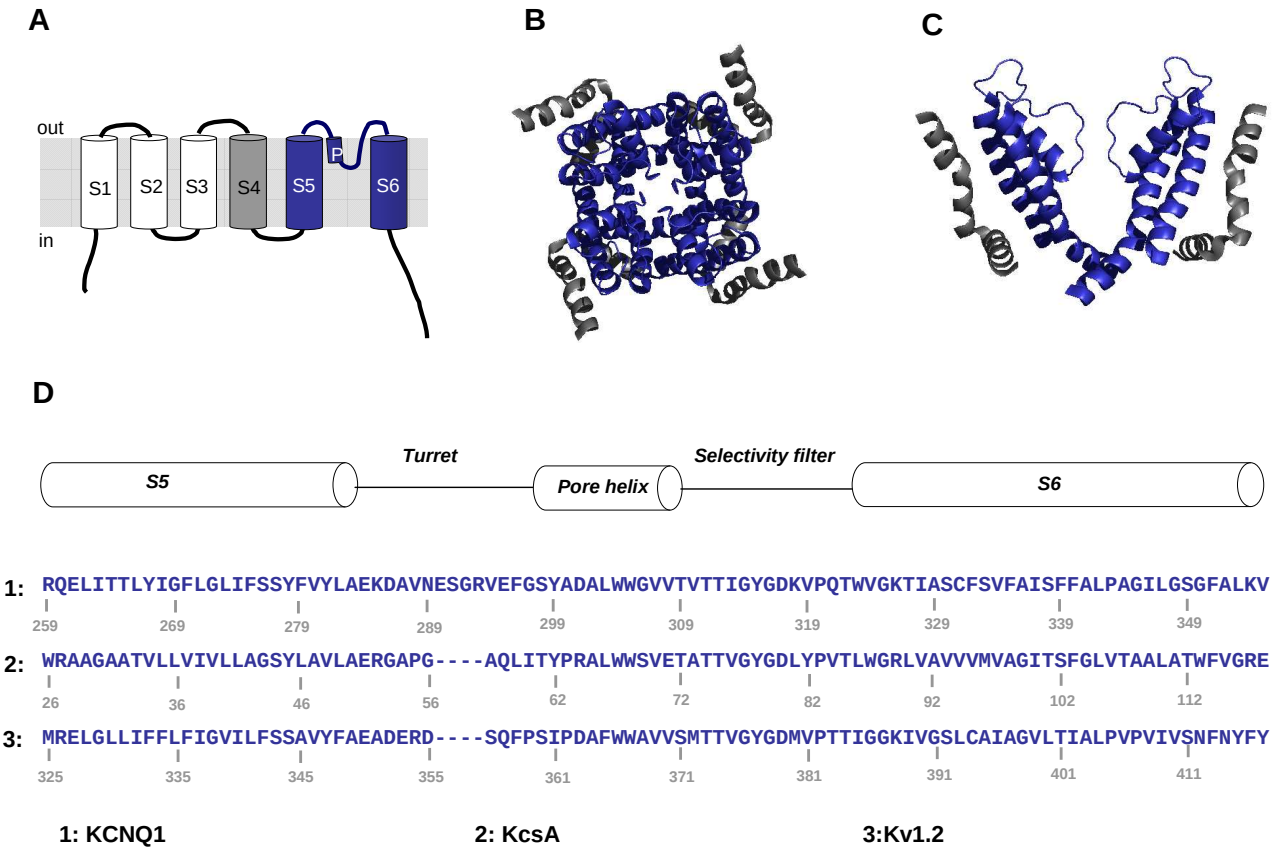

Figure 4.1: Identification and sequence comparison of residues in the pore domain of Kv1.2, KcsA and KCNQ1

(A) Membrane-folding model for a voltage-gated K^+ channel showing six membrane-spanning α helices (white and blue cylinders), and a short pore helix (short blue cylinder). The white helices comprise the voltage-sensing domains; the blue region (S5 through S6) forms the pore domain.

(B) X–ray structure of the S4-S6 region of the Kv1.2 channel viewed from an extracellular vantage with mutated regions highlighted in blue. PDB accession code 2A79. The region from the N terminus through S3 was omitted.

(C) Side view of the Kv1.2 structure, showing only the S5-S6 region from two subunits and the nearby S4 helix from two adjacent subunits.

(D) Sequence alignment of the KCNQ1, KcsA, Kv1.2 channels within the pore domain region. Diagram above indicates secondary structural motifs in Kv1.2.

4.1.1 Expression of KCNQ1 mutants

Together, 106 of the 188 KCNQ1 mutants (56%) resulted in functional channels that mediated recordable currents and 82 mutations lead to non-functional channels. Remarkably, about two-thirds of the 82 nonfunctional mutations (52 out of 82) were localized to a stretch of 39 amino acid residues comprising the turret region, P-helix and selectivity filter. P-helix and selectivity filter of K^+ channels are highly conserved in sequence and structure consistent with an important role for the conduction of K^+ ions. Almost all mutants in these two domains (39 out of 42, i.e. 93%) were nonfunctional. In comparison to the P-helix and selectivity filter, the sequence of the turret region of K^+ channels is not highly conserved and its structure is not well resolved in the available K^+ channel crystal structure. About 54% of the mutants in the KCNQ1 turret region (15 out of 28) could express recordable currents. By contrast, mutations in the membrane-spanning pore-domain segments S5 and S6 and in the S4-S5 linker region mostly produced functional KCNQ1 channels (88 out of 118, i.e. 75%). This data compared well to previous data obtained in comparable mutagenesis screens of *Shaker* channels (Yifrach and MacKinnon R, 2002). In addition, more tryptophan (52%) than alanine (21%) mutants in S6 displayed no functional currents (Table 4.2), indicating that S6 is highly packed in the KCNQ1 pore region.

Table 4.1: Regional functional expressional level for KCNQ1 mutant channels

	Total	functional	nonfunctional	nonfunctional (%)
S4-S5	14	13	1	7%
S5	49	40	9	18%
S6	55	35	20	36%
P turret	28	15	13	46%
P helix and filter	42	3	39	93%
Summary	188	106	82	44%

Table 4.2: Regional functional expressional level for KCNQ1 Ala versus Trp mutant channels

	Total	functional	nonfunctional	nonfunctional (%)
S5_Ala	24	21	3	13%
S5_Trp	25	19	6	24%
S6_Ala	28	22	6	21%
S6_Trp	27	13	14	52%
P_region_Ala	36	11	25	69%
P_region_Trp	34	7	27	79%

Table 4.3: Gating properties of the KCNQ1 mutant channels

		n	$V_{1/2}$(mV)	z	ΔG_0 (kcal/mol)	$\Delta V_{1/2}$ (mV)		n	$V_{1/2}$(mV)	z	ΔG_0 (kcal/mol)	$\Delta V_{1/2}$ (mV)
	wild type	36	-25.3 ± 0.5	2.95±0.06	-1.73±0.05		G245W	5	-21. 3±1.4	2.98±0.06	-1.47±0.12	4±1.5
							G246W	4	-47.3±1.1	2.17±0.09	-2.37±0.14	-22±1.2
							T247W	4	-1.0±1.0	2.24±0.03	-0.06±0.05	24.3±1.1
							W248A	4	-2.7±2.1	1.85±0.08	-0.12±0.09	22.6±2.2
S4-S5							R249W	5	-13.5±1.0	1.72±0.04	-0.53±0.04	11.8±1.1
linker							L250W	6	34.7±0.7	1.28±0.01	1.02±0.02	60±0.9
							L251W	4	51.8±1.6	1.09±0.04	1.30±0.04	77.1±1.7
							G252W	4	-25.5±0.7	2.56±0.07	-1.51±0.08	-0.2±0.9
							S253W	4	-12.9±1.4	1.52±0.07	-0.45±0.05	12.4±1.5
							V254W		NE			
							V255W	4	2.4±1.2	1.94±0.07	0.11±0.05	27.7±1.3
							F256A	5	-10.9±1.0	2.36±0.03	-0.59±0.06	14.4±1.1
							I257W	4	-20.4±0.4	2.03±0.07	-0.96±0.05	4.9±0.6
							H258W	3	35.3±3.6	1.22±0.12	0.97±0.01	60.6±3.6
	R259A	5	28.9 ± 1.5	1.54 ± 0.04	1.02 ± 0.03	54.2±1.6	R259W	5	13.7±0.9	1.82±0.04	0.57±0.03	39±1.0
	Q260A	5	-14.2 ± 0.9	1.74 ± 0.04	-0.57 ± 0.02	11.1±1.0	Q260W	4	10.1±0.8	1.75±0.06	0.41±0.0 4	35.4±0.9
	E261A	7	-27.6 ± 0.7	2.49 ± 0.09	-1. 59 ± 0.08	-2.3±0.9	E261W	5	72.0±1.8	2.02±0.07	3.34±0. 09	97.3±1.9
	L262A	4	-18. 4 ± 2.0	1.77 ± 0.04	-0. 75 ± 0.10	6.9±2.1	L262W		NE			
	I263A	10	-17. 7 ± 0.8	3.37 ± 0.26	-1. 40 ± 0.14	7.6±0.9	I263W	6	-38.2±0.6	3.50±0.10	-3.09±0 .12	-12.9±0.8
	&T264A	6	-4.9 ± 1	1.26 ± 0.03	-0.14 ± 0.03	20.3±1.1	T264W	7	21.7±2.0	1.13±0.02	0.57±0.0 6	47±2.1
	T265A	5	-29.2 ± 0.4	1.91 ± 0.03	-1.29 ± 0.03	-3.9±0.6	T265W	4	-26.1±0.3	3.12±0.12	-1.88±0 .08	-0.8±0.6
	L266A	7	-20. 9 ± 0.3	2.56 ± 0.18	-1. 23 ± 0.10	4.4±0.6	L266W	5	-27.6±1.0	2.84±0.08	-1.81±0 .09	-2.3±1.1
	Y267A	5	-13. 5 ± 0.8	1.17 ± 0.06	-0. 36 ± 0.01	11.8±0.9	Y267W	5	-8.0±0.8	1.90±0.03	-0.35±0 .04	17.3±0.9
S5	&I268A	7	-2.3 ± 1.1	1.42 ± 0.04	0.07 ± 0.03	27.6±1.2	I268W	4	-29.2±0.7	1.93±0.06	-1.31±0. 07	-3.9±0.9
	&G269A	4	-15. 2 ± 1.2	1.88 ± 0.07	-0. 66 ± 0.06	10.1±1.3	G269W		NE			
	F270A	5	-27. 0 ± 0.3	2.61 ± 0.04	-1. 62 ± 0.03	-1.7±0.6	F270W	4	-19.5±1.4	2.43±0.06	-1.10 ± 0.09	5.8±1.5
	L271A	4	-7. 9 ± 0.9	1.42 ± 0.06	-0. 26 ± 0.03	17.4±1.0	L271W	4	-12.2±1.1	2.34±0.06	-0.66± 0.08	13.1
	G272A	4	-26. 4 ± 0.6	3.03 ± 0.14	-1. 84 ± 0.08	-1.1±0.8	G272W	5	-18.3±0.3	2.93±0.08	-1.23± 0.03	7±0.6
	L273A		NE				L273W	7	-21.5±1.2	2.69±0.06	-1.34±0.10	3.8±1.3
	I274A	7	-35. 8 ± 1.2	2.88 ± 0.09	-2. 38 ± 0.13	-10.5±1.3	I274W	6	-49.2±0.6	2.59±0.04	-2.94 ±0.08	-23.9±0.8
	F275A	5	-35. 4 ± 0.7	1.69 ± 0.01	-1. 38 ± 0.04	-10.1±0.9	F275W	5	-1.1±0.8	3.85±0.12	-0.10± 0.07	24.2±0.9
	S276A	5	-18. 8 ± 2.1	3.23 ± 0.23	-1. 42 ± 0.21	6.5±2.2	S276W		NE			
	S277A	4	-28.2 ± 0.3	2.59 ± 0.07	-1.68 ± 0.07	-2.9±0.6	S277W		NE			
	Y278A	4	8.5 ± 0.9	3.02 ± 0.11	0.59 ± 0.08	33.8±1.0	Y278W	4	-6.9±0.6	1.65±0.05	-0.26±0.0 3	18.4±0.8
	F279A	4	-32.3± 0.9	2.93 ± 0.08	-2.19 ± 0.11	-7.0±1.0	F279W	5	-21.6±0.8	3.25±0.12	-1.62±0 .10	3.7±0.9
	V280A		NE				V280W		NE			
	Y281A		NE				Y281W	4	-24.6±1.1	2.69±0.12	-1.53±0.12	0.7±1.2
	L282A	5	-20.9 ± 0.8	1.64± 0.11	-0.79 ± 0.06	4.4±0.9	L282W	4	-8.2±1.6	3.22±0.13	-0.60±0.1 3	17.1±1.7
	A283						A283W		NE			
	E284A		NE				E284W		NE			
	K285A	5	-34.1±1.7	1.75± 0.08	-1.39± 0.14	-8.8±1.8	K285W	4	-32.0±1.6	1.04± 0.09	-0.78± 0.11	-6.7±1.7
	D286A		NE				D286W		NE			
	A287						A287W	4	-20.2±1.2	3.09±0.07	-1.44±0.08	5.1±1.3
	V288A	4	-23.9 ± 2.6	1.88 ± 0.06	-1.03 ± 0.10	1.4±2.6	V288W		NE			
	N289A	5	-24.3 ± 0.6	1.94 ± 0.03	-1.08 ± 0.04	1±0.8	N289W		NE			
P region	E290A	5	-22.2 ± 1.4	3.00 ± 0.29	-1.52 ± 0.12	3.1±1.5	E290W		NE			
	S291A	4	-24.3 ± 1.4	4.13 ± 0.31	-2.33 ± 0.27	1±1.5	S291W	4	-27.5±0.2	3.22±0.20	-2.04±0.11	-2.2±0.5
(Turret)	G292A		NE				G292W		NE			
	R293A	5	21.1 + 0.7	2.31 ± 0.01	-1.13 ± 0.04	4.2±0.9	R293W		NE			
	V294A	5	-25.8 ± 0.8	2.27 ± 0.06	-1.35 ± 0.04	-0.5±0.9	V294W	3	-30.9±1.4	2.10±0.02	-1.50±0 .08	-5.6±1.5
	E295A	5	-21.4 ± 0.9	3.06 ± 0.17	-1.51 ± 0.10	3.9±1.0	E295W		NE			
	F296A		NE				F296W		NA			
	G297A	4	-20.3 ± 3.4	2.73 ± 0.23	-1.33 ± 0.32	5±3.4	G297W	5	-28.4±1.4	3.00±0.09	-1.97±0.14	-3.1±1.5
	S298A		NE				S298W	4	-25.8±0.3	3.06±0.06	-1.81±0.03	-0.5±0.6

		n	$V_{1/2}$(mV)	z	ΔG_0 (kcal/mol)	$\Delta V_{1/2}$ (mV)		n	$V_{1/2}$(mV)	z	ΔG_0 (kcal/mol)	$\Delta V_{1/2}$ (mV)
	Y299A		NE				Y299W		NA			
	A300						A300W	5	-7.5±0.5	3.16±0.08	-0.55±0.04	17.8±0.7
	D301A		NE				D301W		NE			
P region	A302						A302W		NE			
	L303A		NE				L303W		NE			
(pore helix)	W304A		NE				W304					
	W305A		NE				W305					
	G306A		NE				G306W		NE			
	V307A		NE				V307W		NE			
	V308A		NE				V308W		NE			
	T309A		NE				T309W		NE			
	&V310A	4	-34.9 ± 1.9	1.50 ± 0.04	-1.21 ± 0.09	-9.6±2.0	V310W		NE			
	T311A		NE				T311W		NE			
	T312A		NE				T312W		NE			
	I313A		NE				I313W		NE			
P region	G314A		NE				G314W		NE			
	Y315A		NE				Y315A		NA			
(Selectivity	G316A		NE				G316W		NE			
filter)	D317A		NE				D317W		NE			
	K318A		NE				K318W		NE			
	V319A		NE				V319W		NE			
	P320A		NE				P320W		NE			
	Q321A	4	-22.3 ± 0.8	3.27 ± 0.13	-1.68 ± 0.05	3±0.9	Q321W		NE			
	T322A		NE				T322W		NE			
	W323A	5	-18.7 ± 1.1	2.77 ± 0.05	-1.20 ± 0.09	6.6±1.2	W323					
	V324A	7	-27.5 ± 1.8	2.78 ± 0.13	-1.75 ± 0.14	-2.2±1.9	V324W	5	-30.3±0.6	3.47±0.05	-2.42±0 .08	-5±0.8
	G325A		NE				G325W		NE			
	K326A		NE				K326W		NE			
	T327A	5	-27.8 ± 0.5	2.87 ± 0.06	-1.85 ± 0.06	-2.5±0.7	T327W	4	-25.3±0.4	3.03±0.08	-1.77±0 .06	0±0.6
	I328A		NE				I328W		NE			
	A329						A329W		NE			
	S330A	4	-29.0 ± 0.6	2.81 ± 0.07	-1.88 ± 0.08	-3.7±0.8	S330W		NE			
	C331A	4	-31.5 ± 0.7	2.88 ± 0.09	-2.10 ± 0.11	-6.2±0.9	C331W		NE			
	F332A	5	0.6±0.9	3.07±0.07	0.04±0.06	25.9±1.0	F332		NE			
	S333A	4	-21.9 ± 0.8	3.41 ± 0.20	-1. 73 ± 0.16	3.4±0.9	S333W		NE			
S6	V334A		NE				&V334W	4	-3.7±0.8	1.71±0.05	-0.15±0.03	21.6±0.9
	F335A	4	4.8 ± 1.0	1.23 ± 0.01	0.13 ± 0.03	30.1±1.1	F335W		NA			
	A336						A336W	4	-26.9±1.0	1.42±0.05	-0.88±0.06	-1.6±1.1
	I337A	6	-20.7 ± 0.2	1.95 ± 0.04	-0.93 ± 0.01	4.6±0.5	I337W		NE			
	S338A	6	3.8 ± 1.5	1.49 ± 0.05	0.13 ± 0.05	29.1±1.6	S338W	5	-24.9±1.3	2.55±0.13	-1.46±0. 09	0.40±1.4
	&F339A	5	-23.9 ± 1.4	2.24 ± 0.08	-1.25 ± 0.12	1.4±1.5	F339W		NA			
	&F340A	4	-56.1 ± 0.6	2.72 ± 0.08	-3.52 ± 0.11	-30.8±0.8	F340W		NA			
	A341						A341W		NE			
	L342A	6	--51.6 ± 0.8	2.32 ± 0.03	-2.75 ± 0.04	-26.3±0.9	L342W		NE			
	P343A		NE				P343W		NE			
	A344						A344W		NE			
	&G345A	3	-8.3±1.4	1.47 ± 0.06	-0.28± 0.05	17±1.5	G345W		Inward Rectify			
	I346A		NE				I346W	3	15.1±2.4	1.71±0.5	0.59±0.09	40.4±2.4
	L347A	4	36.0 ± 4.9	1.33 ± 0.14	1.06 ± 0.07	61.3±4.9	L347W	5	46.1±1.1	1.63±0.02	1.73±0.03	71.4±1.2
	G348A	4	-27.9 ± 1.0	1.40 ± 0.05	-0.9 ± 0.03	-2.6±1.1	G348W		Inward Rectify			
	S349A	4	-2.8 ± 1.0	2.24 ± 0.08	-0.14 ± 0.05	22.5±1.1	S349W		NE			
	G350A	4	-4.5 ± 0.9	1.36 ± 0.03	-0.14 ± 0.03	20.8±1.0	G350W		NE			
	F351A	4	21.8 ± 0.6	3.20 ± 0.12	1.60 ± 0.06	47.1±0.8	F351W		NA			
	A352						A352W	4	39.5±3.5	1.00±0.02	0.91±0.06	64.8±3.5
	L353A	4	-42.5 ± 2.1	0.86 ± 0.06	-0.84 ± 0.06	-17.2±2.2	L353W	4	-27.8±0.6	3.13±0.08	-2.00± 0.07	-2.5±0.8
	K354A	4	-8.9 ± 0.7	1.93 ± 0.08	-0.39 ± 0.03	16.4±0.9	K354W	4	-6.1±0.4	1.23±0.02	0.17±0.0 1	19.2±0.6
	&V355A	4	-35.5 ± 3.0	1.83 ± 0.04	-1.50 ± 0.15	-10.2±3.0	V355W	3	26.5±1.2	1.26±0.03	0.77±0. 02	51.8±1.3

The midpoint ($V_{1/2}$) and slope (z) of G-V relations are from fits of single Boltzmann functions to data obtained from individual oocytes. n represents the number of experiments. The free energy of KCNQ1 channel activation, ΔG_0, is calculated as $zV_{1/2}F$, and F is the Faraday constant. $\Delta V_{1/2} = V_{1/2}^{mut} - V_{1/2}^{WT}$. Coloring is as follows: blue, $V_{1/2} < -10$ mV; yellow, $V_{1/2} > +10$ mV. NE indicates no functional expression and NA indicates that no mutant was made. Values are shown as mean ± SEM. The mutant channels with macroscopic inactivation are marked with '&' (see Results 4.1.2.2)

4.1.2 Voltage-dependent activation properties of KCNQ1 mutant channels

4.1.2.1 Mutants with intact voltage-dependent activation

Voltage dependent properties were determined for each of the expressing mutants using tail current protocols (Fig. 4.2, 4.3). Activation parameters $V_{1/2}$ and z values were analyzed as described in Experimental Procedures. A summary of results is shown in Table 4.3. The activation of 104 out of 106 expressing KCNQ1 mutants was voltage-gated, closing at negative voltages and opening at positive voltages. A large number of mutant channels (53 out of 104) exhibited only a minor change in the voltage-dependent activation, and such a mutant was defined as having a minor impact on gating if $|\Delta V_{1/2}| \leq 10$ mV. Figure 4.2 shows representative current recordings and conductance (G) versus voltage (V) relations for five exemplary mutants, I263W, L266W, F270W, V324W and T327A. Shapes and positions of the G-V relations were very similar to those of wild-type channels. In contrast, the remaining mutants displayed gating behavior with $|\Delta V_{1/2}|>10$ mV, and were scored as having a major impact on gating. Figure 4.3 shows current families and G-V relations for six exemplary mutants that displayed gating perturbation, R259W, E261W, T264W, Y278W, F340A, and L347W. The $V_{1/2}$ was shifted negatively by 30 mV for F340A, while $V_{1/2}$ was shifted positively by 10 to 100 mV for other five mutants. One of the most drastic alterations was observed for E261W, a mutant where the $V_{1/2}$ of the G-V relation was shifted by ~ 100 mV. The gating perturbation mutants are highlighted in Table 4.3. Apparently, most of them (42 out of 51) produced positive shifts in G-V relations compared with wild type KCNQ1 channels. Interestingly, most mutants in the S4-S5 linker (10 out of 13 mutants) and in S5 and S6 (40 out 73 mutants) exhibited gating perturbation, while only one mutant in the P region (1 out of 18) displayed a prominent gating perturbation (Table 4.4)

Table 4.4: Gating perturbation pattern of KCNQ1 pore mutants

	Total	similar	perturbed	perturbed (%)
S4-S5	13	3	10	77%
S5	40	19	21	53%
S6	33	14	19	58%
P turret	15	15	0	0%
P helix and filter	3	2	1	33%
Summary	104	53	51	49%

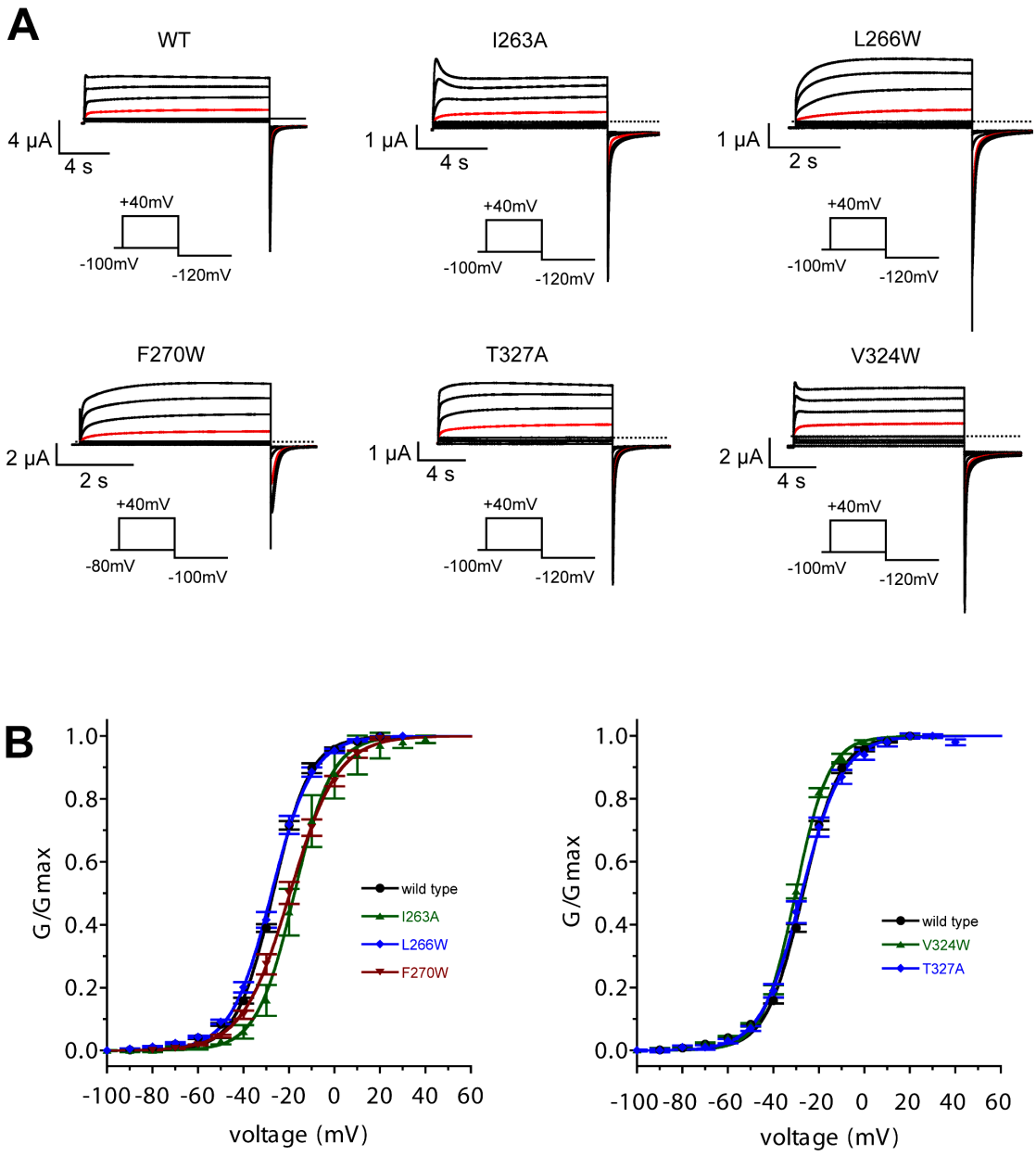

Figure 4.2: Voltage-activation relations for the KCNQ1 mutant channels with gating properties similar to wild-type channel.

(A) Representative current recordings from *Xenopus* oocytes expressing wild-type and five mutant KCNQ1 channels. As indicated below each current recording, holding potential was -100 mV or -80 mV and tail potential was -120 mV or -100 mV. Depolarizations were from holding potential to +40 mV in 20 mV increments. Current traces in red are current responses to voltage steps to -20 mV.

(B) Normalized tail current voltage-activation (G-V) relations for the mutant channels shown above. Smooth curves are single Boltzmann fits to the data with parameters as follows: WT: $V_{1/2}$= -25.3 mV, z=2.95; I263A: $V_{1/2}$= -17.7 mV, z=3.37; L266W: $V_{1/2}$= -27.6 mV, z=2.84; F270W: $V_{1/2}$= -19.5 mV, z=2.43; T327A: $V_{1/2}$= -27.8 mV, z=2.87; V324W: $V_{1/2}$= -30.3 mV, z=3.47.

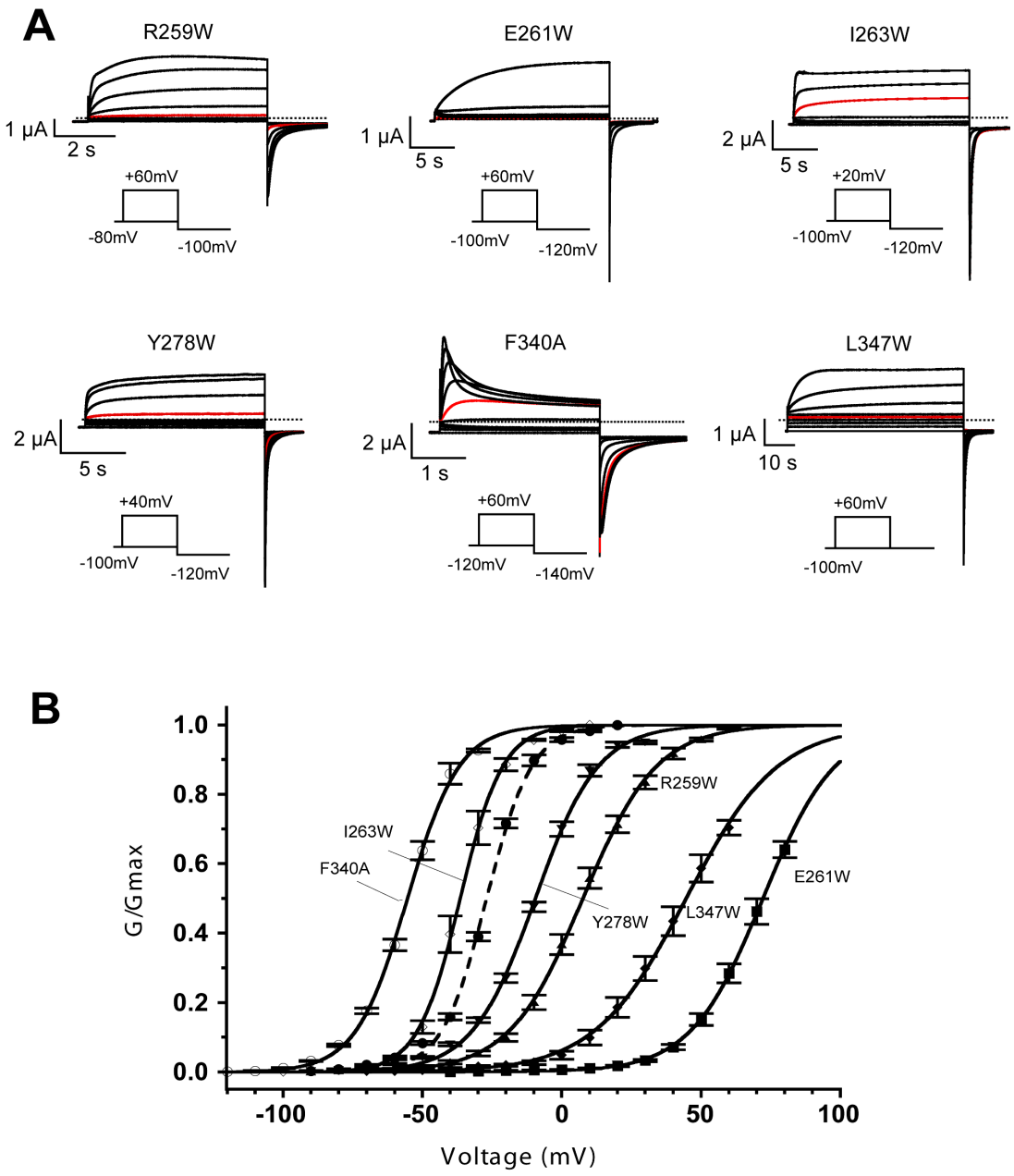

Figure 4.3: Voltage-activation relations for the KCNQ1 mutant channels with altered gating properties.

(A) Representative current recording from *Xenopus* oocytes expressing R259W, E261W, Y278W, L347W, I263W or F340A mutant KCNQ1 channels. As indicated below each current recording, holding potential was -80 or -100, or -120 mV and tail potential was -100 or -120 mV. Depolarizations were from holding potential to the voltage indicated below in 20 mV increments. Current traces in red are current responses to voltage steps to -20 mV.

(B) Normalized tail current voltage-activation (G-V) relations for the mutant channels shown above with wild type as dashed curve. Smooth curves are Boltzmann fits to the data with the following parameters: R259W: $V_{1/2}$=13.7 mV, z=1.82; E261W: $V_{1/2}$=72 mV, z=2.02; Y278W: $V_{1/2}$ = -6.9mV, z=1.65; L347W: $V_{1/2}$ = 46.1mV, z=1.63; I263W: $V_{1/2}$= -38.2mV, z=3.5; F340A: $V_{1/2}$=-56.1 mV, z=2.72.

4.1.2.2 Mutants with macroscopic inactivation

Most mutant channels mediated macroscopic outward currents without any decay like the wild-type channels. However, in a few cases the current displayed a pronounced decay, which increased at more positive test potentials as typical examples are shown in Fig. 4.4A currents mediated by F339A, G269A or V355A mutant channels. This kind of current decay was termed macroscopic inactivation in this study.

As illustrated in Fig. 4.4C, a quantitative assessment of this inactivation was made by comparing at 60 mV the ratio of the peak current during the first 100 ms to the current at the end of a 3-second depolarizing pulse. The ratio represents the extent to which the current decayed upon depolarization. The data showed that the decay increased at more depolarized membrane potentials for F339A, G269A and V355A (Fig. 4.4B).

Nine mutant KCNQ1 channels (T264A, I268A, G269A, V310A, V334W, F339A, F340A, G345A, and V355A) generated prominent macroscopic inactivating currents upon depolarization. The ratio of the peak current to the current at the end of a 3-second pulse stimulation to +60 mV was large than 2 (Fig. 4.4 D).

Interestingly, most of these mutants exhibited gating perturbations. T264A, I268A, G269A, V334W and V345A shifted half-voltage for activation ($V_{1/2}$) to more positive potentials, while F340A and V355A shifted $V_{1/2}$ to more negative potentials (Table 4.3).

4.1.2.3 Mutants with functional inward rectifier currents

G345W and G348W KCNQ1 channels displayed a very distinct gating behavior. Both mutants did not display a typical voltage-dependent activation in the voltage range from -100 mV to +60 mV in ND96 bath solutions (Fig. 4.5A). Instead, functional inward rectifier currents could be recorded in symmetrical K^+ solution from these two mutants (Fig. 4.5B, C). The residues G345 and G348 are positioned near or at the hinge point in opening the channel gate. Mutation of G345 and G348 to large tryptophan resulted in a channel that displayed a large macroscopic conductance at negative membrane voltages where the wild-type channel is normally closed. A constitutively conducting phenotype has been observed in the P475D mutant *Shaker* channel and it was suggested that constitutive activation of the channel resulted from a dramatic perturbation of the closed to open equilibrium (Sukhareva, et al., 2003). A similar mechanism might account for the mutational effect of G345W and G348W KCNQ1 channels.

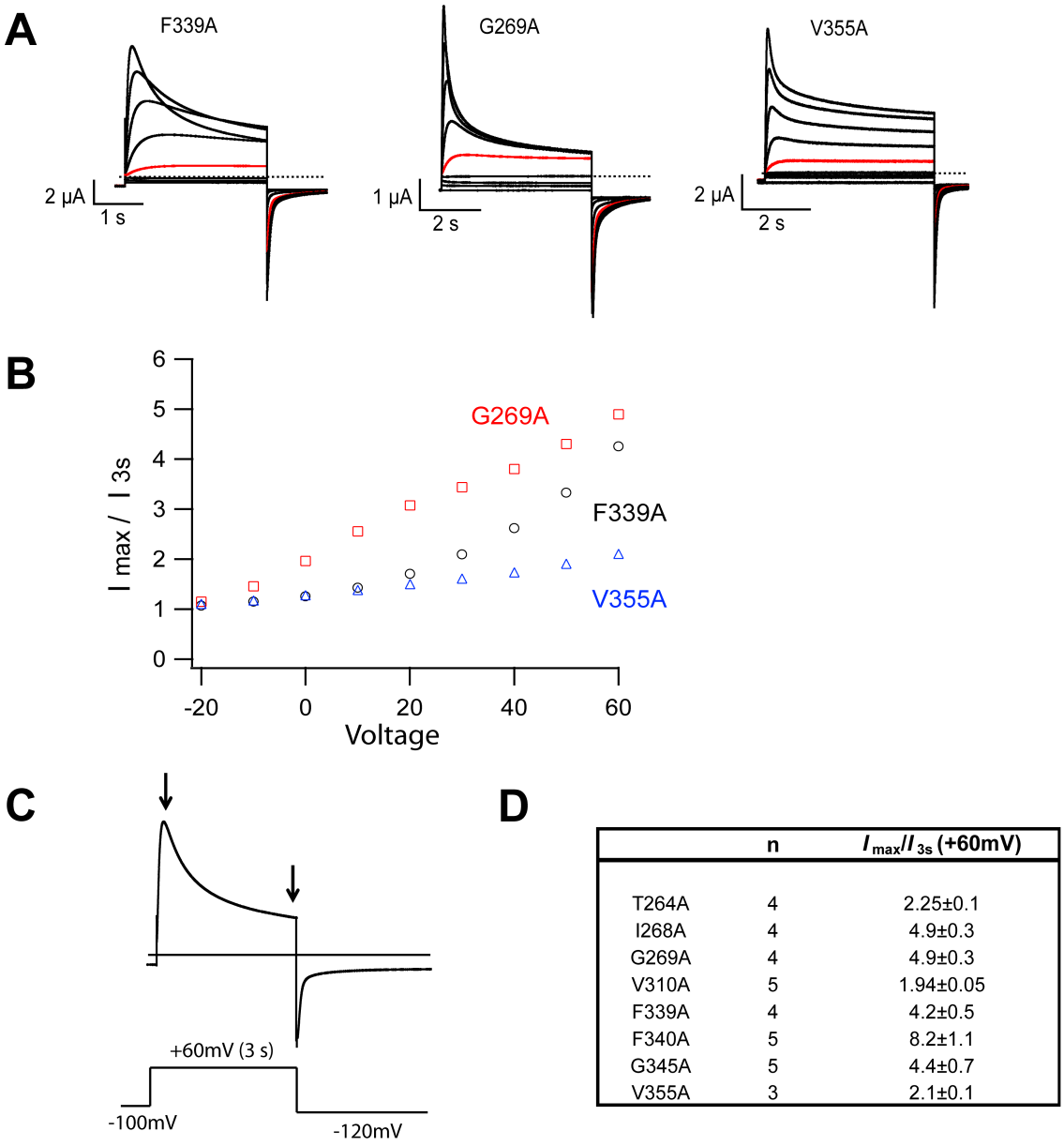

	n	I_{max}/I_{3s} (+60mV)
T264A	4	2.25±0.1
I268A	4	4.9±0.3
G269A	4	4.9±0.3
V310A	5	1.94±0.05
F339A	4	4.2±0.5
F340A	5	8.2±1.1
G345A	5	4.4±0.7
V355A	3	2.1±0.1

Figure 4.4: Macroscopic inactivation of the KCNQ1 mutant channels

(A) Representative current traces recorded for F339A, G269A and V355A mutant channels in 20 mM K^+ bath solution. Currents were evoked by depolarizing voltage steps from -100 mV to +60 mV in 20 mV increments (holding potential, -100 mV; tail potential, -120 mV).

(B) Macroscopic inactivation increased at more positive potentials. The ratio of peak current during the first 100 ms to the current at the end of a 3-second depolarizing pulse (I_{max} / I_{3s}) was calculated at each potential from 3 to 4 recordings for each mutant channel.

(C) Quantitative assessment of macroscopic inactivation for the KCNQ1 mutant channels. Arrows indicate the current amplitudes corresponding to I_{max} and I_{3s}, respectively.

(D) The ratio (I_{max} / I_{3s}) at +60 mV was calculated as indicated in C. n, number of experiments, values are mean ± SEM.

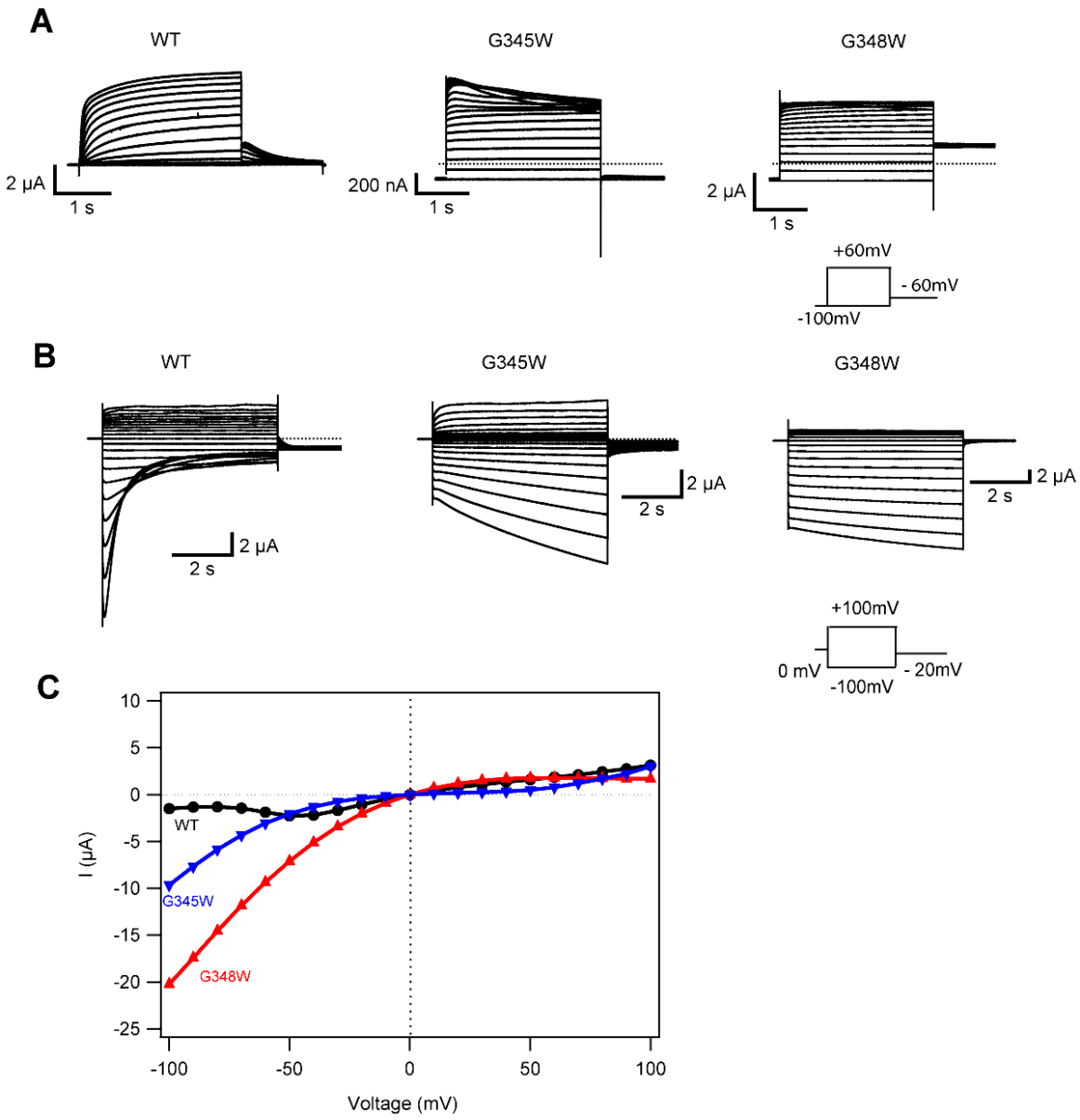

Figure 4.5: Inward rectifying properties of the G345W and G348W KCNQ1 mutant channels

(A) Representative two-electrode voltage clamp current recordings for WT KCNQ1, G345W and G348W mutant channels in ND96 solutions. The currents were evoked by voltage steps ranging from -100 mV to +60 mV in 10 mV increments. Holding potential was -100 mV and tail potential was -60 mV.

(B) Representative two-electrode voltage clamp current recordings for WT KCNQ1, G345W and G348W mutant channels in symmetrical K^+ solutions (140 mM K^+). Currents were evoked by voltage steps ranging from -100 mV to +100 mV in 10 mV increments. Holding potential was 0 mV and tail potential was -20 mV. (C) Current-voltage relationships in symmetrical K^+ solutions for WT KCNQ1, G345W and G348W channels.

4.1.2.4 Comparison of mutational effects on the gate between KCNQ1 and *Shaker* channels

To compare the gating mechanisms of KCNQ1 and *Shaker* channels, mutational effects on the KCNQ1 channel gating were investigated in more detail. A summary of the results was shown in a plot relating $V_{1/2}$ and the slope of the G-V relation (z) (Fig. 4.6 A). Remarkably, KCNQ1 mutants changed mainly $V_{1/2}$, but not z. By contrast, *Shaker* mutants altered $V_{1/2}$ and z, such that z steeply increased when $V_{1/2}$ shifted to more negative potentials. The relationship between $V_{1/2}$ and z for KCNQ1 mutants was however, quite similar to that of mutational effects on gating currents for Shaker mutant channels (Soler-Llavina, et al., 2006) (Fig. 4.6 B). Obviously, the activation gating mechanism of the KCNQ1 channel is quite different from that of the *Shaker* K^+ channel.
To see why this is so, consider first the gating model developed for the *Shaker* K^+ channel (Zagotta et al., 1994): four subunits undergo independently closed to opened transitions, once all subunits have reached a 'permissive' state, the pore opens in a concerted transition. For m transitions with four independent subunits, followed by a concerted pore opening, the following scheme may apply.

$$(C_1 \overset{K_1(V)}{\longleftrightarrow} C_2 \overset{K_2(V)}{\longleftrightarrow} C_3$$
$$\ldots\ldots \overset{K_m(V)}{\longleftrightarrow} C_{m+1})^4 \overset{L}{\longleftrightarrow} O$$

Previous studies revealed that *Shaker* mutants change $V_{1/2}$ and z cooperatively, such that a negative shift of $V_{1/2}$ is accompanied with an increased z, a positive shift of $V_{1/2}$ with a decreased z. It is believed that *Shaker* pore mutants mainly influence the late cooperative transition in the opening process (Yifrach and MacKinnon, 2002). It is not the case for KCNQ1 channel. One possibility is that KCNQ1 mutations might influence 'early' voltage-dependent transition step of each subunits, and the last concerted transition process is not affected. Accordingly, changes in $V_{1/2}$ were not correlated with changes in z as observed in *Shaker*. Alternatively, the KCNQ1 channel might have a different gating mechanism.

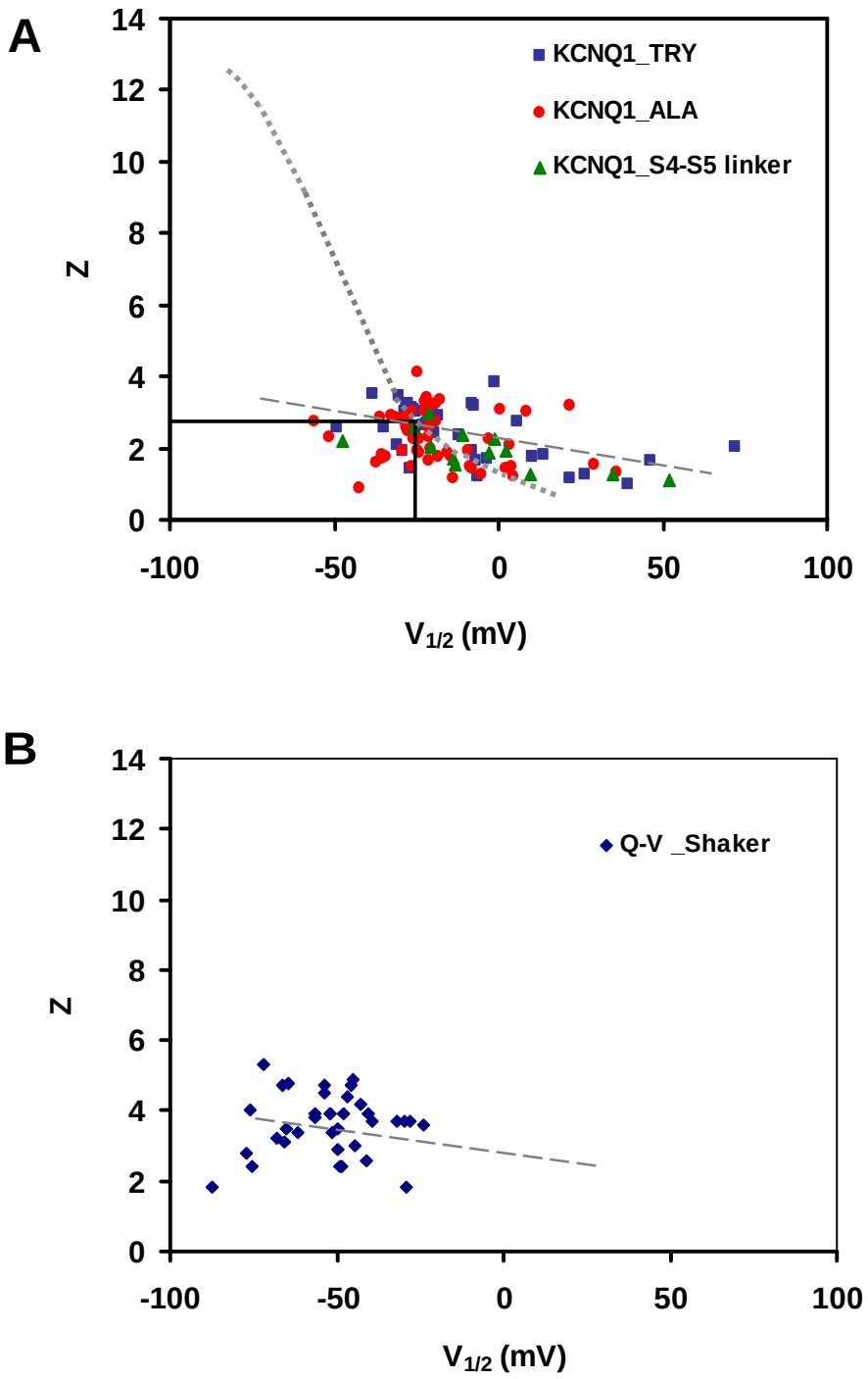

Figure 4.6: Effects of KCNQ1 pore mutations on $V_{1/2}$ and z gating parameters (Table 4.3)
(A) Plot of $V_{1/2}$ and z for KCNQ1 pore mutants. The relationship between $V_{1/2}$ and z for KCNQ1 pore mutants was linearly correlated. The smooth dotted curve represents the correlation of $V_{1/2}$ and z for *Shaker* pore alanine mutants (adopted from the paper by Yifrach and MacKinnon, 2000). (B) Plot of $V_{1/2}$ and z from Q-V relations of Shaker tryptophan pore mutants (data from Solar-Llavina, et al., 2006). Linear correlation of $V_{1/2}$ and z from G-V relations of KCNQ1 pore mutants is shown as a dashed line.

To understand how different the gating sensitive residues are distributed between *Shaker* and KCNQ1, gating perturbation sites were compared specifically between *Shaker* and KCNQ1 channels (data of *Shaker* mutants from Li-Smerin et al., 2000, Hackos et al., 2002, and Yifrach, et al., 2002). According to the sequence alignment given in Figure 4.1, the corresponding residues at S5 and S6 were identified in *Shaker* and KCNQ1. As illustrated in Table 4.6, because of the differences in expression and two-phase of G-V relations of certain *Shaker* mutants, not all positions could be compared. There were 26 mutations which exhibited a gating perturbation ($|\Delta V_{1/2}|$>10mV) in *Shaker*, and 20 mutations in the corresponding positions of KCNQ1. Though the pattern for the gating sensitive residues showed some similarity, mutational effects appeared different in key positions between *Shaker* and KCNQ1. As shown in Table 4.5, gating-sensitive mutations in S5 tended to shift $V_{1/2}$ in the same direction as for *Shaker*, and most of them shifted positively, but those in S6 tended to produce a shift in $V_{1/2}$ in the opposite direction, with a positive shift in KCNQ1 and a negative shift in *Shaker*. This finding implicated a different gating mechanism for the KCNQ1 channel in comparison to *Shaker* channel. A mutation with a positive shift in $V_{1/2}$ may favor the closed state of the channel, whereas the mutation with a negative shift in $V_{1/2}$ may favor the open state. The observation that $V_{1/2}$ of G-V relations were shifted in the opposite direction by S6 mutations was striking. It is suggested that amino acid residues in the S6 helix of KCNQ1 channel might differently be packed in comparison to those of *Shaker* channel.

Table 4.5: Comparison of gating perturbations between *Shaker* and KCNQ1 mutants

$\Delta V_{1/2}$ for Shaker / $\Delta V_{1/2}$ for KCNQ1			
positive / positive	**negative / negative**	**positive / negative**	**negative/ positive**
M393A / R259A	G397W / I263W	V408A (W) / I274A(W)	M393W / R259W
R394W / Q260W		L409A / F275A	A465V / F335A
E395W / E261W		L472A / L342A	I477A(W) / L347A(W)
L398W / T264W			N482W / A352W
I405W / L271W			Y485W / V355W
L409A / F275W			
S412W / Y278W			

As shown in Table 4.6, here listed the mutations in corresponding *Shaker* and KCNQ1 residues, which gave rise to gating perturbation ($|\Delta V_{1/2}| > 10$ mV). Pairs are grouped according to the direction to which the half-voltage for activation was shifted by the mutation. Here, 'positive' means positive shift in $V_{1/2}$ with $\Delta V_{1/2} > +10$ mV and 'negative' means negative shift in $V_{1/2}$ with $\Delta V_{1/2} < -10$ mV. Mutations in S5 are colored in yellow and mutations in S6 are colored in blue.

Table 4.6: Comparison of the mutational effects on gating between *Shaker* and KCNQ1 channels

	Shaker	$V_{1/2}$ (mV)	$\Delta V_{1/2}$(mV)	KCNQ1	$V_{1/2}$(mV)	$\Delta V_{1/2}$(mV)	Shaker	$V_{1/2}$ (mV)	$\Delta V_{1/2}$(mV)	KCNQ1	$V_{1/2}$(mV)	$\Delta V_{1/2}$(mV)
	wild type	-26.5		wild type	-25.3		wild type	-30.5		wild type	-25.3	
	M393A	-6.4	20.1	R259A	28.9	54.2	M393W	-43.9	-13.4	R259W	13.7	39
	R394A	-18.7	7.8	Q260A	-14.2	11.1	R394W	-7.2	23.3	Q260W	10.1	35.4
	E395A	-60.2	-33.7	E261A	-27.6	-2.3	E395W	180.4	210.9	E261W	72	97.3
	L396A			L262A	-18.4	6.9	L396W			L262W		
	G397A	-25.7	0.8	I263A	-17.7	7.6	G397W	-45.3	-14.8	I263W	-38.2	-12.9
	L398A			&T264A	-5	20.3	L398W	21.1	51.6	T264W	21.7	47
	L399A			T265A	-29.2	-3.9	L399W			T265W	-26.1	-0.8
	I400A	-29.1	-2.6	L266A	-20.9	4.4	I400W			L266W	-27.6	-2.3
S5	F401A	two-phase IV	80	Y267A	-13.5	11.8	F401W			Y267W	-8	17.3
	F402A	two-phase IV	80	&I268A	2.3	27.6	F402W			I268W	-29.2	-3.9
	L403A	-20	6.5	&G269A	-15.2	10.1	L403W			G269W		
	F404A	-24.6	1.9	F270A	-27	-1.7	F404A	-35.5	-5	F270W	-19.5	5.8
	I405A	-23	3.5	L271A	-7.9	17.4	I405W	24.9	55.4	L271W	-12.2	13.1
	G406A	-15.6	10.9	G272A	-26.4	-1.1	G406W	-22.3	8.2	G272W	-18.3	7
	V407A	-30.9	-4.4	L273A			V407W			L273W	-21.5	3.8
	V408A	-16.8	9.7	I274A	-35.8	-10.5	V408W	2.1	32.6	I274W	-49.2	-23.9
	L409A	-13.5	13	F275A	-35.4	-10.1	L409W	1.7	32.2	F275W	-1.1	24.2
	F410A	-28.4	-1.9	S276A	-18.8	6.5	F410A			S276W		
	S411A	-25.5	1	S277A	-28.2	-2.9	S411W			S277W		
	S412A	-24.8	1.7	Y278A	8.5	33.8	S412W	25.5	56	Y278W	-6.9	18.4
	A413V	-25.5	1	F279A	-32.3	-7	A413W	-18.1	12.4	F279W	-21.6	3.7
	V414A	-22.5	4	V280A			V414W			V280W		
	Y415A			Y281A			Y415W			Y281W	-24.6	0.7
	F416A	-30.9	-4.4	L282A	-20.9	4.4	F416W			L282W	-8.2	17.1
	A417V	-27.4	-0.9	A283W			A417			A283W		
	V453A	-24.4	2.1	W323A	-18.7	6.6	V453W	-34.2	-3.7	W323		
	W454A	-28.2	-1.7	V324A	-27.5	-2.2	W454A	-24.1	6.4	V324W	-30.3	-5
	G455A	-25.4	1.1	G325A			G455W			G325W		
	K456A			K326A			K456W			K326W		
	I457A	-20	6.5	T327A	-27.8	-2.5	I457W	-13.8	16.7	T327W	-25.3	0
	V458A	-47.2	-20.7	I328A			V458W	-6.7	23.8	I328W		
	G459A	-40.8	-14.3	A329			G459W			A329W		
	S460A	-36.9	-10.4	S330A	-29	-3.7	S460W	94.9	125.4	S330W		
	L461A	-35	-8.5	C331A	-31.5	-6.2	L461W	-32.2	-1.7	C331W		
S6	C462A	-26	0.5	F332A	0.6	25.9	C462			F332W		
	A463V	-27.4	-0.9	S333A	-21.9	3.4	A463			&S333W		
	I464A	-29	-2.5	V334A			I464			V334W	-3.7	21.6
	A465V	-46.3	-19.8	F335A	4.8	30.1	A465W	-59.3	-28.8	F335W		
	G466A			A336			G466W			A336W	-26.9	-1.6
	V467A	-34.4	-7.9	I337A	-20.7	4.6	V467W			I337W		
	L468A	-8.3	18.2	S338A	3.8	29.1	L468W	-47.6	-17.1	S338W	-24.9	0.4
	T469A	-46	-19.5	&F339A	-23.9	1.4	T469W	-36.7	-6.2	F339W		
	I470A	-28	-1.5	&F340A	-56.1	-30.8	I470W	-47.1	-16.6	F340W		
	A471V			A341			A471W			A341W		
	L472A	-13.9	12.6	L342A	-51.6	-26.3	L472W	50.4	80.9	L342W		
	P473A			P343A			P473W			P343W		
	V474A	two-phase IV		A344			V474W			A344W		
	P475A			&G345A	-8.3	17	P475W			G345W		
	V476A	-62	-35.5	I346A			V476W			I346W	15.1	40.4
	I477A	-55.7	-29.2	L347A	36	61.3	I477W	-60.4	-29.9	L347W	46.1	71.4
	V478A	two-phase IV		G348A	-27.9	-2.6	V478W			G348W		
	S479A	-24.8	1.7	S349A	-2.8	22.5	S479W			S349W		
	N480A	NE		G350A	-4.5	20.8	N480W	5.3	35.8	G350W		
	F481A	NE		F351A	21.8	47.1	F481W	-43.7	-13.2	F351W		
	N482A	-36	-9.5	A352			N482W	-47.8	-17.3	A352W	39.5	64.8
	Y483A	two-phase IV		L353A	-42.5	-17.2	Y483W	-31.1	-0.6	L353W	-27.8	-2.5
	F484A	two-phase IV		K354A	-8.9	16.4	F484W	-39	-8.5	K354W	-6.1	19.2
	Y485A	-23	3.5	&V355A	-35.5	-10.2	Y485W	-43.9	-13.4	V355W	26.5	51.8

Data of *Shaker* mutants are from Li-Smerin et al., 2000, Hackos et al., 2002, and Yifrach, et al., 2002). $\Delta V_{1/2} = V_{1/2}^{mut} - V_{1/2}^{WT}$. The corresponding mutants which displayed gating perturbation ($|\Delta V_{1/2}| > 10$ mV) both in *Shaker* and KCNQ1 are colored yellow, and the mutants which showed difference in gating perturbation are colored blue.

4.1.3 Deactivation kinetics of KCNQ1 mutant channels

Previous *Shaker* channel studies (Kanevsky and Aldrich, 1999) indicated that Shaker mutants which altered the transition from the closed state to the open state (C–O) may result from changes in the deactivation rate. To address whether this is also the case for KCNQ1 mutants, I examined the deactivation kinetics for each mutant. Deactivation kinetics were obtained from analysis of the tail currents recorded at -120 mV after a potential step to +40 mV in 100 mM external K^+ solution (shown in Fig. 4.6A). Deactivation time courses were well described with two time constants τ_{fast} and τ_{slow}. Table 4.7 summarizes the deactivation kinetics for each KCNQ1 mutant. Generally, the fast component represented more than 70% of deactivation except for T264W, L342A, I346W and V355W. To investigate whether the mutants change the deactivation, the fast time constants for deactivation (τ_{fast}) of the mutants were compared to the one of the wild type KCNQ1 channel. τ_{fast} was determined as 105±4 ms (n=27) for the wild type KCNQ1 channel. τ_{fast} values within the range of 105±36 ms (mean ± 2 × SD) were regarded as no significant change in deactivation. Mutants with τ_{fast}>141 ms or τ_{fast}<69 ms were considered as having significant changes in deactivation.

Shaker displayed a $V_{1/2}$ shifted to more positive potential had increased the deactivation rate. Vise versa, mutations which shifted $V_{1/2}$ to more negative potential slowed the deactivation rate. These mutants may influence the C–O transition by mainly increasing or decreasing the closing rates, affecting the final concerted opening transition. In KCNQ1, 51 mutants displayed gating perturbation, with 9 mutants producing pronounced negative shifts of $V_{1/2}$ and 42 mutants leading to positive shifts of $V_{1/2}$. Most of the mutants, which produced a negative shift in $V_{1/2}$ for voltage-dependent activation, slowed the deactivation rates (8 out of 9 mutants); while about 40% of the mutants which produced positive shifts of $V_{1/2}$ increased the deactivation rates (17 out 42 mutants). Similar to the gating behavior observed in *Shaker* mutants, these KCNQ1 mutants may also affect the final concerted opening step. However, previous analysis suggested that KCNQ1 mutations may not influence the final concerted opening step in that they altered the gate by shifting $V_{1/2}$ with a small change in z. The results from deactivation kinetics appear to contradict the hypothesis. In conclusion, the gating model proposed for *Shaker* seems not applicable to KCNQ1.

Table 4.7: Deactivation kinetics for the KCNQ1 mutant channels

		Deactivation					Activation		Deactivation					Activation
	KCNQ1	n	τ_{fast} ms	τ_{slow} ms	fast%	leak%	$\Delta V_{1/2}$ mV	KCNQ1	n	τ_{fast} ms	τ_{slow} ms	fast%	leak%	$\Delta V_{1/2}$ mV
	wild type	27	105±4	711±40	90±1	7±1		G245W	4	226±27		100	10±4	4±1.5
								G246W	5	373±37		100	17±10	-22±1.2
								T247W	5	46±2	249±12	87±1	8±2	24.3±1.1
								W248A	5	51±8	266±72	86±2	10±2	22.6±2.2
S4-S5								R249W	4	113±20	556±144	73±4	19±4	11.8±1.1
linker								L250W	8	32±1		100	9±3	60±0.9
								L251W	5	47±14		100	19±4	77.1±1.7
								G252W**	5	55±2	202±28	87±2	10±1	-0.2±0.9
								S253W	4	166±16	599±122	72±7	16±4	12.4±1.5
								V254W						
								V255W	4	102±6	502±26	80±2	12±2	27.7±1.3
								F256A	4	55±13	404±137	90±3	4±2	14.4±1.1
								I257W	5	108±10	584±38	86±2	7±2	4.9±0.6
								H258W**	4	527±30		100	26±4	60.6±3.6
	R259A	7	61±2	507±37	85±1	17±3	54.2±1.6	R259W	9	70±4	393±14	92±1	6±1	39±1.0
	Q260A	4	90±4	469±56	88±1	12±1	11.1±1.0	Q260W	5	61±2		100	5±1	35.4±0.9
	E261A	5	80±4	460±40	81±1	20±3	-2.3±0.9	E261W	3	30±3	182±25	81±1	6±0.1	97.3±1.9
	L262A	4	173±22	840±70	75±2	16±1	6.9±2.1	L262W						
	I263A	5	123±7	720±53	88±1	8±1	7.6±0.9	I263W	4	214±7		100	6.2±0.3	-12.9±0.8
	&T264A**	5	61±7	442±46	62±4	33±2	20.3±1.1	T264W	4	100±6	570±22	64±1	7±1	47±2.1
	T265A	4	144±6	702±12	76±2	21±2	-3.9±0.6	T265W	4	243±9		100	6±2	-0.8±0.6
	L266A	4	117±8	657±79	82±3	8±2	4.4±0.6	L266W	4	144±9		100	8±1	-2.3±1.1
	Y267A	4	80±4		100	22±1	11.8±0.9	Y267W	5	176±13		100	13±1	17.3±0.9
S5	&I268A	5	69±2	373±20	78±1	23±1	27.6±1.2	I268W	7	120±3	714±24	80±1	14±1	-3.9±0.9
	&G269A**	6	92±1	1014±44	86±1	8±1	10.1±1.3	G269W						
	F270A	4	126±8		100	13±2	-1.7±0.6	F270W	4	121±7		100	7±1	5.8±1.5
	L271A	6	172±7	728±28	73±2	12±2	17.4±1.0	L271W	5	185±14		100	10±1	13.1
	G272A	3	92±5	485±23	83±1	7±1	-1.1±0.8	G272W	4	76±2	397±11	81±1	9±1	7±0.6
	L273A							L273W	7	126±3		100	10±1	3.8±1.3
	I274A	5	196±12		100	6±1	-10.5±1.3	I274W	5	342±21		100	21±1	-23.9±0.8
	F275A	5	201±3		100	18±1	-10.1±0.9	F275W	4	104±3		100	13±1	24.2±0.9
	S276A	5	100±9	630±138	93±13	8±2	6.5±2.2	S276W						
	S277A	3	69±5	450±29	92±2	5±1	-2.9±0.6	S277W						
	Y278A	6	140±6		100	16±1	33.8±1.0	Y278W	5	107±7	637±31	88±1	6±1	18.4±0.8
	F279A	4	188±4		100	10±1	-7.0±1.0	F279W	5	70±2	450±20	83±2	10±1	3.7±0.9
	V280A							V280W						
	Y281A							Y281W	6	120±7		100	5±1	0.7±1.2
	L282A**	4	165±7	820±19	70±1	18±2	4.4±0.9	L282W	4	53±3		100	7±1	17.1±1.7
	A283							A283W						
	E284A							E284W						
	K285A	8	238±10		100	20±3	-8.8±1.8	K285W	3	102±7	652±17	84±2	20±1	-6.7±1.7
	D286A							D286W						
	A287							A287W	4	110±4		100	6±1	5.1±1.3
	V288A	5	76±1	480±24	88±1	11±1	1.4±2.6	V288W						
	N289A	5	110±9	500±80	81±3	18±4	1±0.8	N289W						
P region	E290A	5	80±9	460±40	89±2	10±3	3.1±1.5	E290W						
	S291A	3	80±6	490±46	92±2	5±1	1±1.5	S291W	5	135±23		100	9±2	-2.2±0.5
(Turret)	G292A							G292W						
	R293A	6	101±5		100	10±4	4.2±0.9	R293W						
	V294A	5	100±4	630±63	88±1	10±3	-0.5±0.9	V294W**	4	148±6	737±25	78±1	17±2	-5.6±1.5
	E295A	6	107±8	530±23	86±3	9±3	3.9±1.0	E295W						
	F296A							F296W						
	G297A	5	110±9	740±4	96±2	9±2	5±3.4	G297W	4	162±6		100	7±1	-3.1±1.5
	S298A							S298W	5	114±5		100	8±1	-0.5±0.6

	KCNQ1	n	τ_{fast} ms	τ_{slow} ms	fast%	leak%	$\Delta V_{1/2}$ mV	KCNQ1	n	τ_{fast} ms	τ_{slow} ms	fast%	leak%	$\Delta V_{1/2}$ mV
	Y299A							Y299W						
	A300							A300W	8	69±3		100	6±1	17.8±0.7
	D301A							D301W						
P region	A302							A302W						
	L303A							L303W						
(pore helix)	W304A							W304						
	W305A							W305						
	G306A							G306W						
	V307A							V307W						
	V308A							V308W						
	T309A							T309W						
	&V310A	9	91±6	566±37	90±1	9±1	-9.6±2.0	V310W						
	T311A							T311W						
	T312A							T312W						
	I313A							I313W						
P region	G314A							G314W						
	Y315A							Y315W						
(Selectivity	G316A							G316W						
filter)	D317A							D317W						
	K318A							K318W						
	V319A							V319W						
	P320A							P320W						
	Q321A	4	49±3	346±9	93±1	4±1	3±0.9	Q321W						
	T322A							T322W						
	W323A	4	77±2		100	6±1	6.6±1.2	W323						
	V324A	5	88±1	470±30	87±1	13±1	-2.2±1.9	V324W	4	94±4		100	8±1	-5±0.8
	G325A							G325W						
	K326A							K326W						
	T327A	4	145±6		100	9±1	-2.5±0.7	T327W	4	75±6	382±21	87±1	3±1	0±0.6
	I328A							I328W						
	A329							A329W						
	S330A	4	63±2	468±38	91±1	9±1	-3.7±0.8	S330W						
	C331A	5	95±2	559±40	84±1	12±1	-6.2±0.9	C331W						
	F332A**	5	60±2	382±10	90±1	8±1	25.9±1.0	F332W						
	S333A	6	134±6	724±13	82±2	11±1	3.4±0.9	S333W						
S6	V334A							&V334W	4	49±3	284±19	87±1	8±2	21.6±0.9
	F335A	6	119±6	730±53	79±2	16±1	30.1±1.1	F335W						
	A336							A336W	4	317±7		100	22±1	-1.6±1.1
	I337A	3	75±3	496±45	89±1	5±1	4.6±0.5	I337W						
	S338A	5	133±5	678±46	83±1	9±1	29.1±1.6	S338W	6	154±14	1032±45	72±2	20±1	0.40±1.4
	&F339A**	4	96±4	897±22	88±1	7±1	1.4±1.5	F339W						
	&F340A	6	177±11	903±64	70±2	12±2	-30.8±0.8	F340W						
	A341							A341W						
	L342A	5	155±16	492±44	56±5	29±1	-26.3±0.9	L342W						
	P343A							P343W						
	A344							A344W						
	&G345A**	5	105±3	514±33	83±1	18±1	17±1.5	G345W		KIR				
	I346A							I346W**	7	145±8	659±28	47±2	56±1	40.4±2.4
	L347A	6	54±3	450±48	74±2	27±4	61.3±4.9	L347W**	13	75±2	505±20	81±1	16±1	71.4±1.2
	G348A	7	549±44		100	24±1	-2.6±1.1	G348W		KIR				
	S349A**	6	60±1	268±10	90±1	9±1	22.5±1.1	S349W						
	G350A**	6	60±3	237±25	81±1	15±1	20.8±1.0	G350W						
	F351A	5	39±1		100	11±1	47.1±0.8	F351W						
	A352							A352W**	4	218±7		100	14±2	64.8±3.5
	L353A	4	140±2	856±5	75±2	27±1	-17.2±2.2	L353W	4	112±10	621±31	81±2	10±1	-2.5±0.8
	K354A	4	69±2	491±36	87±1	5±1	16.4±0.9	K354W	4	162±7	1380±6	80±1	18±1	19.2±0.6
	&V355A	5	63±1	373±37	88±1	16±2	-10.2±3.0	V355W	5	35±2	164±5	60±2	14±1	51.8±1.3

Deactivation kinetics were normally examined at -120mV after a depolarization to +40 mV. The mutants marked with ** were recorded at -100mV because the leak current increased when these mutants were recorded at -120mV. The $\Delta V_{1/2}$ for voltage-dependent activation (yellow, $\Delta V_{1/2}$ >10 mV; blue, $\Delta V_{1/2}$ < -10 mV) and fast time constant for deactivation kinetics (yellow, fast; blue, slow) were shown as reference.

4.1.4 G_{Rb}/G_K and inactivation properties of KCNQ1 mutant channels

Almost all KCNQ1 mutants which expressed recordable currents displayed voltage-dependent activation. This might indicate that most current expressing mutants produced local rather than global structural changes in the pore (Li-Smerin, 2000). Indeed, the KCNQ1 channel possesses some unique gating properties, which permitted to investigate this further.

Firstly, the KCNQ1 channel exhibits an unusually high relative Rb^+ conductance (G_{Rb}/G_K~ 2.1), while other Kv channels display a $G_{Rb}/G_K \leq 1.0$ (Hille, 2001; Pusch, et al., 2000). Secondly, the KCNQ1 channel undergoes slow onset and voltage independent inactivation. Inactivation of KCNQ1 channels is not obvious from the currents elicited by membrane depolarization, but it is apparent as a 'hook' in tail currents upon repolarization, representing recovery of channels from inactivation. The distinctive conduction and inactivation properties of the KCNQ1 channel are rather fortunate for the mutational investigation because changes in G_{Rb}/G_K and the extent of inactivation represent sensitive indicators for structural changes in the KCNQ1 pore domain impinged by a particular mutation. I examined G_{Rb}/G_K and the extent of inactivation for each mutant KCNQ1 channel by using the protocol described by Seebohm et al. (2003). Briefly, inward Rb^+ or K^+ currents were measured at -120 mV after depolarization to +40 mV for 3 seconds. Oocytes were bath-perfused first with 100 mM Rb^+ followed by 100 mM K^+. Representative current recordings at 100 mM Rb^+ and 100 mM K^+ solutions were shown in Fig. 4.7A.

Consistent with previous data (Seebohm et al., 2003), G_{Rb}/G_K and the degree of inactivation (F_{Inact}) were 2.1±0.03 and 57±1.0% (n = 42) respectively for the wild-type KCNQ1 channel. If the mean value of G_{Rb}/G_K or F_{Inact} for a mutant was within two standard deviations of the mean value for wild-type, the mutant was not considered as having a significantly change in G_{Rb}/G_K or F_{Inact}. About one third of the mutant channels (32 out of 104) generated currents with G_{Rb}/G_K and F_{Inact} properties similar to that of wild type, and the remaining with decreased or increased G_{Rb}/G_k and/or F_{inact} (Fig. 4.7B, Table 4.8).

The pore mutations resulting in functionally expressing channels might affect relative Rb^+ conductance G_{Rb}/G_K and/or the extent of inactivation. A previous study suggested that G_{Rb}/G_K and extent of inactivation are properties of the KCNQ1 channels which are correlated with each other (Seebohm et al., 2003). This proposition was tested by

plotting the degree of inactivation versus the respective G_{Rb}/G_K for wild-type and mutant KCNQ1 channels (Table 4.8 and Fig. 4.7 B). Using Pearson's formula, a correlation coefficient of r = 0.25 was obtained from the KCNQ1 data from this study, demonstrating that G_{Rb}/G_K and the degree of inactivation are uncorrelated and independent parameters. This was an important observation because it permitted me to distinguish at an intuitive level between local and global mutational effects on the KCNQ1 channel pore structure.

Accordingly, changes in both G_{Rb}/G_K and the degree of inactivation indicated a more global effect of a respective mutation, whereas changes in either G_{Rb}/G_K or the degree of inactivation possibly indicate only a local effect of the mutation in the KCNQ1 channel pore structure. Theoretically, a mutation may have no effect or lead to an increase or decrease in G_{Rb}/G_K and (or) the degree of inactivation, or eliminate inactivation. Thus, according to the mutational effects on G_{Rb}/G_K and the degree of inactivation, the mutations were grouped into twelve different categories (I-XII) as illustrated by the grid in Fig. 4.7B. Mutant Kv7.1 channels, which neither displayed largely altered G_{Rb}/G_K nor the degree of inactivation were classified as equivalent to wild-type (category VI). Mutations, which either decreased or increased only G_{Rb}/G_K or the degree of inactivation, were classified as potentially inducing local changes in KCNQ1 channel structure (categories II, V, VI, VII, VIII, and X). Mutations in category I, III, IV, IX, XI, and XII, which produced changes in both G_{Rb}/G_K and the extent of inactivation, probably elicited a more global change in KCNQ1 channel structure. Mutations in each category are listed in Fig. 4.7C respectively.

In addition, some KCNQ1 mutant channels displayed macroscopic inactivation upon depolarization. They also produced a significant change in G_{Rb}/G_K and/or the degree of inactivation. Due to impairment in the activation kinetics by these mutations, they were thought to give rise to a global disruption of pore structure.

Table 4.8: Relative Rb^+ conductance (G_{Rb}/G_K) and inactivation fraction of KCNQ1 pore mutants

		n	G_{Rb}/G_K	Inac%	$\Delta V_{1/2}$(mV)	Deact(ms)		n	G_{Rb}/G_K	Inac%	$\Delta V_{1/2}$(mV)	Deact(ms)
	wild type	**27**	**2.1±0.03**	**57±1**			**G245W**	4	1.90±0.07	56±1	4±1.5	226±27
							G246W	5	2.00±0.04	29±2	-22±1.2	373±37
							T247W	5	2.13±0.06	92±2	24.3±1.1	46±2
							W248A	5	2.09±0.02	90±2	22.6±2.2	51±8
S4-S5							**R249W**	4	2.07±0.05	61±3	11.8±1.1	113±20
linker							**L250W**	8	2.18±0.05	0	60±0.9	32±1
							L251W	5	3.52±0.20	0	77.1±1.7	47±14
							G252W	5	1.90±0.04	26±1	-0.2±0.9	55±2
							S253W	4	2.21±0.06	50.5±0.2	12.4±1.5	166±16
							V254W					
							V255W	4	2.78±0.06	56±1	27.7±1.3	102±6
							F256A	4	2.34±0.16	66±2	14.4±1.1	55±13
							I257W	5	2.28±0.08	43±2	4.9±0.6	108±10
							H258W	4	2.11±0.05	34 ±3	60.6±3.6	527±30
	R259A	7	1.77 ± 0.05	58 ± 2	54.2±1.6	61±2	**R259W**	9	1.78±0.02	63±2	39±1.0	70±4
	Q260A	4	1.98 ± 0.05	55 ± 1	11.1±1.0	90±4	**Q260W**	5	2.08±0.05	63±1	35.4±0.9	61±2
	E261A	5	0.60 ± 0.03	0	-2.3±0.9	80±4	**E261W**	3	0.87±0.05	0	97.3±1.9	30±3
	L262A	4	1.60 ± 0.04	41 ± 4	6.9±2.1	173±22	**L262W**					
	I263A	5	2.37 ± 0.06	62 ± 2	7.6±0.9	123±7	**I263W**	4	1.95±0.05	44±1	-12.9±0.8	214±7
	&T264A	6	2.12 ± 0.09	0	20.3±1.1	61±7	**T264W**	4	1.03±0.04	0	47±2.1	100±6
	T265A	4	2.24 ± 0.11	19 ± 3	-3.9±0.6	144±6	**T265W**	4	1.74±0.02	6±2	-0.8±0.6	243±9
	L266A	4	1.85 ± 0.06	49 ± 2	4.4±0.6	117±8	**L266W**	4	1.44±0.04	9±1	-2.3±1.1	144±9
	Y267A	4	1.48 ± 0.04	0	11.8±0.9	80±4	**Y267W**	5	1.88±0.05	65 ±3	17.3±0.9	176±13
S5	**&I268A**	5	1.41 ± 0.04	93 ± 4	27.6±1.2	69±2	**I268W**	7	0.94±0.01	17±1	-3.9±0.9	120±3
	&G269A	6	1.13 ± 0.04	85 ± 2	10.1±1.3	92±1	**G269W**					
	F270A	4	1.53 ± 0.05	32 ± 1	-1.7±0.6	126±8	**F270W**	4	1.76±0.06	40.0±3.0	5.8±1.5	121±7
	L271A	6	1.82 ± 0.05	43 ± 2	17.4±1.0	172±7	**L271W**	5	1.99±0.07	1.7±0.7	13.1	185±14
	G272A	3	2.11 ± 0.05	34 ± 3	-1.1±0.8	92±5	**G272W**	4	1.12±0.02	44.5±0.8	7±0.6	76±2
	L273A						**L273W**	7	3.14±0.09	60±2	3.8±1.3	126±3
	I274A	5	1.37 ± 0.03	67 ± 3	-10.5±1.3	196±12	**I274W**	5	2.47±0.08	3±2	-23.9±0.8	342±21
	F275A	5	2.00 ± 0.05	29 ± 1	-10.1±0.9	201±3	**F275W**	4	2.21±0.06	78±1	24.2±0.9	104±3
	S276A	5	2.10 ± 0.04	34 ± 2	6.5±2.2	100±9	**S276W**					
	S277A	3	2.02 ± 0.04	58 ± 1	-2.9±0.6	69±5	**S277W**					
	Y278A	6	1.90 ± 0.04	100±2	33.8±1.0	140±6	**Y278W**	5	1.80±0.11	55±3	18.4±0.8	107±7
	F279A	4	2.14 ± 0.07	6 ± 2	-7.0±1.0	188±4	**F279W**	5	1.85±0.06	49±2	3.7±0.9	70±2
	V280A						**V280W**					
	Y281A						**Y281W**	6	2.17±0.06	69±2	0.7±1.2	120±7
	L282A	4	2.34 ± 0.04	55 ± 2	4.4±0.9	165±7	**L282W**	4	2.09±0.06	62±2	17.1±1.7	53±3
	A283						**A283W**					
	E284A						**E284W**					
	K285A	8	2.36 ± 0.13	40 ± 1	-8.8±1.8	238±10	**K285W**	3	2.71±0.12	41±4	-6.7±1.7	102±7
	D286A						**D286W**					
	A287						**A287W**	4	1.90±0.07	56±1	5.1±1.3	110±4
	V288A	5	2.18 ± 0.18	62 ± 1	1.4±2.6	76±1	**V288W**					
	N289A	5	2.13 ± 0.16	56 ± 1	1±0.8	110±9	**N289W**					
P region	**E290A**	5	2.38 ± 0.14	60 ± 4	3.1±1.5	80±9	**E290W**					
	S291A	3	2.50 ± 0.03	57 ± 3	1±1.5	80±6	**S291W**	5	1.55±0.05	39±4	-2.2±0.5	135±23
(Turret)	**G292A**						**G292W**					
	R293A	6	2.15 ± 0.06	64 ± 2	4.2±0.9	101±5	**R293W**					
	V294A	5	1.97 ± 0.08	64 ± 2	-0.5±0.9	100±4	**V294W**	4	2.06±0.09	46±1	-5.6±1.5	148±6
	E295A	6	2.18 ± 0.12	63 ± 4	3.9±1.0	107±8	**E295W**					
	F296A						**F296W**					
	G297A	5	2.15 ± 0.12	63 ± 4	5±3.4	110±9	**G297W**	4	2.46±0.13	70±1	-3.1±1.5	162±6
	S298A						**S298W**	5	1.88±0.04	56±1	-0.5±0.6	114±5

		n	G_{Rb}/G_K	Inac%	$\Delta V_{1/2}$ (mV)	Deact(ms)		n	G_{Rb}/G_K	Inac%	$\Delta V_{1/2}$ (mV)	Deact(ms)
	Y299A						Y299W					
	A300						A300W	8	2.46±0.09	91±2	17.8±0.7	69±3
	D301A						D301W					
P region	A302						A302W					
	L303A						L303W					
(pore helix)	W304A						W304					
	W305A						W305					
	G306A						G306W					
	V307A						V307W					
	V308A						V308W					
	T309A						T309W					
	&V310A	9	1.02 ± 0.05	58 ± 4	-9.6±2.0	91±6	V310W					
	T311A						T311W					
	T312A						T312W					
	I313A						I313W					
P region	G314A						G314W					
	Y315A						Y315A					
(Selectivity	G316A						G316W					
filter)	D317A						D317W					
	K318A						K318W					
	V319A						V319W					
	P320A						P320W					
	Q321A	4	2.48 ± 0.11	77 ± 2	3±0.9	49±3	Q321W					
	T322A						T322W					
	W323A	4	1.89 ± 0.11	50± 4	6.6±1.2	77±2	W323					
	V324A	5	2.06 ± 0.05	74 ± 3	-2.2±1.9	88±1	V324W	4	2.09±0.06	77±1	-5±0.8	94±4
	G325A						G325W					
	K326A						K326W					
	T327A	4	2.04 ± 0.04	42 ± 2	-2.5±0.7	145±6	T327W	4	2.06±0.13	34±1	0±0.6	75±6
	I328A						I328W					
	A329						A329W					
	S330A	4	2.29 ± 0.08	56 ±2	-3.7±0.8	63±2	S330W					
	C331A	5	2.21 ± 0.07	51 ± 3	-6.2±0.9	95±2	C331W					
	F332A	5	0.80±0.04	0	25.9±1.0	60±2	F332					
	S333A	6	1.82 ± 0.05	39 ± 1	3.4±0.9	134±6	S333W					
S6	V334A						&V334W	4	1.01±0.08	59±3	21.6±0.9	49±3
	F335A	6	1.10 ± 0.02	0	30.1±1.1	119±6	F335W					
	A336						A336W	4	0.52±0.03	11±1	-1.6±1.1	317±7
	I337A	3	1.06 ± 0.04	32 ± 1	4.6±0.5	75±3	I337W					
	S338A	5	2.60 ± 0.07	71 ± 3	29.1±1.6	133±5	S338W	6	1.29±0.05	43±4	0.40±1.4	154±14
	&F339A	4	0.60 ± 0.02	18 ± 4	1.4±1.5	96±4	F339W					
	&F340A	6	1.10 ± 0.04	85 ± 4	-30.8±0.8	177±11	F340W					
	A341						A341W					
	L342A	5	1.02 ± 0.04	0	-26.3±0.9	155±16	L342W					
	P343A						P343W					
	A344						A344W					
	&G345A	5	0.69 ± 0.03	76 ± 3	17±1.5	105±3	G345W					KIR
	I346A						I346W	7	1.38±0.06	22±2	40.4±2.4	145±8
	L347A	6	1.73 ± 0.06	26 ± 2	61.3±4.9	54±3	L347W	13	2.30±0.06	0	71.4±1.2	75±2
	G348A	7	1.58 ± 0.04	27 ± 2	-2.6±1.1	549±44	G348W					KIR
	S349A	6	2.19 ± 0.08	33 ± 1	22.5±1.1	60±1	S349W					
	G350A	6	1.85 ± 0.05	13 ± 1	20.8±1.0	60±3	G350W					
	F351A	5	2.91 ± 0.15	0	47.1±0.8	39±1	F351W					
	A352						A352W	4	1.44±0.04	92±2	64.8±3.5	218±7
	L353A	4	1.71 ± 0.06	57 ± 2	-17.2±2.2	140±2	L353W	4	2.10±0.06	30±4	-2.5±0.8	112±10
	K354A	4	1.65 ± 0.07	74 ± 2	16.4±0.9	69±2	K354W	4	1.89±0.07	0	19.2±0.6	162±7
	&V355A	5	0.96 ± 0.06	0	-10.2±3.0	63±1	V355W		1.84±0.07	0	51.8±1.3	35±2

Mutations which induced a change both in G_{Rb}/G_K and inactivation fraction (F_{inac}%) were grey colored. Mutations marked with '&' displayed a strong macroscopic inactivation. $\Delta V_{1/2}$ (half voltage for activation shifted by mutations) for voltage-dependent activation (yellow, $\Delta V_{1/2}$ >10 mV; blue, $\Delta V_{1/2}$ < -10 mV) and fast time constant for deactivation kinetics (yellow, fast; blue, slow) were shown as reference.

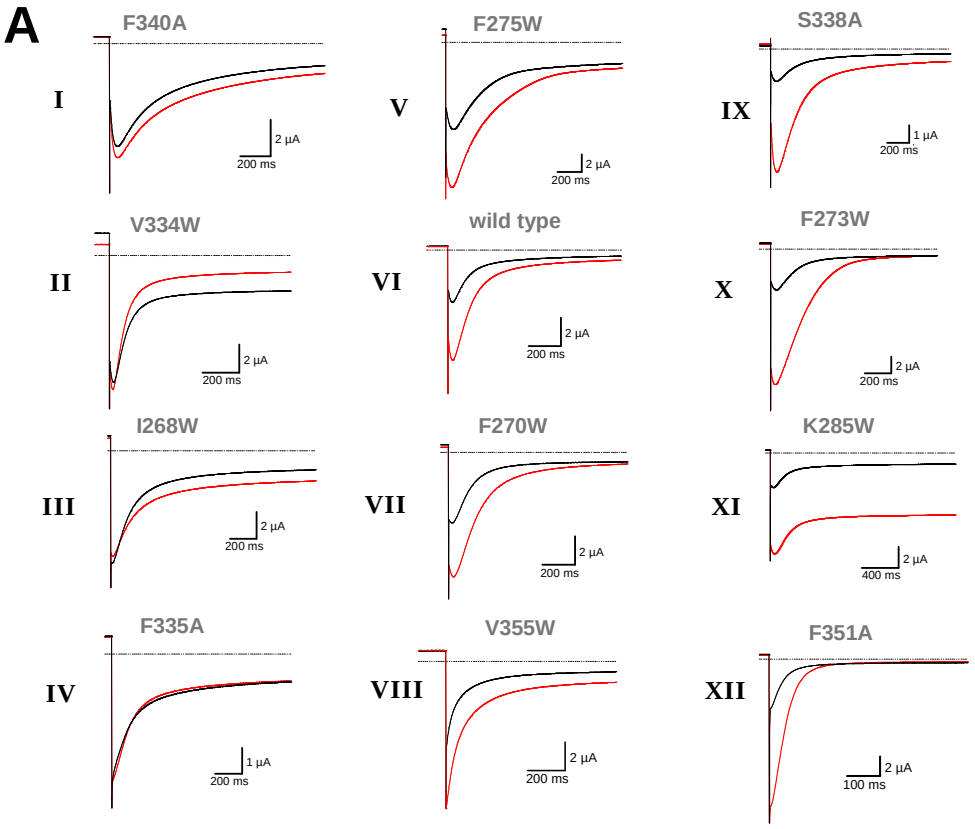
A
I
F340A
2 µA
200 ms
V
F275W
2 µA
200 ms
IX
S338A
1 µA
200 ms
II
V334W
2 µA
200 ms
VI
wild type
2 µA
200 ms
X
F273W
2 µA
200 ms
III
I268W
2 µA
200 ms
VII
F270W
2 µA
200 ms
XI
K285W
2 µA
400 ms
IV
F335A
1 µA
200 ms
VIII
V355W
2 µA
200 ms
XII
F351A
2 µA
100 ms

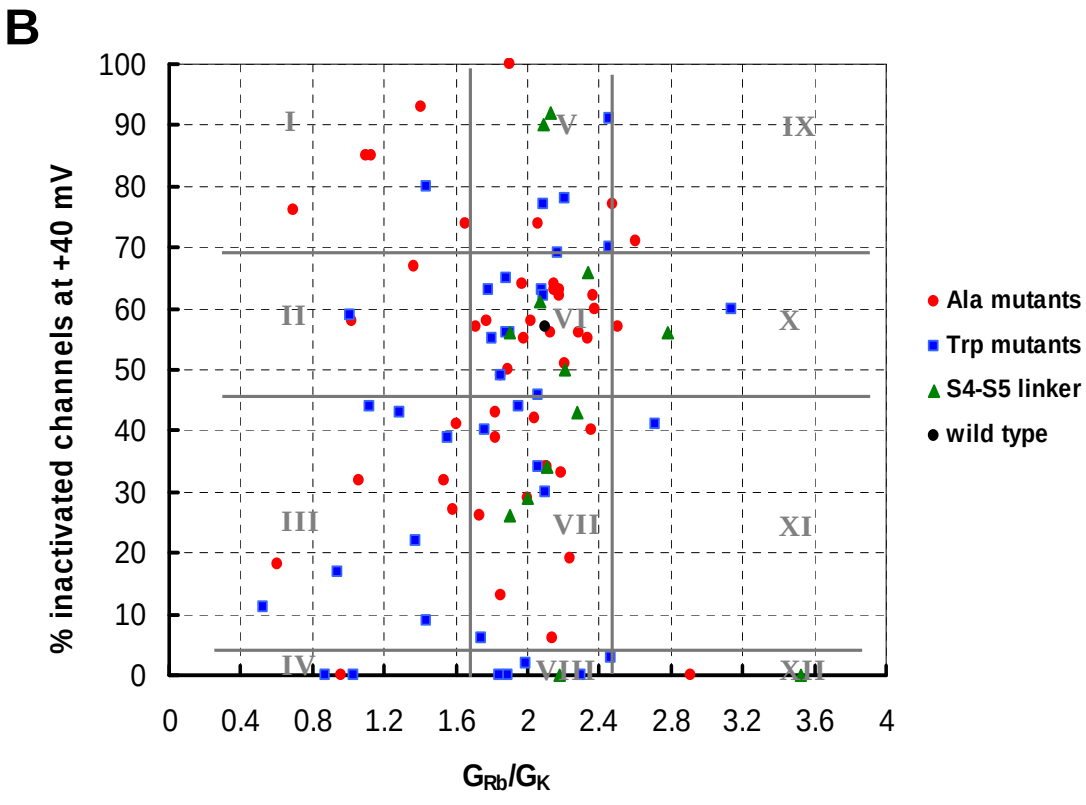
B
% inactivated channels at +40 mV
100
90
80
70
60
50
40
30
20
10
0
0
0.4
0.8
1.2
1.6
2
2.4
2.8
3.2
3.6
4
GRb/GK
I
V
IX
II
VI
X
III
VII
XI
IV
VIII
XII
Ala mutants
Trp mutants
S4-S5 linker
wild type

C

I	*S5*	*S6*	*P region*			**V**	*S5*	*S6*	*P region*	*S4-S5*		**IX**	*S5*	*S6*	*P region*	
	&I268A	*&G345A*					Y278A	Q321A	G297W	T247W				S338A		
	&G269A	*&F340A*					F275W	V324A		W248A						
		K354A						A300W								
		A352W						V324W								
II	*S5*	*S6*	*P region*			**VI**	*S5*	*S6*	*P region*	*S4-S5*		**X**	*S5*	*S6*	*P region*	*S4-S5*
	I274A	*&V310A*					R259A	W323A	V288A	G245W			L273W			V255W
		&V334W					Q260A	S330A	N289A	R249W						
							I263A	C331A	E290A	F256A						
							L266A	L353A	S291A	S253W						
							S277A		R293A							
							L282A		V294A							
							R259W		E295A							
							Q260W		G297A							
							Y267W		A287W							
							Y278W		V294W							
							F279W		S298W							
							Y281W									
							L282W									
III	*S5*	*S6*	*P region*			**VII**	*S5*	*S6*	*P region*	*S4-S5*		**XI**	*S5*	*S6*	*P region*	
	L262A	I337A	S291W				T265A	*T327A*	K285A	G246W					K285W	
	F270A	*&F339A*					L271A	S333A		G252W						
	L266W	G348A					G272A	L347A		I257W						
	I268W	A336W					F275A	*S349A*		H258W						
	G272W	S338W					S276A	G350A								
		I346W					F279A	T327W								
							I263W	L353W								
							T265W									
							F270W									
IV	*S5*	*S6*				**VIII**	*S5*	*S6*		*S4-S5*		**XII**	*S5*	*S6*	*P region*	*S4-S5*
	E261A	F332A					*&T264A*	L347W		L250W				F351A		L251W
	Y267A	F335A					L271W	K354W								
	E261W	L342A					I274W	V355W								
	T264W	*&V355A*														

Figure 4.7: G_{Rb}/G_K and inactivation properties of KCNQ1 pore mutants

(A) Representative current traces for WT and mutant KCNQ1 channels of different groups recorded at -120 mV after 3-second pulse stimulation to +40 mV. Currents recorded in 100 mM K^+ solutions (black traces) were supimposed on those recorded from the same oocyte bathed in 100 mM Rb^+ solutions (red traces). Dotted line indicates the zero-current level. (B) Plot of the degree of channel inactivation at +40 mV *vs*. G_{Rb}/G_K for mutant KCNQ1 channels. See Methods for further details.
(C) Categorization of mutations according to the plot in B.

Taken together, G_{Rb}/G_K and inactivation properties provided a point of view for a pore structural change. Among the 104 mutations that showed functional voltage-dependent activation, 71 mutations were neutral or produced only a local structural change, while 33 mutations induced a global structural change. More mutations of S6 (52%) gave rise to a structural change than those of S5 (30%), indicating the importance of the S6 for the pore structure (Table 4.9). In contrast, almost none of the mutations in the S4-S5 linker produced a change in G_{Rb}/G_k, which suggests that the S4-S5 linker is comparatively distant from the pore (Table 4.9).

Talbe 4.9: Mutational effect on the pore structure of the KCNQ1 channels

	Total	neutral or local	global	global (%)
S4-S5	13	12	1	8%
S5	40	28	12	30%
S6	33	16	17	52%
P turret	15	13	2	13%
P helix and filter	3	2	1	33%
Summary	104	71	33	32%

4.1.5 Mapping of KCNQ1 mutants phenotypes onto the Kv1.2 crystal structure

To interpret the mutational effect in a structural context, I mapped how different mutant phenotypes onto the Kv1.2 channel structure, which served as a model for eukaryotic Kv channel with an open pore conformation.

4.1.5.1 Defects in functional expression

Nonfunctional mutants in S5 and S6 were mapped onto the X-ray structure of the Kv1.2 channel. Space-filling models represent the atoms as spheres whose radii are proportional to the atom's van der Waals radius. The best known of this type of model is the Corey-Pauling-Koltun (CPK) model. Figure 4.8 shows a backbone representation of the S4-S6 region of Kv1.2 X-ray structure with pink CPK (space-filling) representation for residues where mutations produced nonfunctional channels. It is evident that none of the nonfunctional mutants projected outwards. The tolerance of the interface between voltage-sensing and pore domains in Kv channels is consistent with the results from the *Shaker* K^+ channel (Soler-Llavina et al., 2006), which implied the presence of a rather unconstrained interface between voltage sensor and pore domains in Kv channels. In addition, those residues in the external half of the channel that resulted in nonfunctional channels when mutated are presumably involved in packing between S5 and S6 or interact with residues in the reentrant pore loop that forms the selectivity filter. This result is also similar to that observed from the *Shaker* K^+ channel (Soler-Llavina et al., 2006).

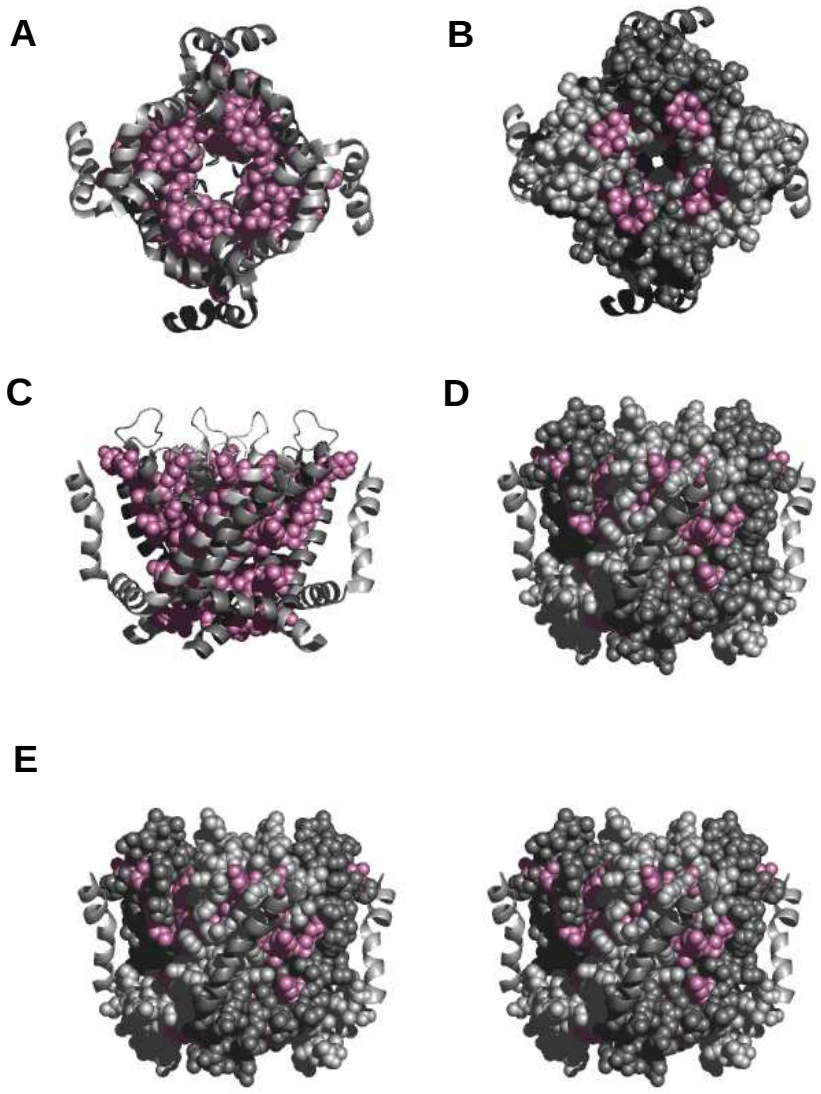

Figure 4.8: Mapping nonfunctional KCNQ1 mutations in S5 and S6 onto the Kv1.2 structure.

Backbone folding model of the S4-S6 region of Kv1.2 viewed from the bottom (A and B) and side (C, D and E). Pink residues (shown as CPK) correspond to the residues in S5 and S6 of KCNQ1 where mutations result in non-functional channels. All other residues in S5-S6 region are shown in grey. E) Stereo side view of the model

However, the results of mapping the residues within the internal half of the channel showed differences between KCNQ1 and *Shaker*. In Table 4.10, the nonfunctional mutations in the internal half of the pore of *Shaker* and KCNQ1 have been compared (data of Shaker from Soler-Llavina et al., 2006, and Yifrach et al., 2002). Mapping the nonfunctional mutations onto Kv1.2 structure illustrated that some KCNQ1 residues positioned at the intracellular leaflet of the membrane were nonfunctional when mutated into tryptophan or alanine, whereas this was not the case in the *Shaker* K^+ channel (Fig. 4.9). nonfunctional mutations in *Shaker* often normal membrane expression, but were non-conducting, as indicated in Table 4.10 (Soler-Llavina et al., 2006). The same may be true for KCNQ1 nonfunctional mutants in the internal half of the pore domain.

Talbe 4.10: Non-functional mutations in the internal half of the pore domain of *Shaker* and KCNQ1.

	Shaker	KCNQ1	Kv1.2
S5	L396W**	L262W	L328
	L399W**		L331
	I400W		I332
		G269W	L335
S6	G466W(A)		G398
	V467W**	I337W	V399
	A471W	A341W	A403
		L342W	L404
	P473W(A)**	P343W(A)	P405
	V474W	A344W	V406
	P475A**		P407
		I346A	V408
	V478W**		V410
		S349W	S411
		SG350W	N412
	F481A		F413

Nonfunctional mutations in *Shaker* and KCNQ1 in the internal half of the pore and the corresponding residues in Kv1.2. ** indicates the non-conducting *Shaker* mutants channels with normal membrane expression.

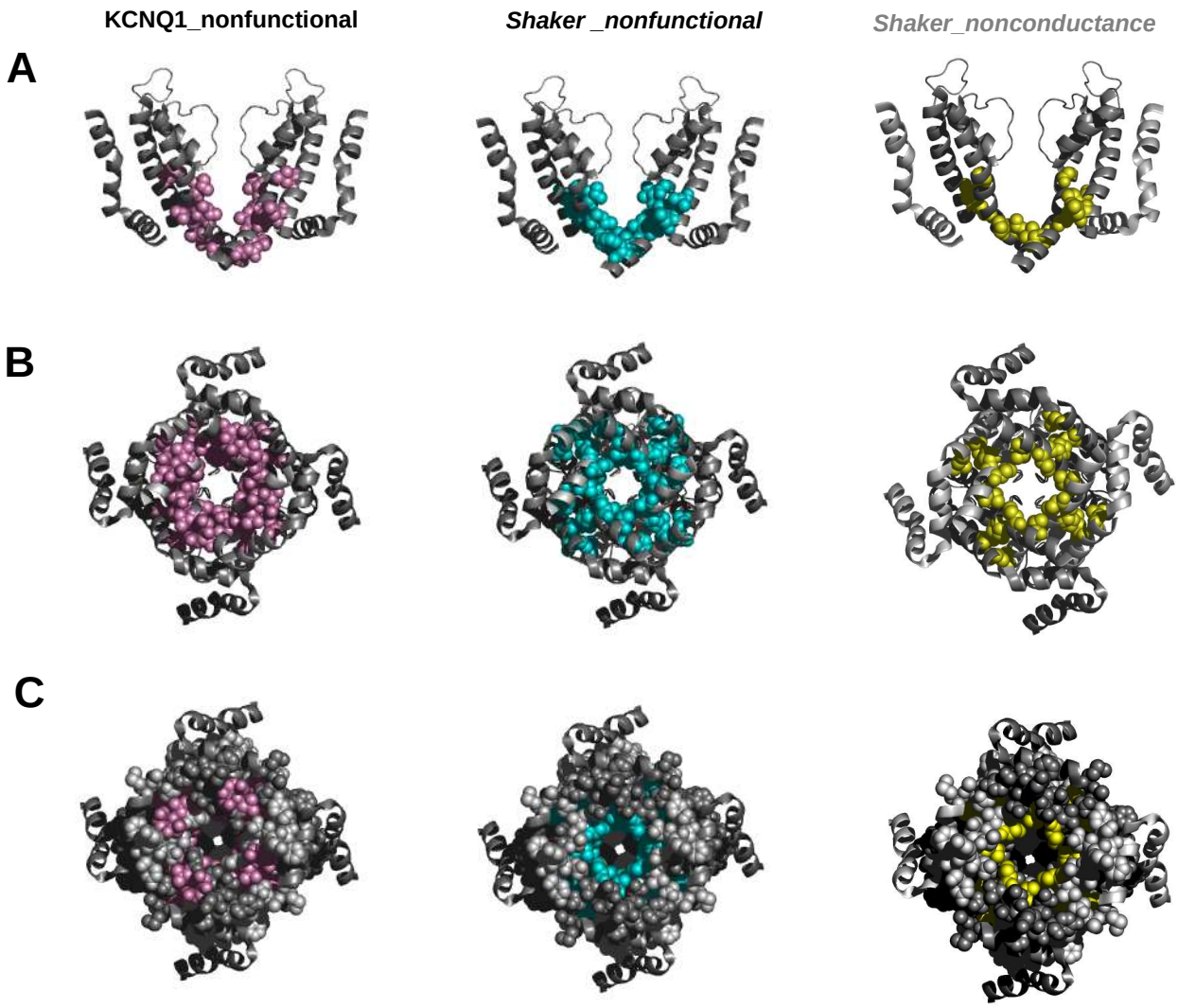

Figure 4.9: Mapping nonfunctional mutations in the internal half of the pore domain of *Shaker* and KCNQ1 onto the Kv1.2 structure.

Backbone folding model of the S4-S6 region of Kv1.2 viewed from the side (A) and the bottom (B). Pink residues (shown as CPK) correspond to residues of KCNQ1 where mutations resulted in nonfunctional channel and blue residues correspond to that of *Shaker.* Yellow residues indicate the residues in *Shaker* where mutations displayed normal membrane trafficking, but were non-conducting. (C) Bottom view of the model with all other residues in S5-S6 region are shown in grey.

4.1.5.2 Perturbation of G_{Rb}/G_K and inactivation properties

KCNQ1 channel exhibits a high relatively higher Rb^+ conductance compared to K^+ (G_{Rb}/G_K). Pusch et al. (2000) have suggested that the large G_{Rb}/G_K is determined by the dependence of flickery open channels on ion occupancy of the pore. Most KCNQ1 pore mutants displayed decreased G_{Rb}/G_K (G_{Rb}/G_K <1.3), only three mutants exhibited prominently increased G_{Rb}/G_K (G_{Rb}/G_K>2.9).

To investigate the structural basis for the high G_{Rb}/G_K properties of KCNQ1 channel, I selected the mutations which yielded a strong perturbation in G_{Rb}/G_K, and mapped the respective residues onto the Kv1.2 structure. It is evident that the residues were located around the inner cavity below the selectivity filter (Fig. 4.10). One group may disturb packing between S5, S6 and P- helix. Another group appears in close contact with the lower activation gate, i.e. the PAG motif. The results indicated that stability of the inner pore cavity may play an important role for a high G_{Rb}/G_K of the KCNQ1 channel.

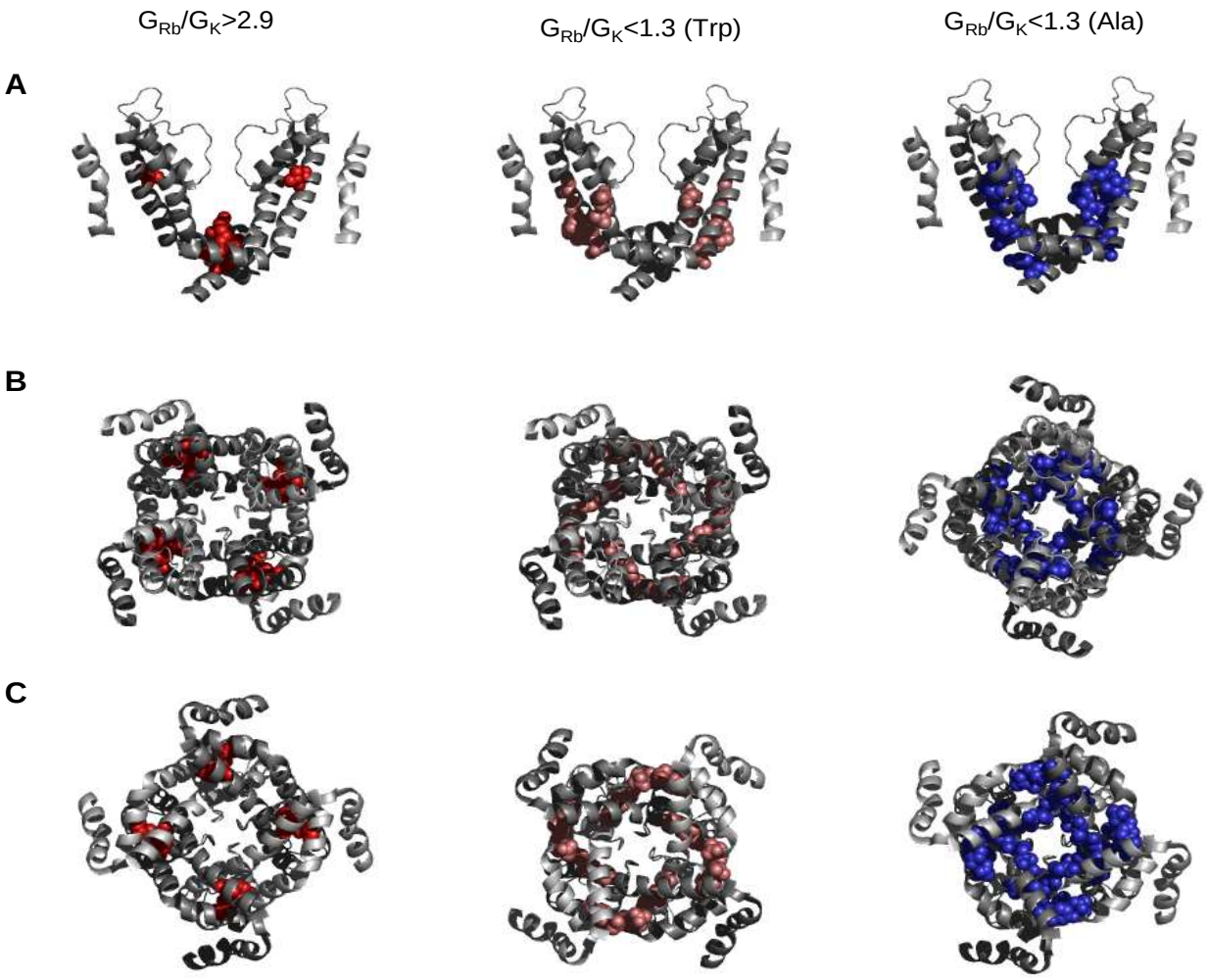

Figure 4.10: Perturbations in G_{Rb}/G_K mapped onto the Kv1.2 structure.

(A) Backbone folding models of the S4-S6 region of Kv1.2 viewed from the side showing S4-S5 linker and S5-S6 region from two subunits and nearby S4 helix from two adjacent subunits with residues where G_{Rb}/G_K>2.9 colored red, those where G_{Rb}/G_K<1.3 when mutated into Trp colored salmon, and those where G_{Rb}/G_K<1.3 when mutated into Ala colored blue. (B) View from the top (outside) colored as in (A). (C) View from the bottom (inside) colored as in (A).

G_{Rb}/G_K>2.9: L273W, F351A, L251W

G_{Rb}/G_K<1.3 (Trp): E261W, T264W, I268W, G272W, V334W, A336W, S338W

G_{Rb}/G_K<1.3 (Ala): E261A, G269A, V310A, F332A, F335A, I337A, F339A, F340A, L342A, G345A, V355A

Another distinct channel property of KCNQ1 is that KCNQ1 undergoes slow-onset, voltage-independent inactivation. KCNQ1 inactivation is different from classical N- and C-type inactivation found in voltage-gated Na^+ channels and Kv channels of the *Shaker* type (Tristani-Firouy, et al.,1998, Pusch, et al., 1998). 17 mutations exhibited no 'hook' inactivation; however, they changed the G_{Rb}/G_K to different extent. In an attempt to understand the molecular mechanism for inactivation, I mapped the mutations that lead to non-inactivation onto the Kv1.2 structure. I separated these mutations into two groups regarding to the different effects on G_{Rb}/G_K: one displayed prevalent Rb^+ conductance and the other group no prevalent Rb^+ conductance. As shown in Figure 4.11, the non-inactivation mutations with $G_{Rb}/G_K<1.0$ are involved in the interaction between pore helix, S5 and S6. In agreement with these data, several lines of evidence indicated the importance of a putative pore helix/S5/S6 interaction for the KCNQ1 inactivation (Shalaby, et al., 1997, Seebohm, et al., 2001, Seebohm, et al., 2005).

The non-inactivating mutation with $G_{Rb}/G_K>1$ are clustered into two groups, one at the interface between the voltage-sensing and pore domains, the other group was concentrated at the interaction sites between C-terminus of S6 and S4-S5 linker. This result implicated the critical role of inter- or intra-subunit interaction for KCNQ1 inactivation.

Macroscopic inactivation is different from 'hook' inactivation. Nine mutants displayed this kind of gating behaviour. The mutants that exhibited macroscopic inactivation upon depolarization sometimes were accompanied with enhanced 'hook' inactivation. Mapping the respective residues onto Kv1.2 structure (Fig. 4.11) revealed that they were located around the inner cavity below the selectivity filter. All these residues were located at the interface within a subunit (I268, G269, V310, V334, F339, and F340) or between neighbouring subunits (T264, G345, and V355). Instability of the open pore might contribute to such a kind of inactivation. However, the mechanism of this kind of gating behavior brought about by mutations needs to be further explored.

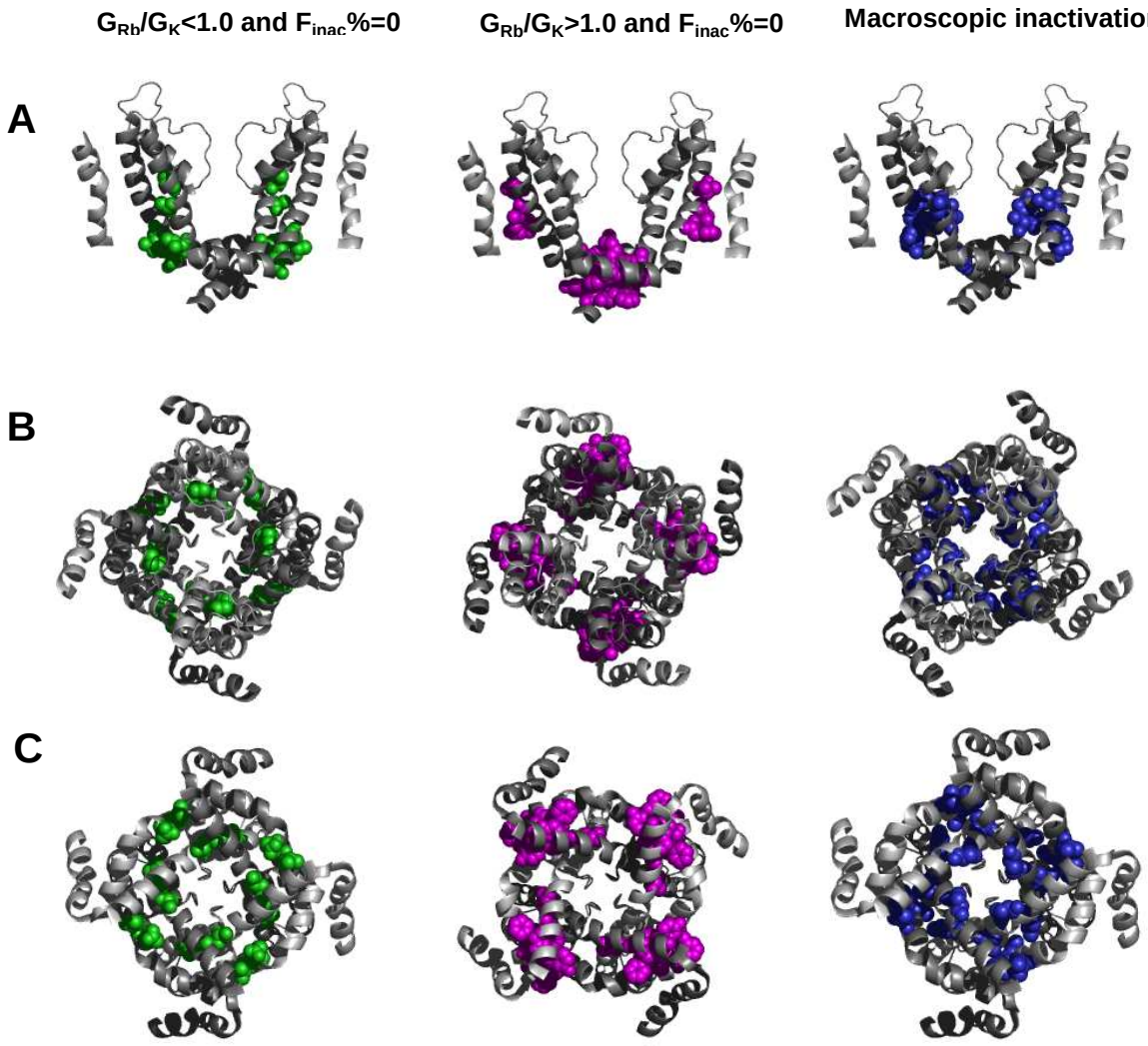

Figure 4.11: Mapping KCNQ1 mutants with no 'hook' inactivation or macroscopic inactivation.
(A) Backbone folding models of the S4-S6 region of Kv1.2 viewed from the side showing S4-S5 linker and S5-S6 region from two subunits and nearby S4 helix from two adjacent subunits with residues where G_{Rb}/G_K < 1.0 and F_{inac}% = 0 colored green, those where G_{Rb}/G_K > 1.0 and F_{inac}% = 0 colored pink, and those where macroscopic inactivation occurred were colored blue. (B) View from the top (outside) colored as in (A). (C) View from the bottom (inside) colored as in (A).
G_{Rb}/G_K < 1.0 and F_{inac}% = 0: E261W, T264W, F332A, F335A, L342A
G_{Rb}/G_K > 1.0 and F_{inac}% = 0: Y267A, L271W, I274W, L347W, F351A, K354W, V355W
Macroinactivation: T264A, I268A, G269A, V310A, V334W, F339A, F340A, G345A, V355A

4.1.5.3 Mutations that induced global structural changes of the pore

Changes in G_{Rb}/G_K and inactivation properties suggested that some mutations give rise to global structural changes. Mapping these mutations onto the Kv1.2 structure showed that most residues were clustered together in the inner half of the pore helix. They were located either near the crossover of the bundle crossing of S6 (close to the intracellular surface), or close to where S5 or S6 are packed against P-helix (close to the membrane center) (Fig. 4.12). Mutations in these regions possibly produced a strong gating perturbation (Fig. 4.13). These regions are important for KCNQ1 channel pore properties, e.g. conductance, activation, and inactivation.

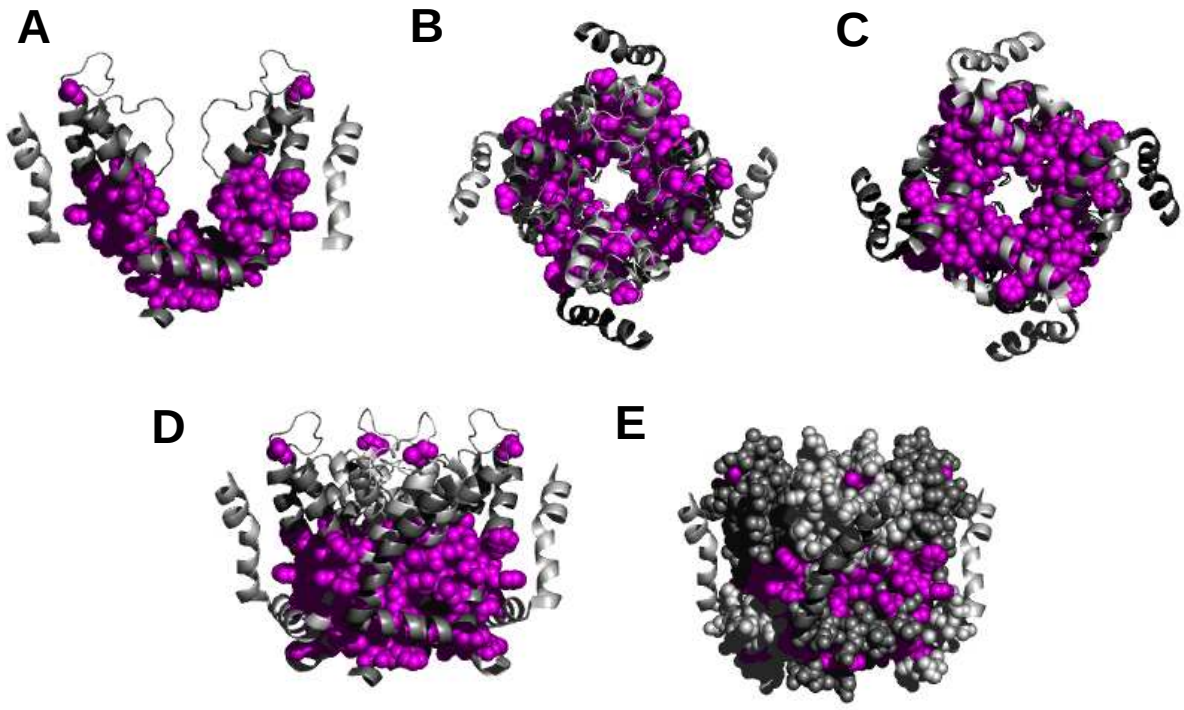

Figure 4.12: Perturbations in the pore structure mapped onto the Kv1.2 structure.
Backbone folding model of the S4-S6 region of Kv1.2 viewed from the side (A and D), top (B) and bottom (C). Purple residues (shown as CPK) correspond to the residues in S5 and S6 of KCNQ1 where mutations result in a global structural change. E) Side view of the model with all other residues in S5-S6 region colored in grey.

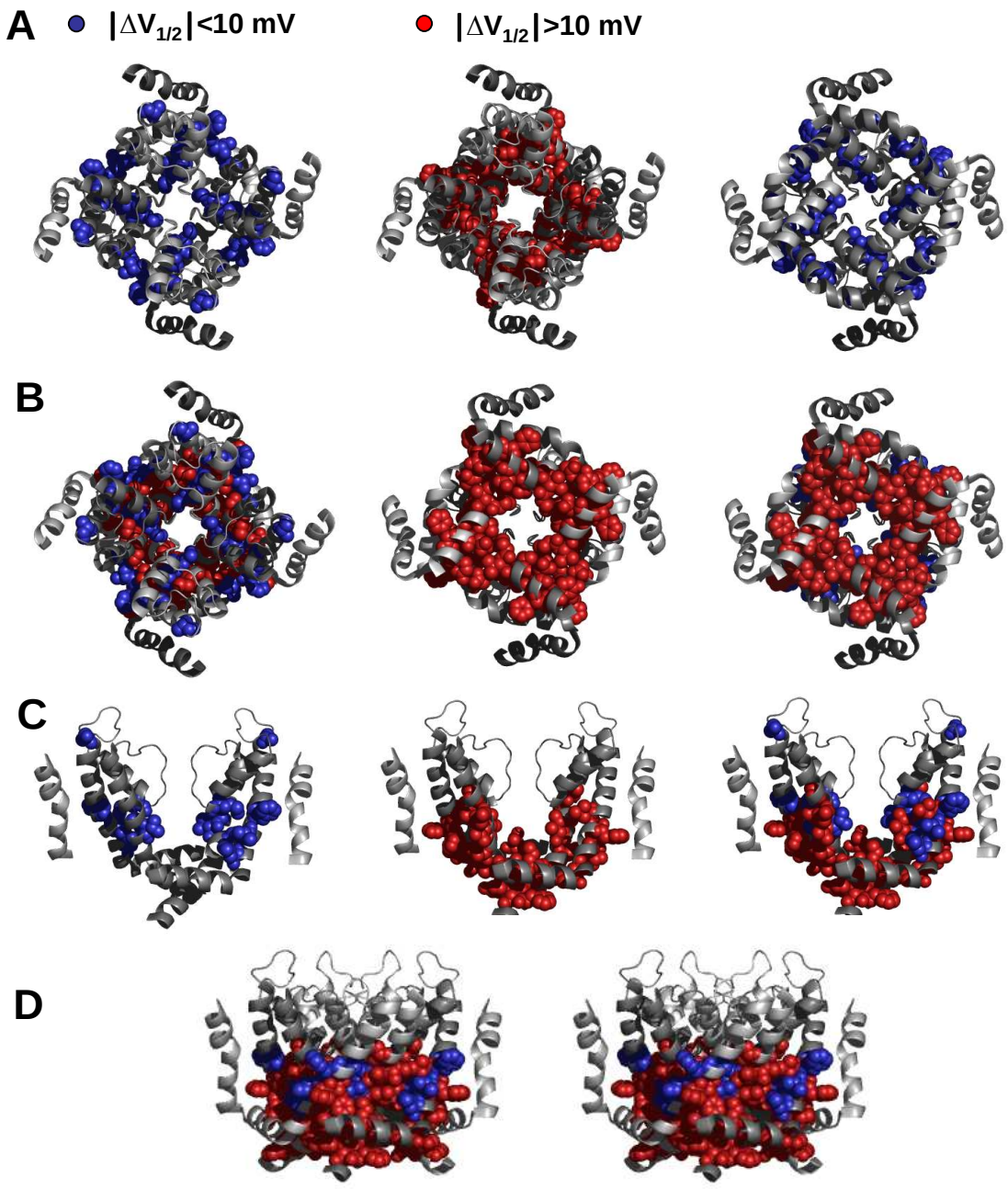

Figure 4.13: Global structural changes mapped onto the Kv1.2 structure.

(A) Backbone folding models of the S4-S6 region of Kv1.2 viewed from the top (outside) with residues where mutations displayed a similar G-V relation to wild-type KCNQ1 ($|\Delta V_{1/2}|$<10mV) are colored blue (shown as CPK) and those strongly perturbed the G-V relation ($|\Delta V_{1/2}|$>10mV) are colored red. $\Delta V_{1/2} = V_{1/2}^{mut} - V_{1/2}^{wt}$

(B) View from the bottom (inside) colored as in (A)

(C) View from the side showing only S4-S5 linker and S5-S6 region from two subunits and nearby S4 helix from two adjacent subunits

(D) Stereo pairs of the Kv1.2 structure viewed from the side with coloring as in (A).

4.1.5.4 Mutations that did not affect the pore structure

Changes in both conductance and inactivation kinetics caused by the pore mutation were used as an indicator for a global structural change in the pore. The residues that did not produce global structural change when mutated were mapped onto the Kv1.2 structure (Fig. 4.14). The gating sensitive residues are concentrated mainly in two groups. One was localized to the interface between voltage-sensor domain and pore domain (I263, Y267, L271, I274, F275, Y278 and L282). The other one was confined to the interaction of S4-S5 linker and C terminus of S6 interact at the internal membrane (S4-S5 linker: G246W, T247, W248, R249, L250, S253, V255, F256, H258, R259, Q260, and S6: L347, S349, G350, L353, K354, V355).

Biophysical studies, combined with the crystal structure of Kv1.2 suggested that coupling between voltage sensor and gate are mediated by interactions between S4-S5 linker and C- terminal end of S6 (Lu et al., 2002; Long et al., 2005). The mutations in this region most probably disturb the coupling between voltage sensor movements and pore opening and closing. Interaction between S4-S5 linker and C terminus of S6 is important for coupling. Prole and Yellen (2006) reported that crosslinking the S4-S5 linker to S6 in the spHCN channel dramatically altered channel gating in the absence of cAMP and converted the channel from a hyperpolarization-activated into a depolarization-activated channel.

Another group of gating sensitive residues was located at the interface between the voltage-sensing and pore domains. Consistent with the finding in this study, tryptophan scanning in the pore region of *Shaker* showed high-impact residues that faced the voltage-sensor domain. Recently, studies from Swartz and coworkers (2006) revealed that the mutations in an external cluster of the interface directly hinder voltage sensor activation, and mutations in an internal cluster domain between S4 and S5 from adjacent subunits appear crucial for the concerted opening transition.

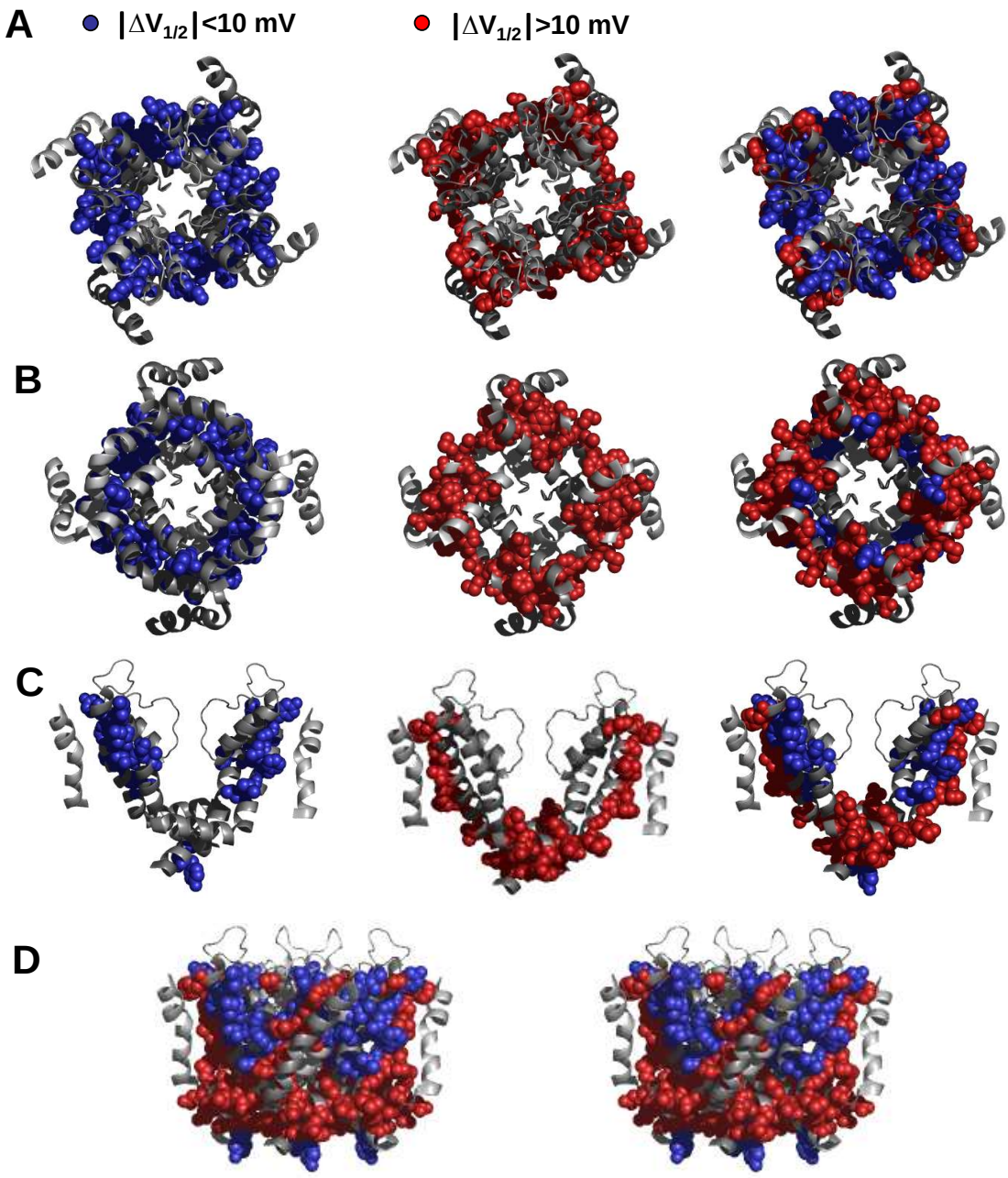

Figure 4.14: No global structural change mapped onto the Kv1.2 structure

(A) Backbone folding models of the S4-S6 region of Kv1.2 viewed from the top (outside) with residues where mutations displayed similar G-V relation to wild-type KCNQ1 ($|\Delta V_{1/2}|$<10mV) are colored blue (shown as CPK) and those strongly perturbed the G-V relation ($|\Delta V_{1/2}|$>10mV) are colored red. $\Delta V_{1/2} = V_{1/2}^{mut} - V_{1/2}^{wt}$

(B) View from the bottom (inside) colored as in (A).

(C) View from the side showing only S4-S5 linker and S5-S6 region from two subunits and nearby S4 helix from two adjacent subunits.

(D) Stereo pairs of the Kv1.2 structure viewed from the side with coloring as in (A).

4.2 Ca^{2+} regulation of the KCNQ1 channel

Mutagenesis studies of the pore region for the KCNQ1 channel described above suggested that the gating mechanism of KCNQ1 was different from that of *Shaker*. A distinct structural feature of KCNQ1 is a long C-terminus attached to the pore. Two possible CaM binding sites have been identified within the C-terminus of KCNQ family channels (Yus-Najera, et al., 2002), and previous studies indicated that CaM was an important Ca^{2+} sensor, which mediated Ca^{2+} sensitivity of KCNQ2/3 heteromultimers (Gamper and Shapiro, 2005). Recent study showed that CaM binding was essential for KCNQ1/KCNE1 channel assembly (Shamgar, et al, 2006; Ghosh et al., 2006). Possibly, the gate of KCNQ1 is allosterically regulated by Ca^{2+}/CaM.

4.2.1 Ca^{2+} regulation of KCNQ1 and KCNQ1/KCNE1 (I_{Ks}) currents

To test whether KCNQ1 or KCNQ1/KCNE1 was directly activated by intracellular Ca^{2+}, I used the *Xenopus* oocyte expression system and recorded KCNQ1 or KCNQ1/KCNE1 mediated currents from inside-out patches. The intracellular Ca^{2+} concentration $[Ca^{2+}]_i$ was manipulated by perfusion of buffered solutions directly onto excised patches. KCNQ1 of KCNQ1/KCNE1 currents displayed pronounced ‘’run-down’’ in excised patches because of depletion of lipid component PIP_2 (Zhang et al. 2003). Therefore, vanadate and fluoride were added to the intracellular solutions as lipid phosphatase inhibitors. Intracellular Ca^{2+} was buffered by adding 5 mM EGTA to the desired $[Ca^{2+}]_i$.
In this experimental set-up, the voltage for half-maximal activation ($V_{1/2}$) was -32 ± 2 mV for KCNQ1 channels at nominally Ca^{2+}-free conditions. Increasing free $[Ca^{2+}]_i$ induced a concentration-dependent leftward shift of the activation curve such that $[Ca^{2+}]_i$ = 0.025 µM, the $V_{1/2}$ was -51±3 mV and $[Ca^{2+}]_i$ = 0.1 µM, it was -59 ± 1 mV (Fig. 4.15A). KCNQ1/KCNE1 channels activation appeared even more Ca^{2+}-sensitive. Under nominally zero Ca^{2+} conditions, KCNQ1/KCNE1 currents could only be recorded at potentials above +20 mV and $V_{1/2}$ was 80 ± 4 mV. Increasing free $[Ca^{2+}]_i$ also produced a concentration-dependent leftward shift of the activation curve for KCNQ1/KCNE1 currents such that $[Ca^{2+}]_i$ = 0.025 µM, the $V_{1/2}$ was 34 ± 2 mV and $[Ca^{2+}]_i$ = 0.1 µM, it was 27 ± 3 mV (Fig. 4.15B). Apparently, an increase in $[Ca^{2+}]_i$ from 0 to 0.1 µM induced a left shift in the activation curve by -22 mV for KCNQ1, and by -50 mV for

KCNQ1/KCNE1 (Fig. 4.15C).

The left shift in the activation curve induced by an increase in $[Ca^{2+}]_i$ was not observed upon bath perfusion with Mg^{2+} at concentrations of up to 5mmol/L (Fig. 4.15B), indicating that Ca^{2+} regulation of KCNQ1 or KCNQ1/KCNE1 did not arise from a charge effect. An increase of $[Mg^{2+}]_i$ inhibited the current amplitude of KCNQ1/KCNE1 at +60 mV, shifted half-maximal voltage for activation positively ($V_{1/2}$ = 80 ± 4mV (n=4) at 0 mM $[Mg^{2+}]_i$; 112 ± 6 mV (n = 4) at 4.6 mM $[Mg^{2+}]_i$), while KCNQ1 channel alone displayed no significant change in voltage-dependent activation when $[Mg^{2+}]_i$ increased. Mg^{2+}-induced inhibition on KCNQ1/KCNE1 might result from neutralization of PIP_2 in the membrane because of a high concentration of $[Mg^{2+}]_i$. Taken together, these results demonstrate that voltage sensitivity and activation by intracellular Ca^{2+} were closely linked in KCNQ1 and KCNQ1/KCNE1 channels.

Ca^{2+}-regulation of KCNQ1/KCNE1 channel allows for its activation at physiological potentials. To investigate whether Ca^{2+} regulation of KCNQ1/KCNE1 has physiological relevance, it was tested how fast KCNQ1/KCNE1 channels could respond to the change in $[Ca^{2+}]_i$. A fast application system was used in inside-out patches in order to switch different Ca^{2+} concentration solutions within milliseconds. When $[Ca^{2+}]_i$ was rapidly increased or decreased at depolarized membrane potentials, I_{Ks} channel amplitudes responded accordingly by a rapid increase or decrease, respectively. Fitting the response curve to a single-exponential function, the time constant for the Ca^{2+}-responses were 923 ± 237 ms and 370 ± 80 ms (n = 4) respectively (Fig. 4.15 D). These experiments were carried out with the aid of Dr. K. Benndorf, University of Jena. Ca^{2+} response of KCNQ1/KCNE1 channels was rapid and fully reversible. This observation may provide a molecular basis for understanding the Ca^{2+} sensitivity reported for cardiac I_{Ks} currents at high stimulation rates (Bai, et al., 2005).

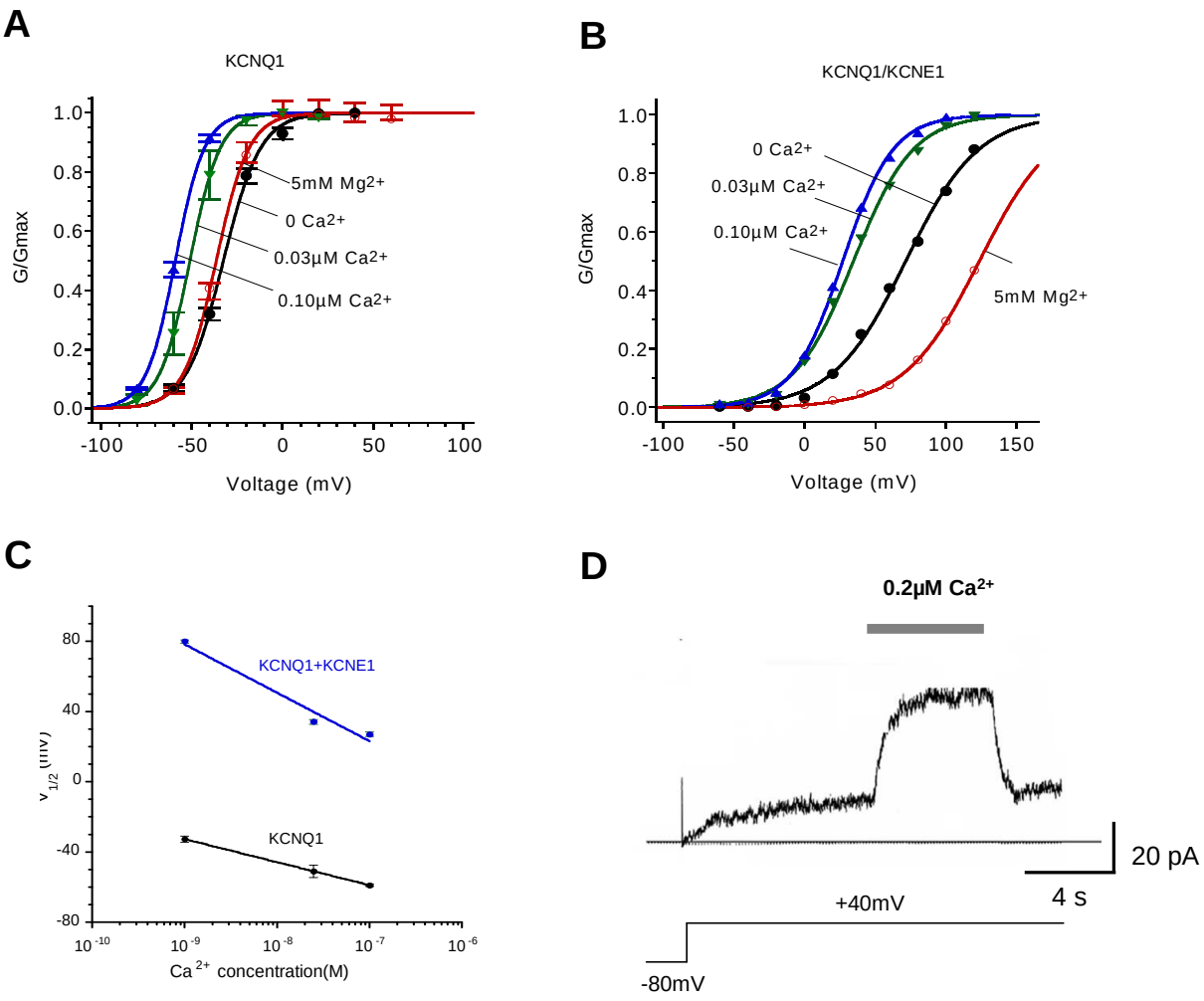

Figure 4.15: Ca^{2+}-sensitivity of KCNQ1 and KCNQ1/KCNE1 channels in inside-out patches.
Normalized conductance-voltage (G-V) relations for KCNQ1 (A) and KCNQ1/KCNE1 (B) at 0 µM [Ca^{2+}] (black), 0.03 µM [Ca^{2+}] (green) , 0.1 µM [Ca^{2+}] (blue) and 5 mM [Mg^{2+}] (red). Conductance was determined from tail currents recorded upon repolarizations to −120 mV and normalized to the observed maximum conductance (G_{max}). Data points were fit with the Boltzmann equation $G = G_{max}/(1 + \exp[-(x - V_{1/2}) \times zF/RT])$, where $V_{1/2}$ is the midpoint voltage, z is the gating valence, F is Faraday's constant, R is the gas constant, and T is absolute temperature in K. (C) Plot of mean values for $V_{1/2}$ vs. $[Ca^{2+}]_i$ for KCNQ1 and KCNQ1/KCNE1 channels. (D) Rapid response of KCNQ1/KCNE1 channels to intracellular [Ca^{2+}] change. KCNQ1/KCNE1 macroscopic currents at +40 mV were activated by a rapid [Ca^{2+}] increase and deactivated by a rapid [Ca^{2+}] decrease. The data was done in collaboration with Dr. K. Benndorf, Universität Jena.

4.2.2 CaM mediated Ca^{2+}-sensitivity of KCNQ1 or KCNQ1/KCNE1 channels

I used two approaches to ascertain whether these Ca^{2+}-regulated effects were mediated by CaM for KCNQ1 or KCNQ1/KCNE1. Firstly, I examined the impact of the CaM antagonist W-7 on the expressed currents in inside-out macropatches. Currents were evoked by a depolarization voltage step to +60 mV or +80 mV from a holding potential of -80 mV. Bath application of the CaM antagonist W-7 (50 µmol/L) potently and reversibly inhibited both KCNQ1 and KCNQ1/KCNE1 (Fig. 4.16A). This inhibition suggested that Ca^{2+}-CaM was important for KCNQ1 or KCNQ1/KCNE1 channel activity. Secondly, I attempted to replace endogenous CaM with the Ca^{2+}-insensitive CaM_{1234} by overexpression of CaM_{1234}. As illustrated in Fig. 4.16B, when comparing coexpression of KCNQ1/KCNE1 with wild-type CaM, coexpression of KCNQ1/KCNE1 with CaM_{1234} markedly reduced current amplitude and produced a pronounced right-shift of $\Delta V_{1/2}$ = +35 mV in the voltage-dependence activation (from $V_{1/2}$ = 37 ± 3 mV to $V_{1/2}$ = 73 ± 3 mV; n = 4) (Fig. 4.16C). Similar results for KCNQ1 were observed by Shamgar, et al (2006), coexpression of KCNQ1 with CaM_{1234} markedly suppressed the currents and produced a right-shift of $\Delta V_{1/2}$ = + 25 mV in the voltage-dependence of channel activation. Thus, CaM confers Ca^{2+} sensitivity of KCNQ1 or KCNQ1/KCNE1 channels

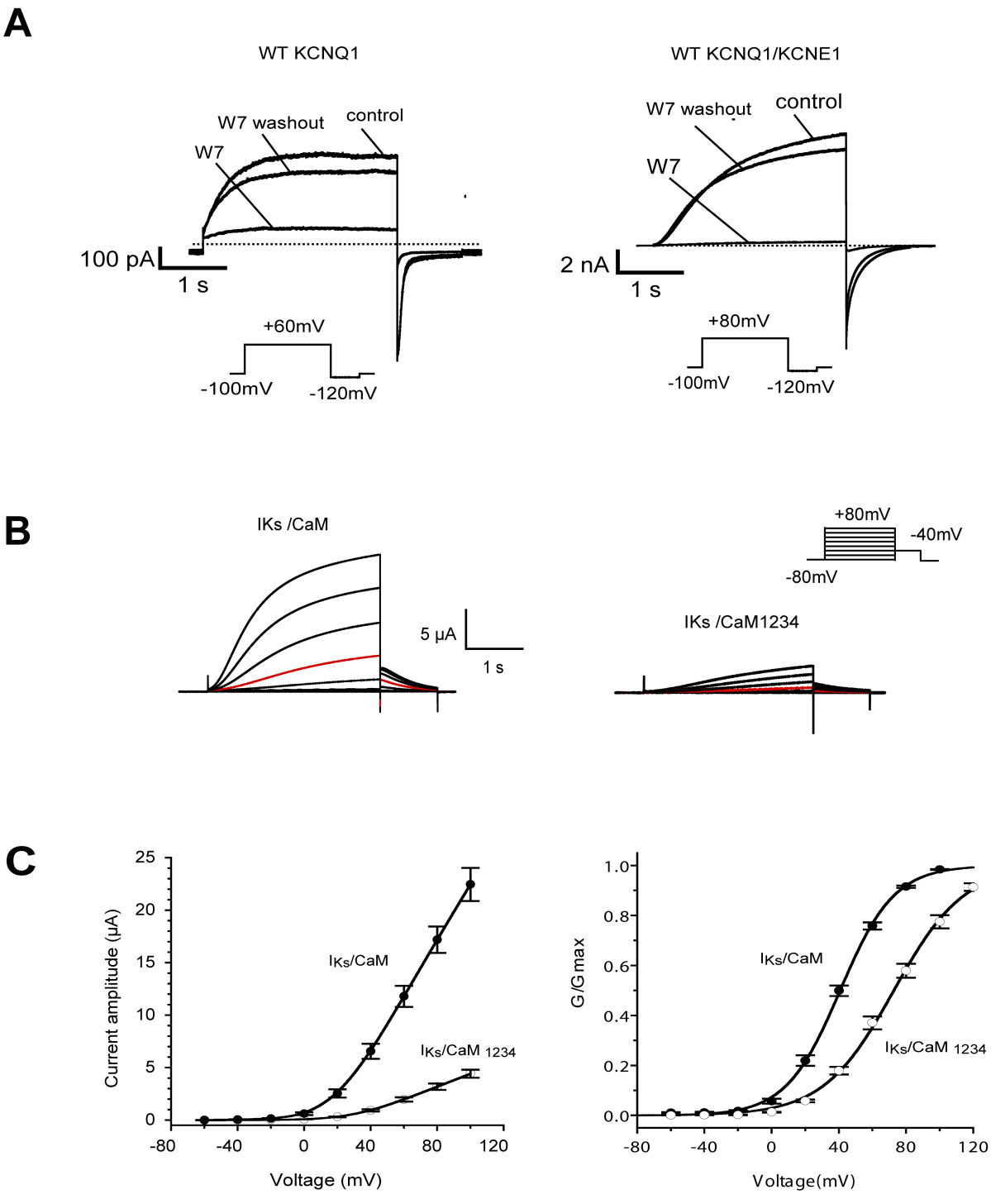
A
WT KCNQ1
W7 washout
control
W7
100 pA
1 s
+60mV
-100mV
-120mV
WT KCNQ1/KCNE1
W7 washout
control
W7
2 nA
1 s
+80mV
-100mV
-120mV
B
IKs /CaM
5 µA
1 s
+80mV
-40mV
-80mV
IKs /CaM1234
C
Current amplitude (µA)
IKs/CaM
IKs/CaM 1234
Voltage (mV)
G/Gmax
IKs/CaM
IKs/CaM 1234
Voltage(mV)

Figure 4.16: CaM mediated Ca^{2+} regulation of KCNQ1 and KCNQ1/KCNE1 channels.

(A) Application of the CaM antagonist W-7 to KCNQ1 or KCNQ1/KCNE1 channels strongly inhibited the current amplitude. The W-7 inhibitory effects were rapid and reversible. Representative recordings of KCNQ1 and KCNQ1/KCNE1 currents evoked by depolarization as indicated from inside-out macropatches bathed in 0.1µM [Ca^{2+}] without or with 50 µM W-7 and after washout.

(B) Impact of the WT CaM and the Ca^{2+}-insensitive CaM_{1234} mutant on KCNQ1/KCNE1 recorded from two-electrode voltage clamp in *Xenopus* oocytes. Representative current traces for coexpression of KCNQ1/KCNE1 (I_{Ks}) with wild type CaM and CaM_{1234}. The channels were activated by voltage steps from -80 mV to +80 mV in 20 mV increments, and tail currents were measured at -40 mV (holding potential, -80 mV)

(C) The current-voltage relations of I_{KS} channels coexpressed with either WT CaM (black squares) or the Ca^{2+}-insenstive CaM_{1234} mutant (empty squares) (n=4) are plotted in the left panel. Normalized conductance-voltage (G-V) relation of KCNQ1/KCNE1 coexpressed with WT CaM or CaM_{1234} (empty squares) are shown in the right panel. Coexpression of KCNQ1/KCNE1 with CaM $_{1234}$ markedly suppressed the currents and produced a pronounced right-shift of G-V curves.

4.2.3 Ca^{2+}-sensitivity of KCNQ1 pore mutants

The finding in this study indicated that the gate of the KCNQ1 channel was controlled by a change in membrane voltage and in Ca^{2+}, reminiscent of the Ca^{2+}-regulated and voltage-dependent BK channel. As proposed by Aldrich (Cui and Aldrich, 2000), the free energy provided by voltage and Ca^{2+} in activating KCNQ1 channels are simply additive

$$\Delta G_{V,\,Ca} = \Delta G_V + \Delta G_{Ca} \qquad (1)$$

The energetic additivity indicates that the electrical and the Ca^{2+} binding energies can compensate for each other to sustain the channel open probability. Thus, to maintain P_0 = 0.5, $\Delta\Delta G_{Ca}$ must exactly counterbalance any change in the electrical component of the free energy:

$$\Delta\Delta G_V = -\,\Delta\Delta G_{Ca} \qquad (2)$$

According to the Boltzmann function, the energetic additivity results in a relationship:

$$\Delta\,(zeV_{1/2}) = -\,\Delta\Delta G_{Ca} \qquad (3)$$

which underlies the shift of the G-V relation on the voltage axis with various $[Ca^{2+}]_i$ for the wild-type and mutant KCNQ1 channels. $\Delta(zV_{1/2})$ directly reflects the change in the Ca^{2+} binding contribution to the ΔG of opening in response to an increase in $[Ca^{2+}]_i$.

To test whether mutants with gating perturbation changed the Ca^{2+} sensitivity of KCNQ1 channels, R259W, Q260W, E261W, F340A, and F351A were chosen specifically since they could elicit big macroscopic currents in the two-electrode voltage clamp which was necessary for successfully performing inside-out patch recording. Then the voltage-dependent activity of R259W, Q260W, E261W, F340A, and F351A was investigated at different $[Ca^{2+}]_i$ in inside-out patch configuration. The results are summarized in Table 4.11 and Fig. 4.17A. The data showed that mutations altered voltage-dependent gating in nominally 0 µM $[Ca^{2+}]_i$. Increasing $[Ca^{2+}]_I$ induced a leftward shift of the activation curve for R259W, Q260W, F340A, and F351A mutant channels. However, E261W mutant channels did not show any response to a change in $[Ca^{2+}]_i$ between 0 and 0.2 µM. (Fig. 4.17A).

I plotted $\Delta(zV_{1/2})$ induced by increased $[Ca^{2+}]_i$ for wild-type and mutant channels (Fig. 4.17B). R259W and F340A did not alter $\Delta zV_{1/2}$, indicating that they did not affect the KCNQ1 channels' Ca^{2+}-dependent activation. However, Q260W, E261W and F351A exhibited a decreased $\Delta zV_{1/2}$. The data suggested that KCNQ1 pore mutations can affect Ca^{2+} sensitivity of KCNQ1 gating. This directly confirmed that the gate of KCNQ1 channels is controlled by both voltage and Ca^{2+}.

Table 4.11: Gating parameters of wild type and mutant KCNQ1 channels at various intracellular [Ca^{2+}] from inside-out patches.

		0µM [Ca^{2+}]			0.025µM [Ca2+]			0.1µM [Ca2+]	
	n	$V_{1/2}$ (mV)	z	n	$V_{1/2}$ (mV)	z	n	$V_{1/2}$ (mV)	z
wild type	3	-33±2	2.5±0.1	3	-51±4	3.3±0.1	3	-59.0±0.8	3.2±0. 1
R259W	4	-7±1	2.5±0.1	4	-25±1	2.9±0.1	6	-32±1	3.7±0.1
Q260W	5	-2±2	1.60±0.08	4	-22.8±0.5	3.5±0.1	4	-25.2±0.3	3.5±0 .1
E261W	4	76±2	1.51±0.02	6	75±1	1.24±0.02	4	74.6±0.1	1.16±0.04
F340A	5	-40±1	2.0±0.1	4	-60±2	2.7±0.2	3	-68±2	2.66±0.05
F351A	4	43±2	1.92±0.04	4	9±1	2.5±0.1	4	6.4±0.7	2.8±0.1

Currents were recorded from inside-out macropatches. Bath solutions contained free Ca2+ concentration as indicated. The midpoint ($V_{1/2}$) and slope (z) of conductance-voltage relations are the mean ± SEM. Values were obtained from single Boltzmann functions fit to data of individual patches. n represents the number of patch recordings. Conductance was determined from tail currents recorded at -120 mV after voltage steps from -60 mV to +100 mV for 3 seconds.

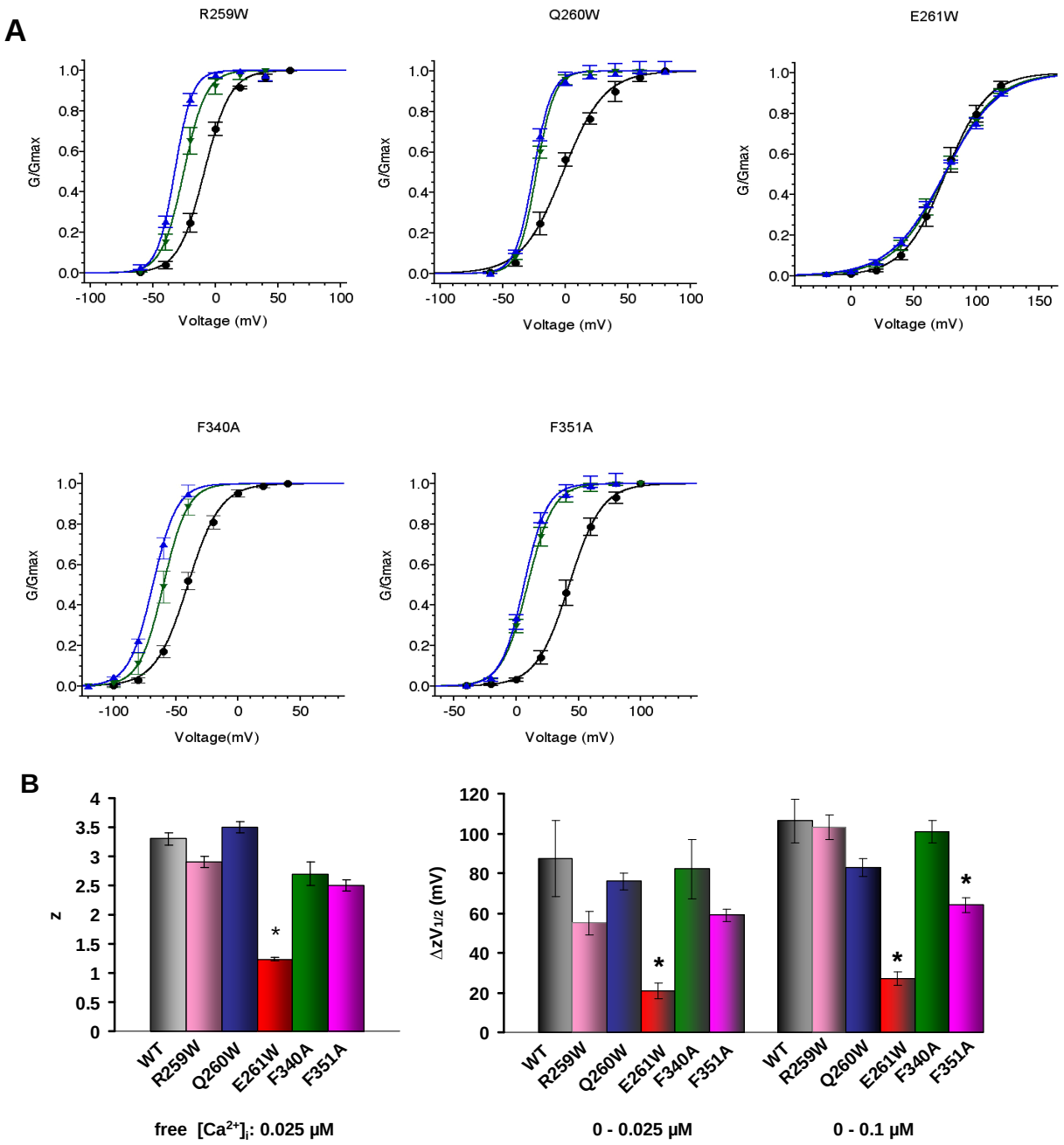

Figure 4.17: Voltage- and Ca^{2+}-regulation of wild-type and mutant KCNQ1 channels

(A) Conductance-voltage relations for currents recorded from inside-out patches over a range of voltage steps at different free Ca^{2+} concentrations (black: 0 µM; green: 0.025 µM; blue: 0.1µM). Conductance was determined from tail currents recorded upon repolarizations to −120mV and normalized by the observed maximum conductance (G_{max}). Data points were fit with the Boltzmann equation $G = G_{max}/(1 + \exp[-(x - V_{1/2}) \times zF/RT])$, where $V_{1/2}$ is the midpoint voltage, z is the gating valence, F is Faraday's constant, R is the gas constant, and T is absolute temperature in K. (B) Averaged parameters obtained from the fits of conductance-voltage relations for wild type and mutant KCNQ1 channels. Parameters were obtained at the $[Ca^{2+}]_i$ as indicated below the plots. $\Delta(zV_{1/2})=zV_{1/2}$ at lower $[Ca^{2+}]_i$–$zV_{1/2}$ at higher $[Ca^{2+}]_i$ (right) were calculated from each patch and then averaged (mean ± SEM; n=3 to 5). *, P<0.05, compared with wild type KCNQ1 channel.

4.3 KCNE1 and KCNQ1

Several potassium outward currents determine repolarization of cardiac action potentials, including the slowly activating delayed rectifier K^+ current, I_{Ks}. The I_{Ks} current is formed by the co-assembly of two proteins: KCNQ1 α-subunits and KCNE1 β-subunits (Barhanin et al. 1996; Sanguinetti et al. 1996). The most prominent effects of coexpression with KCNE1 are a markedly slowed activation and an increase in current magnitude compared to homotetrameric KCNQ1 channels. In addition, I_{Ks} channels exhibit altered relative Rb^+ conductance and no detectable inactivation when compared with KCNQ1 channels. The molecular mechanisms of the KCNE1 mediated changes in KCNQ1 channel gating are not well understood, but it has been suggested that the β-subunits may interact with the pore domain of KCNQ1 subunits (Romey et al. 1997; Tai & Goldstein, 1998; Melman et al. 2004). Here, I investigated the importance of amino acid residues in the KCNQ1 pore region for KCNE1 modulation.

4.3.1 Temperature-dependent I_{Ks} channels

Since I_{Ks} channels displayed very slow activation and did not saturate with prolonged depolarization, it was difficult to evaluate the voltage dependency of activation for I_{Ks} channels at room temperature (22℃). Previous studies have shown a temperature dependency in I_{Ks} channel activition (Seebohm, et al., 2001). I examined the temperature dependency of I_{Ks}. Representative current recording from Xenopus oocytes coexpressing KCNQ1 and KCNE1 at 22℃ and 32℃ are shown in Fig. 4.18. An increase in temperature enhanced the macroscopic currents, accelerated activation, and deactivation kinetics of KCNQ1/KCNE1 channel, consistent with the data published before (Seebohm, et al., 2001). Importantly, I_{Ks} currents saturated within 3 seconds depolarization pulse stimulation at 32℃, which allowed further investigation of the voltage-dependent activation properties for I_{Ks} currents.

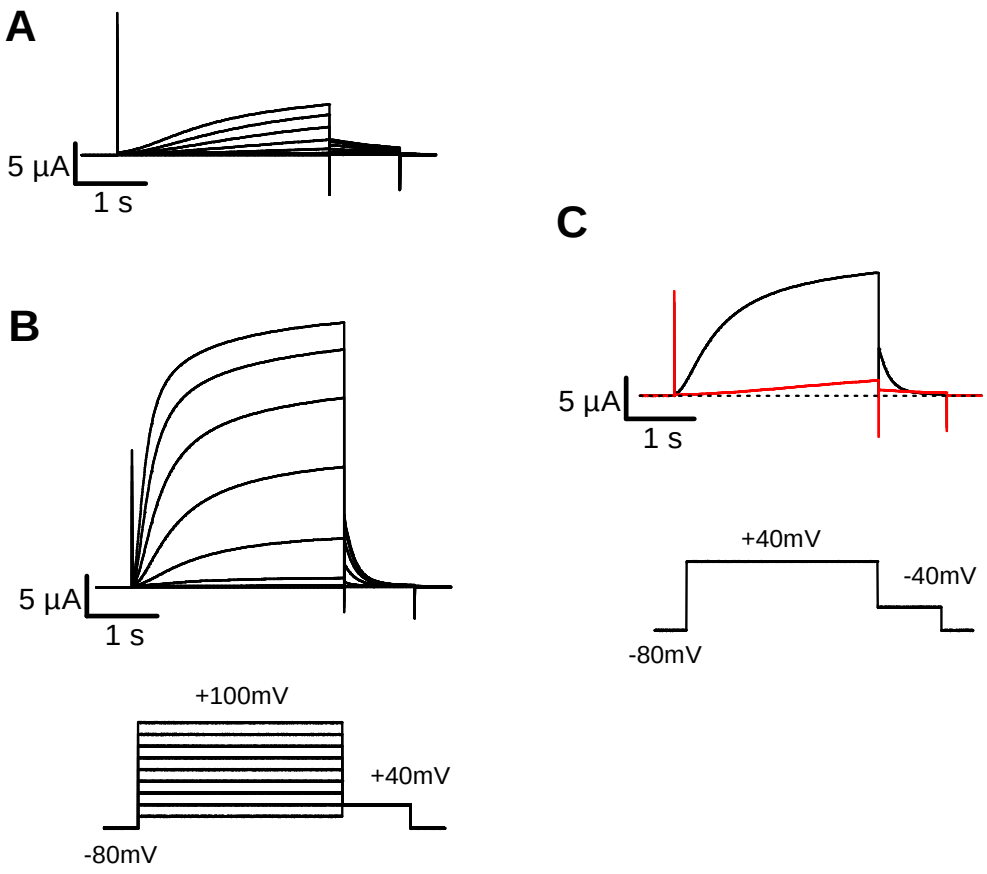

Figure 4.18: Temperature dependency of I_{Ks} channels.

(A) Representative voltage-dependent I_{Ks} current recording obtained with the two-electrode voltage clamp from *Xenopus* oocytes expressing KCNQ1/KCNE1 channels with the voltage protocol shown in the inset at 22℃.

(B) Recording performed at 32 ℃ using the same pul se protocol as in A.

(C) I_{Ks} current traces recorded at 22℃ (red colored) and at 32℃ (black colored) from same *Xenopus* oocyte are imposed with 3-second depolarizing voltage steps to + 40 mV followed by a 1-second step to -40 mV from a holding potential of – 80 mV.

4.3.2 KCNE1 effects on KCNQ1 pore mutants

KCNE1 is a gating modifier for KCNQ1. Assembly of KCNE1 with KCNQ1 leads to a great change in pore gating properties, e.g. slowing down the activation kinetics, positive shift of the voltage-dependent activation curve, deletion of inactivation, and alteration of G_{Rb}/G_K. To examine how KCNE1 may interact with the pore of KCNQ1 and modulate gating properties of the KCNQ1 channel, I chose to examine the mutant channel that obeyed the following criteria:

1. Functional expression
2. G_{Rb}/G_K : $(G_{Ala}+G_{Trp})/2 > 1.7$
3. 'hook' inactivation
4. Activation and current saturation

According to the data of KCNQ1 mutants in this study described before, 13 residues in the pore region were chosen as candidates for further experiments.

- S5: R259, Q260, I263, L266, F270, F275, Y278, F279, L282,
- Pore helix: A300W
- S6: W323A, V324, T327, A352W, L353

I coexpressed KCNQ1 pore mutations with KCNE1 in *Xenopus* oocytes to examine whether the pore mutations perturbed KCNE1 modulation of KCNQ1 gating. Injection of KCNE1 cRNA into oocytes generated a I_{Ks}-like current by coassembly with endogenous oocytes KCNQ1 (Sanguinetti, et al. 1996). I only analyzed the currents elicited by coexpression of KCNQ1 with KCNE1 that were larger than those induced by expression of KCNE1 alone.

Most of these KCNQ1 pore mutants generated recordable currents except of I263A and A352W when coexpressed with KCNE. Table 4.12 and Fig. 4.19 summarized KCNE1 modulations on the KCNQ1 pore mutants. The half-voltage for activation ($V_{1/2}$) was compared between the mutant alone and mutant with KCNE1.

The differences in $V_{1/2}$ ($\Delta V_{1/2}$) were calculated according to the following equation:

$$\Delta V_{1/2} = V_{1/2}^{mut/E1} - V_{1/2}^{mut}$$

where $V_{1/2}^{mut/E1}$ and $V_{1/2}^{mut}$ are $V_{1/2}$ values for KCNQ1 mutants coexpressed with KCNE1 or KCNQ1 mutant alone.

The differences in ΔGo brought by KCNE1 interaction were also calculated by the equation:

$$\Delta\Delta G_0 = \Delta G_0^{mut/E1} - \Delta G_0^{mut}$$

where $\Delta G_0^{mut/E1}$ and ΔG_0^{mut} are ΔG_0 values for KCNQ1 mutant coexpressed with KCNE1 or KCNQ1 mutant alone.

For wild-type KCNQ1, KCNE1 shifted $V_{1/2}$ of the activation curve by + 55 mV and the free energy difference for channel activation at 0 mV ($\Delta\Delta G_0$) was about + 3 kcal/mol compared with KCNQ1 channel alone. A great number of mutants could be modulated by KCNE1 similarly to that of wild-type KCNQ1. Four mutants (L266W, F275W, Y278A and F279A) strongly disturbed the KCNE1 gating modulation: $V_{1/2}$ could not be shifted positively by KCNE1 and $\Delta\Delta G_0$ was less than 1.0 kcal/mol (Fig. 4.19).

Shown in Fig. 4.20 and Fig. 4.21 are representative current recordings and G-V relations for these mutants in the absence and presence of KCNE1. When expressed alone, F275W and Y278A exhibited gating perturbation, while L266W and F279A displayed similar gating behavior as wild type KCNQ1 channels. Coexpression of these four mutants with KCNE1 did shift voltage-dependent activation although activation kinetics slowed down at room temperature. In contrast, coexpression of L263W with KCNE1 yielded a large shift in half voltage of activation ($V_{1/2}$) by +100 mV. Interestingly, L263W mutation alone induced a pronounced negative shift in $V_{1/2}$ by -12.9 mV.

Table 4.12 KCNE1 gating modulations on KCNQ1 pore mutants

KCNQ1					KCNQ1/KCNE1				KCNE1 efffect	
	n	$V_{1/2}$ mV	z	ΔGo kcal/mol	n	$V_{1/2}$ mV	z	ΔGo kcal/mol	$\Delta V_{1/2}$ mV	ΔΔGo kcal/mol
WT	36	-25.3±0.3	2.95±0.06	-1.73±0.05	40	24.6±0.7	1.74±0.03	1.0±0.04	59.9±0.08	2.73±0.07
R259A	5	28.9 ± 1.5	1.54 ± 0.04	1.02 ± 0.03	6	71.4±1.1	1.39 ±0.03	2.29±0.05	42.5±1.8	1.27±0.06
R259W	5	13.7±0.9	1.82±0.04	0.57±0.03	6	94.4±0.9	1.53±0.02	3 .33±0.05	80.7±0.13	2.76±0.06
Q260A	5	-11.9 ± 0.5	1.32 ± 0.04	-0.36 ± 0.03	5	48.1±0.8	1. 59±0.03	1.77±0.04	60.0±0.8	2.13±0.05
Q260W	4	10.1±0.8	1.75±0.06	0.41±0.04	4	81.7±1.9	1.54±0.06	2 .91±0.17	71.7±0.9	2.5±0.18
I263A	10	-17.7± 0.8	3.37 ± 0.26	-1.40± 0.14		Small current				
I263W	6	-38.2±0.6	3.50±0.10	-3.09±0.12	4	62.5±2.3	1.33±0.0 2	1.92±0.08	100.7±2.4	5.01±0.14
L266A	7	-20.9± 0.3	2.56 ± 0.18	-1.23± 0.10	4	38.1±0.6	1.59 ±0.03	1.40±0.04	59.0±0.07	2.66±0.11
L266W	5	-27.6±1.0	2.84±0.08	-1.81±0.09	4	-23.8±0.9	1.79±0. 06	-0.98±0.07	-3.8±1.3	0.83±0.15
F270A	5	-27.0±0.3	2.61±0.04	-1.62±0.03	4	26.5±1.4	1.91±0.0 6	1.16±0.05	53.5±1.4	2.78±0.06
F270W	4	-19.5±1.4	2.43±0.06	-1.10±0.09	4	19.0±1.3	2.21±0.0 7	0.97±0.08	38.5±1.9	2.07±0.12
F275A	4	-35.4±0.7	1.69±0.01	-1.38±0.04	4	43.9±0.1	1.83±0.0 3	1.85±0.02	79.3±0.7	3.23±0.05
F275W	5	-1.1±0.8	3.85±0.12	-0.10±0.07	5	13.1±1.0	1.93±0.09	0.57±0.02	14.2±1.3	0.67±0.05
Y278A	4	8.5±0.9	3.02±0.11	0.59±0.08	4	4.6±0.8	2.05±0.08	0.2 2±0.03	3.9±1.2	-0.37±0.09
Y278W	5	-6.9±0.6	1.65±0.05	-0.26±0.03	4	64.4±0.6	1.16±0.03	1.72±0.04	71.3±0.9	1.98±0.05
F279A	4	-32.3±0.9	2.93±0.08	-2.19±0.11	4	-46.4±0.8	2.28±0. 10	-2.44±0.15	14.1±1.2	-0.25±0.17
F279W	5	-21.6±0.8	3.25±0.12	-1.62±0.10	4	46.0±1.1	1.58±0.0 5	1.68±0.07	67.6±1.4	3.30±0.13
L282A	5	-23.0 ± 1.5	1.55 ± 0.14	-0.84 ± 0.12	4	26.2±0.8	2. 05±0.04	1.24±0.02	49.2±1.7	2.06±0.12
L282W	4	-8.2±1.6	3.22±0.13	-0.60±0.13	6	32.8±1.5	1.94±0.06	1.46±0.06	41.0±2.2	2.06±0.14
A300W	4	-7.5±0.5	3.16±0.08	-0.55±0.04		Small current				
W323A	5	-18.7±1.1	2.77±0.05	-1.20±0.09	5	43.3±1.6	1.66±0.0 4	1.66±0.04	62.0±1.9	2.86±0.10
V324A	7	-27.5 ± 1.8	2.78 ± 0.13	-1.75 ± 0.14	4	16.9±1.7	2. 05±0.02	0.80±0.07	44.4±2.5	2.55±0.16
V324W	4	-30.3±0.6	3.47±0.05	-2.42±0.08	4	46.4±1.4	1.54±0.0 5	1.65±0.06	76.7±1.5	4.07±0.10
T327A	5	-27.8 ± 0.5	2.87 ± 0.06	-1.85 ± 0.06	4	20.8±1.7	1. 57±0.03	0.75±0.06	48.6±1.8	2.60±0.09
T327W	4	-25.3±0.4	3.03±0.08	-1.77±0.06	3	70.0±3.1	1.33±0.0 2	2.12±0.07	95.3±3.1	3.90±0.09
A352W	4	39.5±3.5	1.00±0.02	0.91±0.06		Small current				
L353A	5	-42.5±2.1	0.86±0.06	-0.84±0.06	4	25.6±2.2	1.87±0.0 6	1.09±0.06	74.2±2.5	1.93±0.09
L353W	4	-27.8±0..6	3.13±0.08	-2.00±0.07	4	44.2±0.8	1.55±0. 07	1.58±0.07	72.0±1.0	3.58±0.11

Parameters of voltage dependence (half-activation voltage $V_{1/2}$ and slope z) for KCNQ1/KCNE1 were obtained by fitting the data to single Boltzmann function. Conductances were determined from tail currents recorded at -40 mV after 3-seconds voltage steps ranging from -80 mV to +80 mV in the condition of 32℃. The free energy of the channel a ctivation, ΔG_0, is calculated as $zV_{1/2}F$ (in kcal/mol). Data for KCNQ1 mutants alone are from Table. 4.3. Values are means ± SEM. n, number of experiment. Half-activation voltage shifted by coexpression with KCNE1 was calculated as follows: $\Delta V_{1/2} = V_{1/2}^{mut/E1} - V_{1/2}^{mut}$, where $V_{1/2}^{mut/E1}$ and $V_{1/2}^{mut}$ are $V_{1/2}$ values for KCNQ1 mutants coexpressed with KCNE1 or KCNQ1 mutant alone. The differences in ΔGo brought by KCNE1 interaction was also calculated by the equation: $\Delta\Delta G_0 = \Delta G_0^{mut/E1} - \Delta G_0^{mut}$, where $\Delta G_0^{mut/E1}$ and ΔG_0^{mut} are ΔG_0 values for KCNQ1 mutant coexpressed with KCNE1 or KCNQ1 mutant alone.

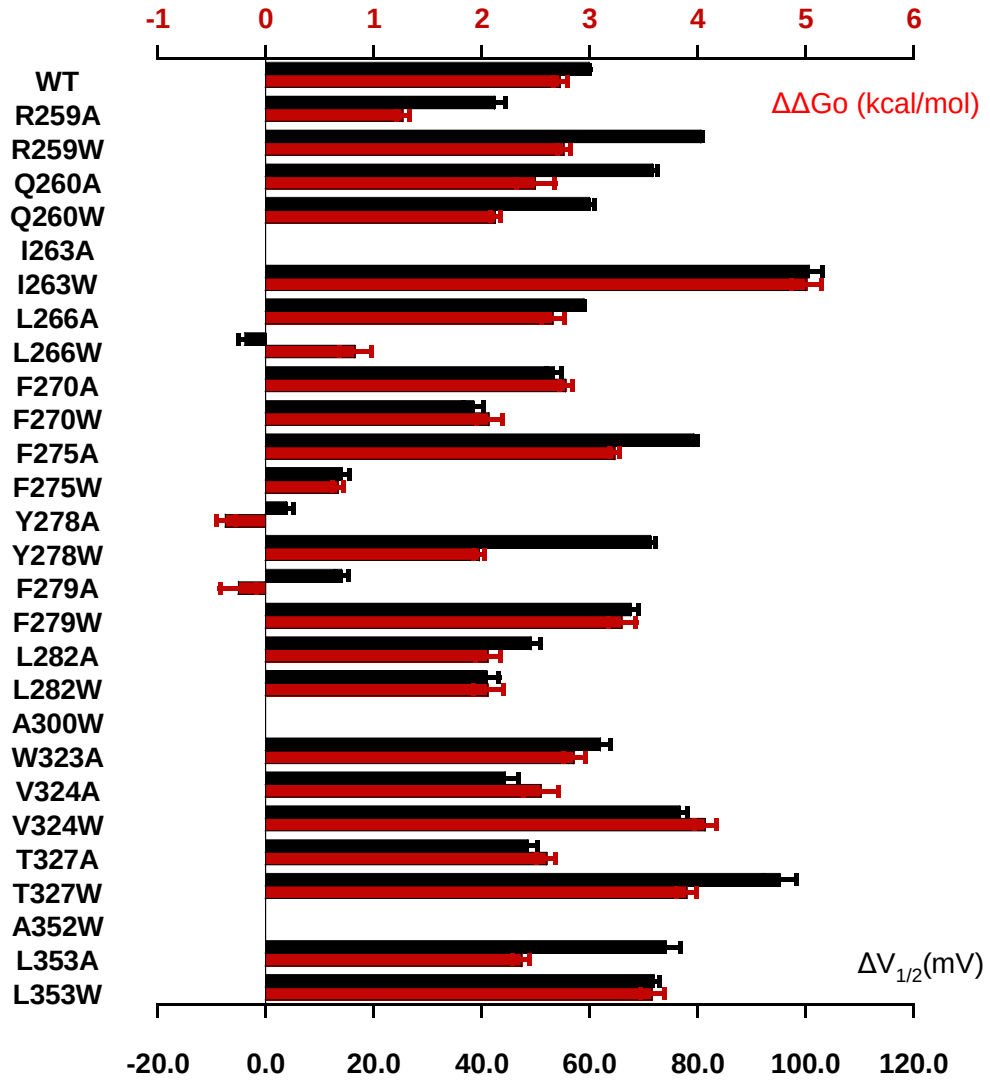

Figure 4.19: KCNE1 gating modulations on the KCNQ1 pore mutants.

As shown in Table 4.12, $\Delta V_{1/2}$ (black bars) and $\Delta\Delta G_0$ values (red bars) are plotted against KCNQ1 mutant types. Values are shown as mean ± SEM.

No detectable currents in I263A /KCNE1, A300W/KCNE1 and A352W/KCNE1.

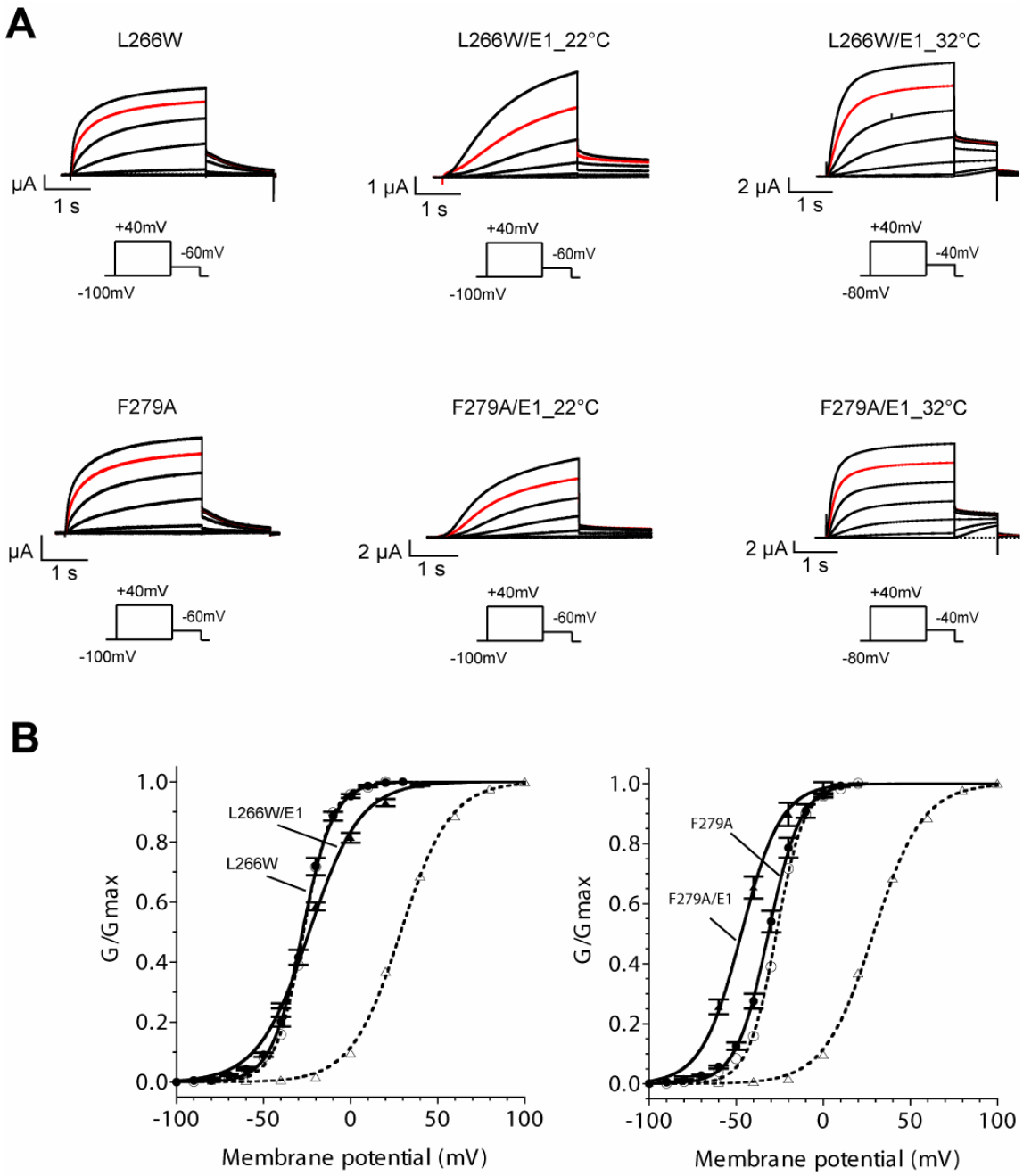

Figure 4.20: Defect of KCNE1 modulation by L266W and F279A KCNQ1 mutations.

A) Representative current recordings of L266W and F279A mutant KCNQ1 channels in the absence (performed at 22℃) and presence of KCNE1 (performed at 22℃ and 32℃). Currents were evoked by voltage steps from holding potential to +40 mV in 20 mV increment, holding potentials and tail potentials were shown in the inset. Current traces in red are the current responses to voltage step to +20 mV.

B) G-V relationships for the mutants in the absence of (filled circles) or presence of KCNE1 (32℃, filled triangle). Dashed lines indicate G-V relationship for wild-type KCNQ1 (open square) and KCNQ1/KCNE1 (32℃, open triangle). Normalized conductance–voltage relations were fitted to single Boltzmann functions with parameters listed in Table 4.12. Data are shown as mean ± SEM.

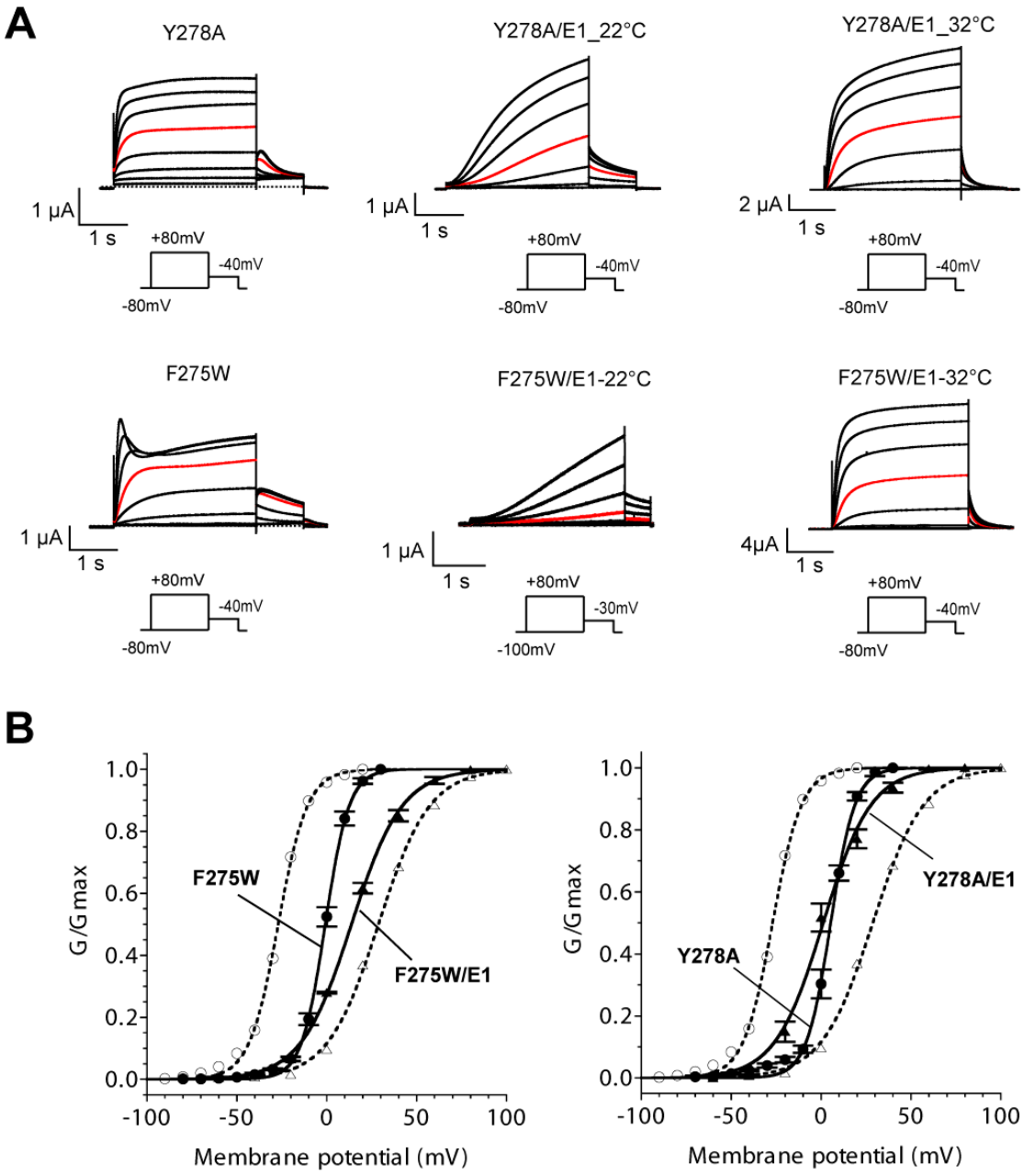

Figure 4.21: Defect of KCNE1 modulation by F275W and Y278A KCNQ1 mutations.

(A) Representative current recording for F275W andY278A mutant KCNQ1 channels in the absence (performed at 22℃) and presence of KCNE1 (performe d at 22℃ and 32℃). Currents were evoked by voltage steps from holding potential to +80 mV in 20 mV increment, holding potentials and tail potentials were shown in the inset. Current traces in red are the current responses to voltage step to +20 mV.

(B) G-V relationships for mutants alone (filled circle) or with KCNE1 (32℃, filled triangle) as indic ated. Dashed lines indicate G-V relationship for wild-type KCNQ1 (open squares) and with KCNE1 (32℃, open triangles). Normalized conductance–voltage relations were fitted to single Boltzmann functions with parameters listed in Table 4.12. Data are shown as mean ± SEM.

5 Discussion

5.1 Gating of KCNQ1 channel

The purpose of my study is to investigate the gating mechanism of the KCNQ1 channel. Residues in the pore region were systematically mutated and the mutational effects on the voltage-dependent activation were evaluated. Remarkably, KCNQ1 pore mutations perturb gating by changing half voltage for activation ($V_{1/2}$), but almost not the slope (z) of the activation curves (G-V), In contrast, *Shaker* pore mutations change $V_{1/2}$ and z such that a negative shift in $V_{1/2}$ is accompanied with a steep increase in z (Li-Smerin et al., 2000; Yifrach and MacKinnon, 2002). The gating mechanism of the *Shaker* Kv channel is thought (Zagotta et al., 1994) to involve relatively independent voltage dependent movements within four subunits followed by a concerted pore opening transition step

$$(C_1 \overset{K_1(V)}{\leftrightarrow} C_2 \overset{K_2(V)}{\leftrightarrow} C_3$$
$$\ldots\ldots \overset{K_m(V)}{\leftrightarrow} C_{m+1})^4 \overset{L}{\leftrightarrow} O$$

Shaker pore mutants, which affect channel activation in change in $V_{1/2}$ and z, mainly alter the final cooperative opening step. A possible explanation for the gating behavior of KCNQ1 is that KCNQ1 mutants might affect ‘early’ voltage-dependent transition steps in each subunit but not a concerted transition process. However, analysis of deactivation kinetics suggests that most KCNQ1 mutations do affect a final opening step. In conclusion, KCNQ1 gating may involve a different mechanism.

Voltage-gated K^+ channels have very similar membrane spanning domains, but exhibit a considerable diversity in their extra-membranous domains (Hille, 2001). For example, *Shaker* and KCNQ1 subunits possess distinct cytoplasmic channel assembly domains. The A-domain in the KCNQ1 C-terminus confers channel

assembly, while the ‘T1 domain’ in the *Shaker* N-terminus drives tetramerization and assembly specificity in *Shaker* Kv channel. The contrasting localizations mean, that only KCNQ1 possesses C-terminal assembly domain, which is directly attached to the pore. This may have an important influence on KCNQ1 gating. Probably the activation gate of KCNQ1 is dually controlled by voltage and ligands which bind to the C-terminus, reminiscent of BK and HCN channels.

5.1.1 Interface between voltage-sensor and the pore region

The distribution of non-expressing KCNQ1 mutants indicates that the packing between S5, S6, the P-helix, and the hinge region of S6 are very sensitive to mutation, but not that between the voltage sensor and the pore domain (Fig. 4.8). The interface between voltage sensor and pore domain is rather tolerant to mutation. The results showed that much of the transmembrane interface between voltage sensor and pore domain is relatively unconstrained, which is consistent with mutagenesis studies of *Shaker* (Soler-Llavina et al., 2006) and compatible with the X-ray structure of Kv1.2 channel (Long et al., 2005). Also, this observation confirms the proposed modular nature of voltage sensor and pore domains in Kv channels.

Previous studies of *Shaker* suggested that gating of the Kv channel involves two consecutive movements of voltage sensors. The first movement moves the bulk of the gating charge and corresponds to movement of the four voltage sensor domains between resting (R) and activated (A) states. The second motion results in a small amount of gating charge movement during the concerted opening step (Ledwell and Aldrich, 1999). Recent studies of *Shaker* indicated that mutations in an external cluster of the interface directly interfere with voltage-sensor activation (Soler-Llavina et al., 2006). Mutations in the equivalent positions of KCNQ1 (L271W (A), F275W, Y278A (W) and L282W) produce positive shifts in $V_{1/2}$ without a global structural change in the pore (Fig. 5.1). The residues are hydrophobic and substitution by a small alanine or a large tryptophan residue gave rise to gating perturbation. The

mutational effects might arise from a direct interaction between channel domains that interfere with voltage sensor movement. Alternatively, the mutations may alter the interaction of channel domains with lipids that might be critical for voltage sensor movement.

Interaction of the voltage sensor with the membrane lipid is functionally important (Lee et al., 2004; 2005), and lipid modification within the external leaflet has pronounced effects on voltage sensor activation (Ramu et al. 2006; Schmidt et al., 2006). This view is supported by molecular dynamics simulations, which demonstrated that the voltage sensor domain induces a local deformation of the lipid bilayer (Sands and Sansom, 2007).

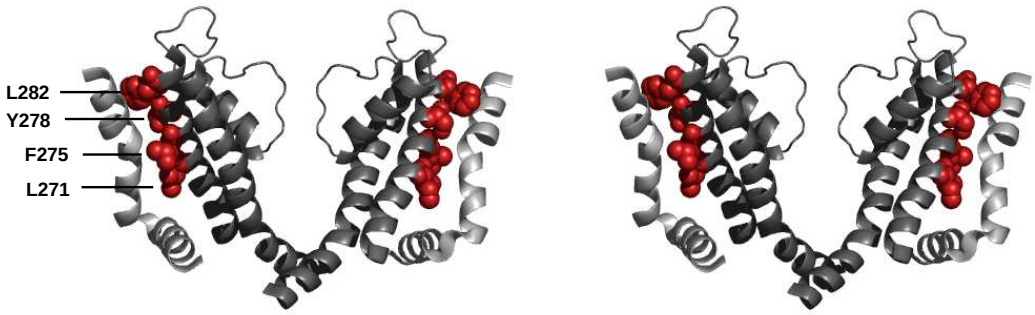

Figure 5.1: Mutations in the external half of the interface between voltage-sensor and the pore. Stereo pairs of the S4-S6 region viewed from the side showing only two subunits and the neighbouring S4 helix from two adjacent subunits with the gating-sensitive residues in the external half of the interface (colored red, shown CPK).

Interestingly, mutations in the inner half of the interface between voltage sensor and pore domains appear important for the coupling between voltage sensor movement and channel opening in *Shaker* (Soler-Llavina et al., 2006). Corresponding mutations in KCNQ1 (E261W, T264W and Y267A) induce not only gating perturbation, but also a global structural change in the pore (Fig. 5.2), raising the possibility that mutational effects on the coupling might result from direct influence of the S6 gate.

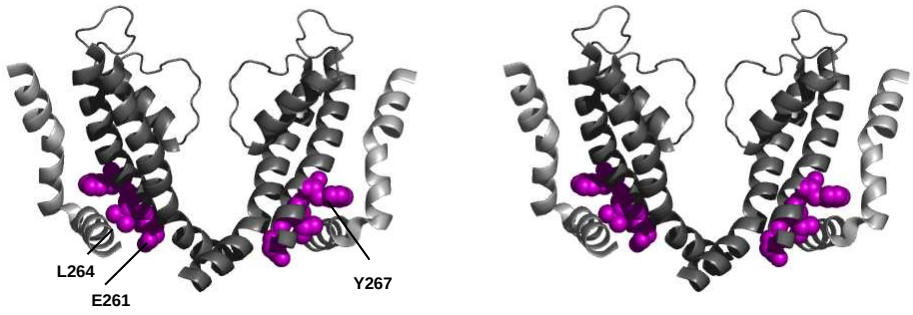

Figure 5.2: Gating-sensitive residues in the internal half of the interface between voltage-sensor and the pore. Stereo pairs of the S4-S6 region viewed from the side showing only two subunits and the neighbouring S4 helix from two adjacent subunits with the gating-sensitive residues in the internal half of the interface (colored magenta, shown CPK).

5.1.2 S4-S5 linker and C-terminal of S6

Biophysical and structural data on Kv1.2 suggested that the S4-S5 linker and C-terminus of S6 are quite important for coupling between voltage sensor movement and Kv channel opening and closing (Lu et al., 2002; Caprini, et al., 2005; Long et al., 2005). Consistent with these studies, this study demonstrates that gating-sensitive residues in KCNQ1 are located in both the S4-S5 linker and the C-terminus of S6 (Fig. 4.14). Note that different to the *Shaker* channel, the gate of KCNQ1 may be dually controlled by voltage and ligands (Ca^{2+}). The C-terminus of S6 may not only be involved in coupling to voltage sensor movements, but also to ligand conformational change. This picture might account for the different mutational effects that were observed at the equivalent positions of S6 in *Shaker* and KCNQ1 channels, where $V_{1/2}$ of G-V relations are shifted to opposite directions (Table 4.5).

5.1.3 The intracellular gate of KCNQ1

The results in the present study demonstrate that mutations in the intracellular half of S6, especially the mutations near the hinge point (PAG motif) either result in a channel with no recordable currents, or induce a global structural change (Fig. 4.8, Fig. 4.12). This implicates the importance of the intracellular half of S6 in channel gating. The advantage of my study is that a pore structural change of KCNQ1 could be inferred from G_{Rb}/G_K and inactivation properties. The results show that mutations in this region display strong alterations in G_{Rb}/G_K and inactivation properties, suggesting a global structural change in the pore. The mutations result in a channel with gating perturbation, which might result from a more general structural distortion of the S6 gate.

The results in my study suggest that activation of KCNQ1 appears to involve a PAG motif located closer to the C-terminus of the S6 domain by acting as a bending point as proposed for *Shaker* channels (Seebohm et al., 2006) (Fig. 5.3). A PVP motif is highly conserved in Kv1-KvX channels. This corresponds to an IPG motif in EAG and ERG channels and a PAG motif in KCNQ channels. Labro et al. (2003) showed that mutation of the second proline in the PVP motif to a glycine or alanine residue significantly impaired normal activation in Kv1.5. The results indicate an important difference in the activation gate of Kv and KCNQ channel families.

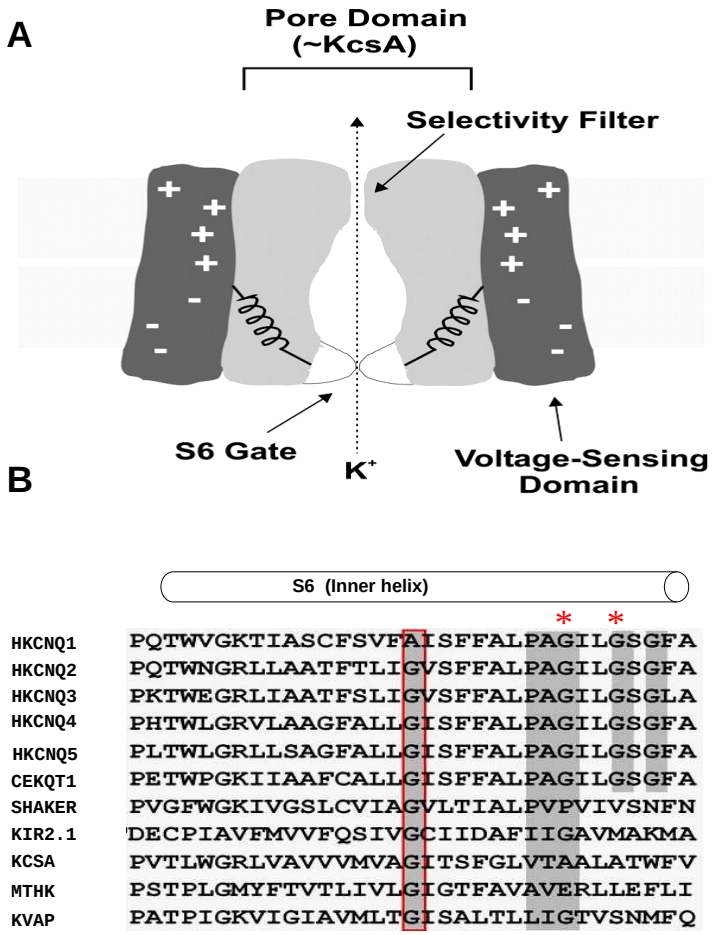

Figure 5.3: The intracellular gate region of K^+ channels.

(A) Cartoon of a Kv channel showing separate voltage-sensing and pore domains and an S6 activation gate towards the intracellular side of the pore. (B) Sequence alignment of several K^+ channels with the position of G345 and G348 marked by *. The gating hinge (box red) and PAG motif are indicated.

Glycine is regarded as a residue that confers flexibility to α-helix structure. Mutation of G345 or G348 into alanine results in a channel with voltage-dependency, while mutation into tryptophan results in a channel exhibiting inward rectifier property. The results indicate that the flexibility of G345 and G348 are important for KCNQ1 channel function.

Similar to the observations in my study, mutagenesis studies of the S6 activation gate in *Shaker* revealed that hydrophilic substitutions at P475 resulted in a channel that displays a large conductance at negative membrane voltages where the wild-type channel is normally closed (Hackos et al., 2002, Sukhareva et al., 2003). It was suggested that constitutively conducting mutants perturb the closed to open equilibrium in a way that allows for opening of the activation gate without prior activation of the voltage sensors. Further experiments are needed to clarify the inward rectifier phenotype observed in G345W and G348W channels.

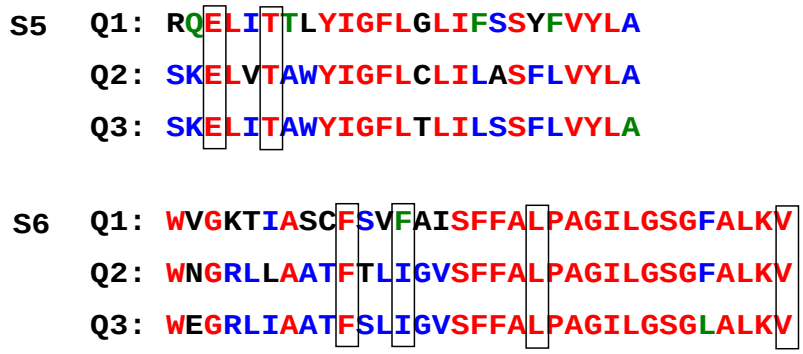

Figure 5.4: Sequence alignment of S5 and S6 between KCNQ1, KCNQ2, and KCNQ3. Residues which result in the channel with small G_{Rb}/G_K and no inactivation when mutated into Trp or Ala are boxed.

5.2 G_{Rb}/G_K and inactivation of KCNQ1

Despite of the high sequence homology of KCNQ channel subtypes, they display different biophysical properties. KCNQ1 exhibits a relatively high G_{Rb}/G_K and undergoes inactivation upon depolarization, whereas KCNQ2, KCNQ3 display a relatively small G_{Rb}/G_K and do not inactivate. Sequence alignment between KCNQ1, KCNQ2, and KCNQ3 indicates that residues which give rise to small Rb^+ conductance and no inactivation when mutated are conserved among the KCNQ family (Fig. 5.4), implicating that the mutational effects depend on sequence context. Mapping the residues onto the Kv1.2 structure showed that they were potentially involved in the interaction of P-helix with S5 and S6 below the selectivity filter (Fig. 4.11, left column). Consistent with the finding in this study, previous studies from Seebohm et al. (2003) demonstrated that mutations within this region produced particularly large effects on both G_{Rb}/G_K and inactivation, which appears to be tightly correlated. However, the mutagenesis scanning of the pore region in my studies illustrated that these two parameters are not correlated.

5.2.1 Conductance of KCNQ1

KCNQ1 channel displays unique relatively high Rb^+ conductance compared with K^+ (G_{Rb}/G_K). It has been proposed that high G_{Rb}/G_K of KCNQ1 is related to the dependence of a fast flickery process in opened channels on ion occupancy within the pore (Pusch, et al., 2000). Rb^+ is able to stabilize a flicker-open state because the selectivity filter in the open state has a different pore occupancy in high Rb^+ compared to high K^+ (Morais-Cabral et al. 2001). In agreement with this idea, results of the present study revealed that residues sensitive to a change in G_{Rb}/G_K were clustered into two groups (Fig. 4.10). One group was involved in the interaction of P-helix with S5 and S6 at the bottom of selectivity filter. Another one was in close contact with the

intracellular activation gate, which apparently influences stability of the open channel (Fig. 4.10). This indicated that the inner cavity of the pore domain may determine high G_{Rb}/G_K of KCNQ1. The selectivity filter has been reported to determine ion conduction properties in *Shaker* Kv channels (Kirsch et al., 1992). By contrast, the inner cavity is apparently involved in the discrimination among monovalent cations in KCNQ1 channels. In support of my observations, recent studies demonstrated that K^+ selectivity could be regulated through judicious engineering of cavity residues in Kir3.2 channels (Bichet et al., 2006). It seems likely that the interactions between permeant ions and KCNQ1 channel cavity influence ion selectivity and channel block by means of an electrostatic effect.

5.2.2 Inactivation of KCNQ1

The mechanism of KCNQ1 inactivation is not well characterized. Its biophysical characteristics differ from classical N and C-type inactivation of *Shaker*-like Kv channels. K^+ ions modulate C-type inactivation at an external pore site and N-type inactivation involves a direct pore occlusion at an internal site (Yellen, 2002). The inactivation of KCNQ1 is markedly prevented by the presence of KCNE1 (Pusch et al., 1998; Tristani-Firouzi and Sanguinetti, 1998). It has been suggested that this modification in channel kinetics is accomplished by the C-terminus of KCNE1 protruding into the KCNQ1 complex and binding to the pore loop (Romey et al. 1997). The data in the present study showed that residues, where mutations induced no inactivation but normal G_{Rb}/G_K were located at the interface between voltage sensor and C-terminus of S6 (Fig. 4.11, middle column). This indicated that inter- or intra-subunit interactions might play a role in KCNQ1 inactivation. Interestingly, most mutations which attenuated inactivation also changed the voltage-dependence of activation. There might be a coupling between inactivation and activation gating. Recent studies has shown that inactivation is also an intrinsic property of KCNQ4 and KCNQ5 channels (Jensen et al., 2007) Inactivation mechanisms for these KCNQ

channel subtypes might be similar.

Some mutations in the pore region of KCNQ1 induced a voltage-dependent macroscopic inactivation, not observed in wild-type KCNQ1. Previous studies regarded such kind of inactivation as enhanced inactivation (Seebohm et al., 2005). Molecular modeling of these residues onto the Kv1.2 structure showed that they were located around the inner cavity below the selectivity filter, and they were involved in the interaction with the intracellular gate (Fig. 4.11, right column). Interestingly, macroscopic inactivation has been also observed in the chimera KCNQ1*S6*Q2, which is constructed by introducing S6 of KCNQ2 into KCNQ1 (Seebohm et al., 2006). These results suggest that instability at the intracellular gate might contribute to this macroscopic inactivation.

Remarkably, recent studies revealed that mutations in CaM binding domains of C-terminus of KCNQ1 also induced such a macroscopic inactivation (Shamgar et al., 2006). In contrast to *Shaker* Kv channel, the gate of KCNQ1 is dually controlled by voltage sensor and ligand (Ca^{2+}/CaM). Previous studies from Ca^{2+} regulated SK channels suggested that Ca^{2+} binding induced the formation of the dimeric complex of CaM binding domains, which would drive a rotation between the S6 helices to open the gate (Schumacher et al., 2001). Mutations in CaM binding domains tend to disrupt the dimerization of CaMBD in the C-terminus, which in turn affects stability of the intracellular gate. Macroscopic inactivation induced by mutations in CaM binding domains may be regarded as another indication that KCNQ1 is voltage- and ligand-gated channel.

The mechanism, by which the channels become refractory to the applied stimulus, is commonly referred to as ‘desensitization’ or ‘inactivation’. Recent studies of MthK channel, a prokaryotic Ca^{2+}- activated K^+ channel, suggested that the desensitization of MthK arises from slippage of the interface of RCK domains of C-terminus, resembling that of a glutamate receptor (Sun et al., 2002; Kuo et al., 2007). Strikingly, previous studies of HCN channel, a cAMP-activated Kv channel, suggested that inactivation in HCN channels results from reclosure of the activation gate resembling the process of desensitization in ligand-gated channel (Shin et al., 2004). Similar to

HCN channel, KCNQ1 channel is also a ligand-gated Kv channel, and the inactivation mechanism of KCNQ1 is different from N-type or C-type inactivation. It is proposed that the inactivation of KCNQ1 channel might also arise from reclosure of the activation gate (Fig. 5.5). Depolarization leads to voltage-sensor movement and channel opening, but then weak linkage between voltage sensor and gate "fails," and the activation gate slips back to its shut position. Ca^{2+}/CaM may act either by opposing this slippage or by favoring the opening equilibrium.

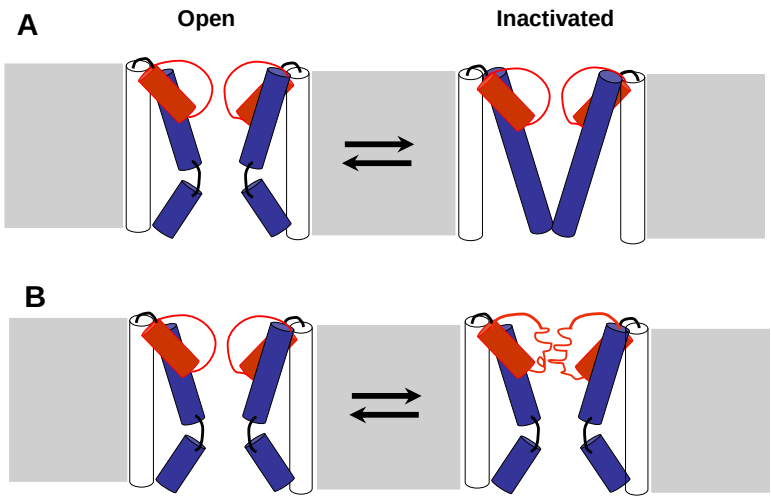

Figure 5.5: Cartoon of KCNQ1 inactivation & C-type inactivation of Kv channels.
(A) KCNQ1 inactivates resulting from reclosure of the activation gate. (modified from Shin et al., 2004). (B) C-type inactivation of Kv channels involves rearrangement of the selectivity filter.

5.3 Ca^{2+} regulation of KCNQ1

The mutagenesis studies of KCNQ1 in this study suggest that gating of KCNQ1 might be dually controlled by voltage and ligands. Previous studies showed that elevation of $[Ca^{2+}]_i$ in guinea pig ventricular myocytes enhanced I_{Ks} currents (Tohse et al. 1990). Moreover, CaM binding sites have been identified within the C-terminus of KCNQ channel family (Yus-Najera et al., 2002). Nevertheless, the attempt to define whether and how Ca^{2+}/CaM regulates any of the KCNQ homologs have produced conflicting results (Wen et al., 2002; Gamper et al., 2005; Gamper et al., 2006; Ghosh et al., 2006). Moreover, Ca^{2+}/CaM do not appear to regulate KCNQ1 or I_{Ks} currents in a heterologous system (Gamper et al., 2005). The present study provides new evidence that KCNQ1 and I_{Ks} channels are Ca^{2+}-regulated and that CaM confers Ca^{2+}-sensitivity to KCNQ1 and I_{Ks} current. This observation provides a molecular basis for the Ca^{2+} regulation of I_{Ks} in native myocytes. Most importantly, the results strongly support the idea that KCNQ1 is a ligand-gated and voltage-dependent K^+ channel.

An increase in intracellular $[Ca^{2+}]$ enhances the I_{Ks} current amplitude. Enhancement of current amplitudes can be accounted for by Ca^{2+}-induced leftward shifts in G-V curves. Application of the CaM antagonist W-7 markedly inhibits wild-type KCNQ1 and I_{Ks} currents and its effect is reversible, suggesting that CaM mediates Ca^{2+} regulation of KCNQ1 or I_{Ks} activity. In agreement with these data, coexpression of KCNQ1 or I_{Ks} channels with a Ca^{2+}-insensitive CaM mutant markedly attenuated the currents and produced a right-shift in the G-V curve of I_{Ks} channels expressed in *Xenopus* oocytes. The results suggest that CaM acts as a Ca^{2+} sensor that stimulates I_{Ks} channel activity. This dual voltage and Ca^{2+} dependence of I_{Ks} channel is somewhat reminiscent of the large-conductance Ca^{2+}-activated BK channel behavior (Fig. 5.6).

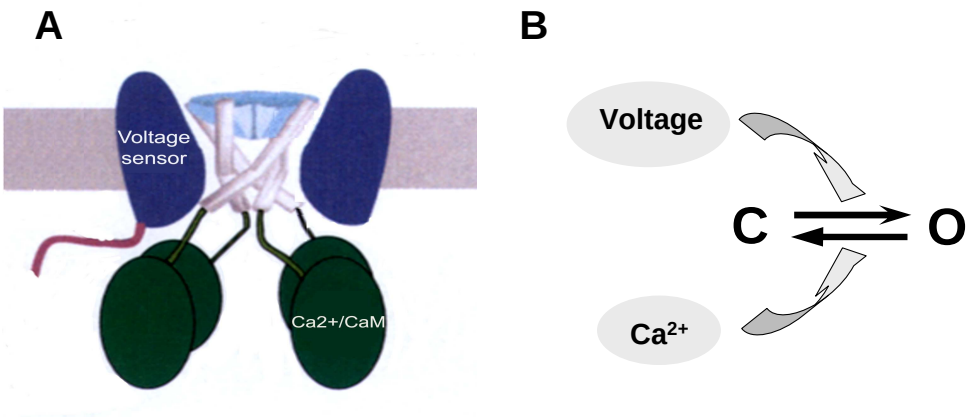

Figure 5.6: Allosteric gating model for KCNQ1 channels. A, Illustration of KCNQ1 channel regulation by voltage and Ca2+/CaM. B, KCNQ1 channel gating is regulated by voltage and Ca2+.

KCNQ1 pore mutations attenuate or completely abolish Ca^{2+} sensitivity, supporting the notion that gating of KCNQ1 is allosterically regulated by voltage sensor and Ca^{2+}. R259W, Q260W, E261W, F351A and F340A perturbed gating in nominal 0 Ca^{2+}, indicating that the coupling between voltage-senor movement and pore opening may be affected by these mutations. However, only E261W and F351A attenuated Ca^{2+}-sensitivity (Fig. 4.17). As shown in Figure 5.7, the residue E261 is located at S5, but it is in close contact with the gating hinge where S6 bending occurs upon channel opening. The residue F351 is located at the C-terminus of S6 below the hinge point. Both mutations E261W and F351A are thought to give rise to global structural changes according to their conduction and inactivation properties. Loss of Ca^{2+} sensitivity by E261W and F351A might arise from structural distortion of the activation gate, leading to decreased response to voltage and Ca^{2+}.

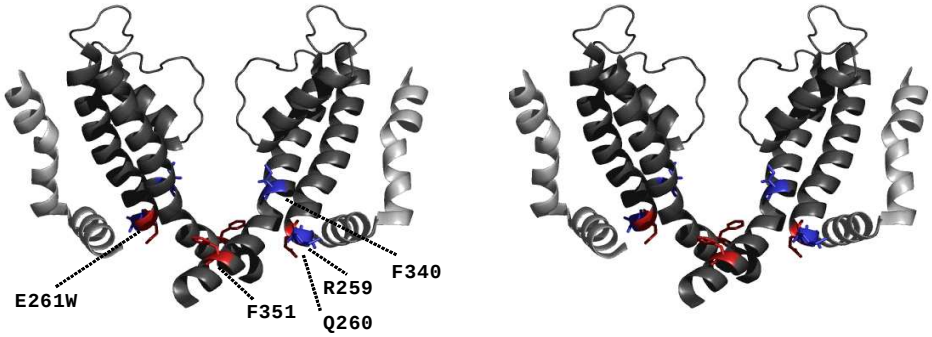

Figure 5.7: Distribution of mutants which attenuate the Ca^{2+} sensitivity of KCNQ1.

X-ray structure of Kv1.2 showing only the S5-S6 region from two subunits and the neighboring S4 helix from two adjacent subunits with the tested pore mutations colored. R259W, Q260W and F340A do not change the Ca^{2+} sensitivity (in blue), while E261W and F351A attenuate the Ca^{2+} sensitivity (in red).

The findings in my study revealed that increases in $[Ca^{2+}]_i$ in the range of from 0 to 100 nM caused left-shifts in G-V curves for KCNQ1 or I_{Ks}, but further rises in $[Ca^{2+}]$ (< 1 µM) did not produce further shifts. Apparently, Ca^{2+}-sensitivity of KCNQ1 or I_{Ks} is not observed when $[Ca^{2+}]_i$ is above 100nM. The observations may well explain conflicting data on Ca^{2+} sensitivity of KCNQ1 or I_{Ks} in heterologous expression systems published before, where increasing $[Ca^{2+}]_i$ by ionomycin ($[Ca^{2+}]_i$ > 0.1 nM) did not produce any change in current amplitude for KCNQ1 or I_{Ks} (Gamper et al., 2006), but reducing $[Ca^{2+}]_i$ by injecting BAPTA or EGTA had pronounced effects on current amplitude (Ghosh et al., 2006). The results in the present study demonstrate that the Ca^{2+} response of I_{Ks} is rapid, and kinetics of the Ca^{2+}-induced rise in I_{Ks} amplitude occurs within the time frame of a single action potential, implicating a physiological significance for Ca^{2+} regulation of I_{Ks}.

In line with this finding, recent studies illustrated that CaM binding is essential not only for proper channel gating, but also for channel folding and assembly (Shamgar et al., 2006; Ghosh et al., 2006), as is the case for the SK K^+ channel and the L-type Ca^{2+}

channel (Xia et al., 1998; Lee, 2003; Peterson et al., 1999). CaM acts as a chaperon which constitutively binds to the channel early in biogenesis of the channel complex and confers Ca^{2+}-regulation of channel. KCNE1 greatly increases KCNQ1 surface expression, indicating that KCNE1 may facilitate I_{Ks} channel assembly. KCNE1 might assemble with CaM-tethered KCNQ1 during the biogenesis of the channel complex, leading to enhancement of channel surface expression.

The results in this study show KCNE1 enhances the Ca^{2+}-sensitivity of KCNQ1. Raising [Ca^{2+}] from 0 to 0.1μM induced a left shift in G-V relation by 22 mV for KCNQ1, but 50mV for KCNQ1/KCNE1. Interestingly, the ß1 subunit of BK channels also increases Ca^{2+} sensitivity, marked by a more hyperpolarizing shift in the *G–V* relationship at a given Ca^{2+} concentration (Cox and Aldrich, 2000; Nimigean and Magleby, 2000; Qian and Magleby, 2003). Previous studies suggested that the ß1 subunit affects functional coupling between calcium binding and channel opening rather than calcium binding affinity (Cox and Aldrich, 2000; Nimigean and Magleby, 2000). KCNE1 might modify Ca^{2+} sensitivity of KCNQ1 gating through a mechanism similar to that proposed for the ß1 subunit of BK channels.

5.4 How KCNE1 interacts with KCNQ1

Though homomeric KCNQ1 channels are functional, physiological function of human cardiac KCNQ1 channels requires coassembly with single transmembrane domain ancillary subunits from the KCNE family (Barhanin et al., 1996; Sanguinetti et al., 1996). The interaction between pore forming α subunits and β subunits is a continuing subject for investigation. So far, how KCNE peptides can fit within α subunit tetramer and modulate gating of KCNQ1 is not well understood.

Several pieces of evidence indicate that KCNE1 interacts with the KCNQ1 pore. Specific residues within KCNE1 influence KCNQ1 gating. First, co-immunoprecipitation of chimeric α subunits with KCNE peptides demonstrates

physical interaction of these KCNE peptides with the potassium channel pore-lining region. Second, a specific region within the TM domains of KCNE protein impinges upon channel gating (Melman et al. 2004). Moreover, previous studies show that KCNE1 transmembrane residue T58 is required for voltage-dependent activation via interaction with F340 in the KCNQ1 S6 domain, placing KCNE1 close to the KCNQ1 channel pore (Panaghie et al., 2006). Here, the importance of the pore region of KCNQ1 for the gating control by KCNE1 has been investigated.

KCNE1 has multiple effects on KCNQ1 gating, including slowing of activation, shifting the voltage dependence of activation to more positive potentials, decreasing G_{Rb}/G_K, and removal of inactivation (Barhanin et al., 1996; Sanguinetti et al., 1996; Sesti and Goldstein, 1998; Yang and Sigworth, 1998). Pore mutations have their own caveats with regard to the possible changes in other channel gating properties. In the present study, I only chose residues in the KCNQ1 pore region which are not sensitive to a change in G_{Rb}/G_K and inactivation properties to investigate the KCNE1 gating modulation. Mapping these residues onto KcsA and Kv1.2 structure reveals that they are located at the periphery of the pore domain (Fig. 5.8). Apparently, there is space around these residues to accommodate KCNE1. It provides a good starting point to study how KCNE1 interacts with the pore of KCNQ1.

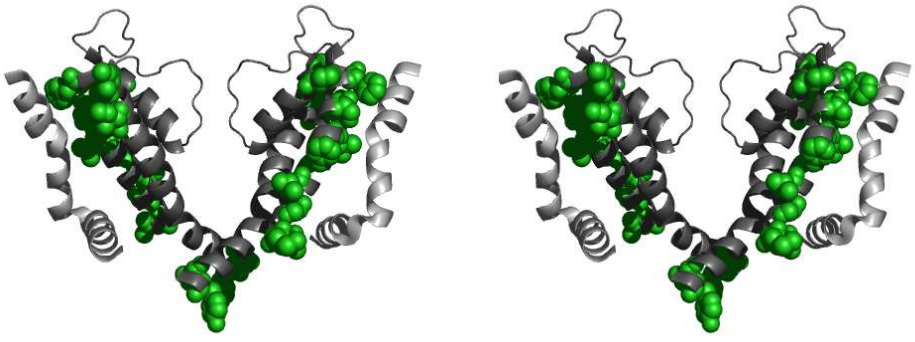

Figure 5.8: Distribution of residues which are insensitive to global structural changes. X-ray structure of Kv1.2 showing only the S5-S6 region from two subunits and the neighboring S4 helix from two adjacent subunits with the residues which are insensitive to global structural changes.

I_{Ks} currents exhibit very slow activation and do not saturate with prolonged depolarization (Pusch, et al., 2000). Previous study, therefore, examined the voltage-dependent activation of I_{Ks} isochronically (Tapper and George, 2000; Rocheleau et al., 2006; Chen et al., 2007), severely limiting the investigation of perturbation in the voltage-dependent activation for I_{Ks} currents. To circumvent this problem, the present study took advantage of the temperature-dependency of I_{Ks} currents. I_{Ks} reached steady-state activation at 32℃ within tes t potentials of 3-second activation. This allowed examining quantitatively mutational effects on voltage-dependent activation kinetics.

Voltage-dependent activation properties for KCNQ1 mutants were compared in the absence and presence of KCNE1. Most mutations did not alter KCNE1 gating modulation, indicating that these residues were not important for KCNE1 gating modulation. Four mutations (L266W, F275W, Y278A and F279A), however, impaired KCNE1 modulation on channel gating. Strikingly, L263W enhanced KCNE1 effect by shifting the $V_{1/2}$ for activation by about +100 mV. The observations indicated that these residues may be critical to KCNQ1 interaction with KCNE1.

Mapping these residues onto Kv1.2 structure shows that they are located to the S5 helix. F275, F278 and F279 are located at the interface between voltage-sensor and pore domain (Fig. 5.9). It is possible that interaction sites between KCNE1 and the pore region of KCNQ1 are state-dependent. KCNE1 transmembrane domain most likely undergoes cooperative movement upon channel opening. As a consequence, different residues in S5 are closer to the residing KCNE subunit at the closed and open states. KCNE1 is most likely in close contact with L266 at the closed state, but F275, Y278, F279 at the open state.

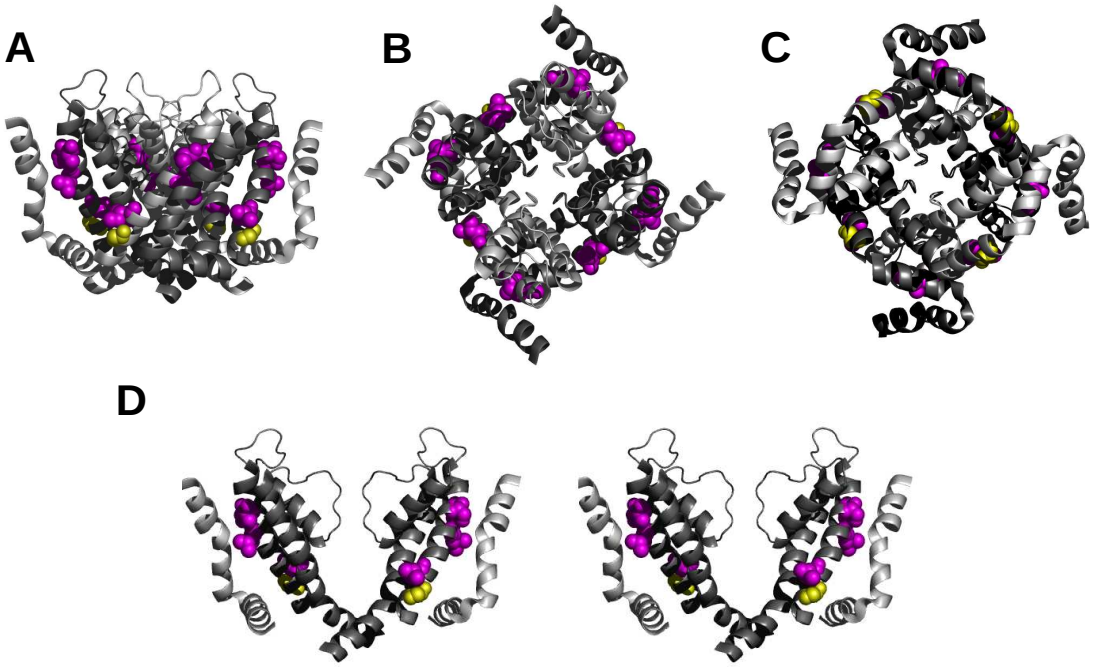

Figure 5.9: Defect of KCNE1 gating modulation mapped onto the Kv1.2 structure. (A) Backbone folding models of the S4-S6 region of Kv1.2 viewed from the side showing S4-S5 linker and S5-S6 region. The residues where the mutations attenuate KCNE1 modulation are colored magenta (L266, F275, Y278 and F279) and the residue where the mutation enhances KCNE1 effect is colored in yellow (L263). (B) View from the top (outside) colored as in (A). (C) View from the bottom (inside) colored as in (A). (D) Side view of stereo pairs of two subunits and nearby S4 helix from two adjacent subunits colored as in (A).

Previous studies indicated that KCNE1 interacts with the KCNQ1 pore, and specific residues within the KCNE domains are responsible for the gating control of KCNQ1 (Melman et al. 2002; Melman et al. 2004). KCNE1 has been shown to interact with KCNQ1 S6 because T58V KCNE1 appeared to rescue the phenotype of F340W (Melman, et al. 2004; Panaghie et al. 2006). Noted that the F340W mutant exhibits constitutive activation and macroscopic inactivation when expressed alone, indicating a dramatic structural change by F340W. Here, the findings in my study indicate that

mutations in S5 impair gating modulation by KCNE1, suggesting an important role of the interaction between S5 of KCNQ1 and KCNE1. The most important point is that these mutants do not give rise to a pore structural change when expressed alone.

Most interestingly, the activation of Kv3.1 and Kv3.2 is slowed by both KCNE1 and KCNE3 with minimal changes in voltage dependence (Lewis et al., 2004), suggesting that the observed contrasting effects of KCNE1 and KCNE3 are relatively specific to KCNQ1. Recent studies demonstrated that S4 of KCNQ1 is a critical determinant for the effects of KCNE1 and KCNE3 on KCNQ1 gating. Unique S4 charge paucity of KCNQ1 facilitates its unique conversion to a leak channel by KCNE3. Strikingly, loss of single S4 charges (R231 or R237) produced constitutively active KCNE1-KCNQ1 channels (Panaghie and Abbott. 2007), raising the possibility of KCNE1 interaction with KCNQ1 S4. It appears that KCNE1 modulates the voltage-dependency of KCNQ1 gating through voltage sensor and pore region.

Previous studies showed that the KCNE1 C-terminus is critical for modulation of KCNQ1 channel gating (Tapper and George, 2000). Removal of cytoplasmic domain adjacent to the transmebrane domain eliminated a hallmark of KCNE1 effects, the slow activation/deactivation kinetics of the KCNQ1/KCNE1 complex (Tapper and George, 2000). Mutations in the KCNE1 C-terminus have significant effects on voltage-dependence of the KCNQ1/KCNE1 channel (Rocheleau et al., 2006). The findings in this study suggested that the activation gate of KCNQ1 is allosterically regulated by voltage-sensors and Ca^{2+}/CaM. Therefore, the C-terminus of KCNE1 may exert its influence on channel gating through an interaction with the C-terminus of KCNQ1.

6 Summary

KCNQ channels (Kv7) represent a family of voltage-gated K^+ channels that play a major role in brain and cardiac excitability. Coassembly of KCNQ1 and the KCNE1 β subunit produces the I_{Ks} current that is crucial for repolarization of the cardiac action potential in the heart. Despite its physiological importance, the gating mechanism of KCNQ1 remains undetermined.

The objective of this study is to investigate the gating properties of the KCNQ1 channel by mutagenesis scanning. For this purpose, each residue in the KCNQ1 pore region (from G245 to V355) was systematically mutated into a small residue (alanine) and/or a bulky residue (tryptophan). cRNAs encoding the mutant channels were injected into *Xenopus* oocytes and the mutational effects on the voltage-dependent activation, conductance and inactivation were evaluated by the two-electrode voltage clamp technique. Changes in G_{Rb}/G_K and the extent of inactivation caused by KCNQ1 mutations were used as indicators for structural changes in the pore. This allowed evaluation of whether the mutation produces a local or a global structural change at an intuitive level, which provides more insight into the mutational effects on channel gating.

The results suggest that the gating mechanism of KCNQ1 is quite different from that of *Shaker* which was studied extensively via mutagenesis scanning before. Remarkably, KCNQ1 pore mutations perturb gating by changing half voltage for activation ($V_{1/2}$), but almost not the slope (z) of the activation curves. In contrast, *Shaker* pore mutations change $V_{1/2}$ and z cooperatively, such that a negative shift of $V_{1/2}$ is accompanied with a steep increase in z. The gating mechanism of the Kv channel is thought to involve relatively independent voltage-dependent movements within each of the four subunits followed by a concerted pore opening transition step:

$$(C_1 \overset{K_1(V)}{\longleftrightarrow} C_2 \overset{K_2(V)}{\longleftrightarrow} C_3$$
$$\ldots\ldots \overset{K_m(V)}{\longleftrightarrow} C_{m+1})^4 \overset{L}{\longleftrightarrow} O$$

Shaker pore mutants are believed to mainly influence the final cooperative opening step. This is not the case for KCNQ1. A possible explanation for the gating behavior of KCNQ1 is that KCNQ1 mutants might affect ‘early’ voltage-dependent transition steps in each subunit but not a concerted transition process. However, analysis of

deactivation kinetics suggests that most KCNQ1 mutants do affect the final concerted opening step. KCNQ1 gating may involve a different mechanism.

In contrast to *Shaker*, KCNQ1 possesses a large C-terminus where the binding sites for a Ca^{2+} sensor Calmodulin have been identified. In this study, the results from inside-out patch clamp experiments show that an increase in [Ca^{2+}] from 0 to 100nM induces a leftward shift in G-V curves of KCNQ1 channels. Application of the Calmodulin antagonist W-7 markedly inhibits the KCNQ1 currents, suggesting that Calmodulin mediates the Ca^{2+} regulation of the KCNQ1 channel. Additionally, I have identified the KCNQ1 pore mutations which attenuate the Ca^{2+} sensitivity. These results suggest that the gating of KCNQ1 is dually controlled by voltage and Ca^{2+}, which might account for the different gating kinetics of KCNQ1 and *Shaker* channels.

KCNE1 is an ancillary β subunit with a single transmembrane domain. Assembly of KCNE1 with KCNQ1 leads to a great change in the pore gating properties, e.g. slowing down the activation kinetics, positive shift of the voltage-dependent activation curve, deletion of inactivation and alteration in G_{Rb}/G_K. The interaction of KCNE1 with the KCNQ1 pore has been further explored in this study. Loss of KCNE1 gating modulation caused by some KCNQ1 pore mutations suggests that KCNE1 might interact with KCNQ1 pore through specific positions.

7 References

Aggarwal SK, MacKinnon R 1996. Contribution of the S4 segment to gating charge in the Shaker K^+ channel. *Neuron* 16:1169–77

Bai CX, Namekata I, Kurokawa J, Tanaka H, Shigenobu K, Furukawa T 2005. Role of nitric oxide in Ca2+ sensitivity of the slowly activating delayed rectifier K+ current in cardiac myocytes. *Circ Res.* 96: 64–72.

Barhanin J, Lesage F, Guillemare E, Fink M, Lazdunski M, and Romey G (1996). K(V)LQT1 and lsK (minK) proteins associate to form the I(Ks) cardiac potassium current. *Nature* 384: 78–80.

Bichet D, Grabe M, Jan YN, Jan LY (2006). Electrostatic interactions in the channel cavity as an important determinant of potassium channel selectivity. *Proc Natl Acad Sci U S A* 103:14355-60.

Caprini M, Fava M, Valente P, Fernandez-Ballester G, Rapisarda C, Ferroni S, Ferrer-Montiel A (2005). Molecular compatibility of the channel gate and the N terminus of S5 segment for voltage-gated channel activity. *J Biol Chem* 280:18253–64

Chen H, Goldstein SA (2007). Serial perturbation of MinK in IKs implies an {alpha}-helical transmembrane span traversing the channel corpus. *Biophys J* [Epub ahead of print]

Chen J, Mitcheson JS, Tristani-Firouzi M, Lin M, Sanguinetti MC (2001). The S4-S5 linker couples voltage sensing and activation of pacemaker channels. *Proc Natl Acad Sci USA* 98:11277–82

Cox DH, Aldrich RW. Role of the beta1 subunit in large-conductance Ca(2+)-activated K(+) channel gating energetics. Mechanisms of enhanced Ca(2+) sensitivity (2000). *J Gen Physiol* 116:411-32

Cui J, Aldrich RW (2000). Allosteric linkage between voltage and Ca(2+)-dependent activation of BK-type mslo1 K(+) channels. *Biochemistry* 39:15612-9.

Decher N, Chen J, Sanguinetti MC (2004). Voltage-dependent gating of hyperpolarization-activated, cyclic nucleotide-gated pacemaker channels: molecular coupling between the S4-S5 and C-linkers. *J Biol Chem* 279:13859–65.

Dedek K and Waldegger S (2001). Colocalization of KCNQ1/KCNE channel subunits in the mouse gastrointestinal tract. *Pflügers Arch* 442: 896–902.

del Camino D, Holmgren M, Liu Y, Yellen G (2000). Blocker protection in the pore of a voltage-gated K^+ channel and its structural implications. *Nature* 403:321–25

del Camino D, Yellen G (2001). Tight steric closure at the intracellular activation gate of a voltage-gated K^+ channel. *Neuron* 32:649–56

Delmas P, Brown DA (2005). Pathways modulating neural KCNQ/M (Kv7) potassium channels. *Nat Rev Neurosci* 6:850-62.

Doyle DA, Morais Cabral J, Pfuetzner RA, Kuo A, Gulbis JM, Cohen SL, Chait BT, MacKinnon R (1998). The structure of the potassium channel: molecular basis of K^+ conduction and selectivity. *Science* 280:69–77

Gamper N, Li Y, Shapiro MS (2005). Structural requirements for differential sensitivity of KCNQ K+ channels to modulation by Ca2+/calmodulin. *Mol Biol Cell* 6:3538-51.

Ghosh S, Nunziato DA, Pitt GS (2006). KCNQ1 assembly and function is blocked by long-QT syndrome mutations that disrupt interaction with calmodulin. *Circ Res* 98:1048-54.

Grabe M, Lai HC, Jain M, Nung Jan Y, Yeh Jan L (2007). Structure prediction for the down state of a potassium channel voltage sensor. *Nature* 445:550-3.

Grahammer F, Herling AW, Lang HJ, Schmitt-Graff A, Wittekindt OH, Nitschke R, Bleich M, Barhanin J, and Warth R (2001). The cardiac K^+ channel KCNQ1 is essential for gastric acid secretion. *Gastroenterology* 120: 1363–1371.

Grunnet M, Jespersen T, MacAulay N, Jorgensen NK, Schmitt N, Pongs O, Olesen SP, Klaerke DA (2003). KCNQ1 channels sense small changes in cell volume. J Physiol 549:419-27

Hackos DH, Chang TH, Swartz KJ (2002). Scanning the intracellular S6 activation gate in the shaker K+ channel. *J Gen Physiol* 119:521-32.

Heitzmann D, Koren V, Wagner M, Sterner C, Reichold M, Tegtmeier I, Volk T, Warth R (2007). KCNE beta subunits determine pH sensitivity of KCNQ1 potassium channels. *Cell Physiol Biochem* 19:21-32.

Hill B (2001). Ion Channels of Excitable membranes. Sunderland, MA: Sinauer Assoc. Inc.

Hodgkin AL, Huxley AF (1952). A quantitative description of membrane current and its application to conduction and excitation in nerve. *J. Physiol.* 117:500–44

Holmgren M, Shin KS, Yellen G (1998). The activation gate of a voltage-gated K^+ channel can be trapped in the open state by an intersubunit metal bridge. *Neuron* 21:617–21.

Isacoff EY, Jan YN, Jan LY (1991). Putative receptor for the cytoplasmic inactivation gate in the Shaker K^+ channel. *Nature* 353:86–90.

Jennifer L, Ledwell, and Richard W. Aldrich (1999). Mutations in the S4 Region Isolate the Final Voltage-dependent Cooperative Step in Potassium Channel Activation. *J Gen Physiol* 113:389-41.

Jensen HS, Grunnet M, Olesen SP (2007). Inactivation as a new regulatory mechanism for neuronal Kv7 channels. *Biophys J* 92:2747-56.

Jentsch TJ (2000). Neuronal KCNQ potassium channels: physiology and role in disease. *Nat Rev Neurosci* 1:21-30.

Jespersen T, Rasmussen HB, Grunnet M, Jensen HS, Angelo K, Dupuis DS, Vogel LK, Jorgensen NK, Klaerke DA, and Olesen SP (2004). Basolateral localisation of KCNQ1 potassium channels in MDCK cells: molecular identification of an N-terminal targeting motif. *J Cell Sci* 117: 4517–4526.

Jespersen T, Grunnet M, Olesen SP (2005). The KCNQ1 potassium channel: from gene to physiological function. *Physiology (Bethesda)* 20:408-16.

Jiang Y, Lee A, Chen J, Cadene M, Chait BT, MacKinnon R (2002). Crystal structure and mechanism of a calcium-gated potassium channel. *Nature* 417:515–22.

Jiang Y, Lee A, Chen J, Ruta V, Cadene M, Chait BT, MacKinnon R (2003). X-ray structure of a voltage-dependent K^+ channel. *Nature* 423:33–41.

Kanevsky M, Aldrich RW (1999). Determinants of voltage-dependent gating and open-state stability in the S5 segment of Shaker potassium channels. *J Gen Physiol* 114:215-42.

Kirsch GE, Drewe JA, Taglialatela M, Joho RH, DeBiasi M, Hartmann HA, Brown AM (1992). A single nonpolar residue in the deep pore of related K^+ channels acts as a K^+:Rb^+ conductance switch. *Biophys J* 62:136-44.

Kuo A, Gulbis JM, Antcliff JF, Rahman T, Lowe ED, Zimmer J, Cuthbertson J, Ashcroft FM, Ezaki T, Doyle DA (2003). Crystal structure of the potassium channel KirBac1.1 in the closed state. *Science* 300:1922–26.

Kuo MM, Baker KA, Wong L, Choe S (2007). Dynamic oligomeric conversions of the cytoplasmic RCK domains mediate MthK potassium channel activity. *Proc Natl Acad Sci U S A* 104:2151-6.

Kurokawa J, Motoike HK, Rao J, and Kass RS (2004). Regulatory actions of the A-kinase anchoring protein Yotiao on a heart potassium channel downstream of PKA phosphorylation. *Proc Natl Acad Sci USA* 101: 16374–16378.

Labro AJ, Raes AL, Snyders DJ (2005). Coupling of voltage sensing to channel opening reflects intrasubunit interactions in kv channels. *J Gen Physiol* 125:71-80.

Lai HC, Grabe M, Jan YN, Jan LY (2005). The S4 voltage sensor packs against the pore domain in the KAT1 voltage-gated potassium channel. *Neuron* 47:395-406

Latorre R, Olcese R, Basso C, Gonzalez C, Munoz F, Cosmelli D, Alvarez O (2003). Molecular coupling between voltage sensor and pore opening in the Arabidopsis inward rectifier K+ channel KAT1. *J Gen Physiol* 122:459-69.

Ledwell JL, Aldrich RW (1999). Mutations in the S4 region isolate the final voltage-dependent cooperative step in potassium channel activation. *J. Gen. Physiol* 113:389–414.

Lee A, Zhou H, Scheuer T, Catterall WA (2003). Molecular determinants of Ca(2+)/calmodulin-dependent regulation of Ca(v)2.1 channels. *Proc Natl Acad Sci U S A* 100:16059-64.

Lee AG (2004). How lipids affect the activities of integral membrane proteins, *Biochim Biophys Acta* 1666**:** 62–87.

Lee SY, Lee A, Chen J, MacKinnon R (2005). Structure of the KvAP voltage-dependent K+ channel and its dependence on the lipid membrane. *Proc Natl Acad Sci U S A* 102:15441-6.

Li-Smerin Y, Hackos DH, Swartz KJ (2000). A localized interaction surface for voltage-sensing domains on the pore domain of a K+ channel. *Neuron* 25:411-23.

Liu YS, Sompornpisut P, Perozo E (2001). Structure of the KcsA channel intracellular gate in the open state. *Nat Struct Biol* 8:883–87

Long SB, Campbell EB, Mackinnon R (2005a). Crystal structure of a mammalian voltage-dependent Shaker family K^+ channel. *Science* 309:897–903

Long SB, Campbell EB, Mackinnon R (2005b). Voltage sensor of Kv1.2: structural basis of electromechanical coupling. *Science* 309:903–8

Loussouarn G, Park KH, Bellocq C, Baro I, Charpentier F, and Escande D (2003). Phosphatidylinositol-4,5-bisphosphate, PIP2, controls KCNQ1/KCNE1 voltage-gated potassium channels: a functional homology between voltage-gated and inward rectifier K^+ channels. *EMBO J* 22: 5412–5421.

Lu Z, Klem AM, Ramu Y (2001). Ion conduction pore is conserved among potassium channels. *Nature* 413:809–13.

Lu Z, Klem AM, Ramu Y (2002). Coupling between voltage sensors and activation gate in voltage-gated K^+ channels. *J Gen Physiol* 120:663–76

Marten I, Hoshi T (1998). The N-terminus of the K channel KAT1 controls its voltage-dependent gating by altering the membrane electric field. *Biophys J* 74:2953-62.

Marx SO, Kurokawa J, Reiken S, Motoike H, D'Armiento J, Marks AR, and Kass RS (2002). Requirement of a macromolecular signaling complex for beta adrenergic receptor modulation of the KCNQ1-KCNE1 potassium channel. *Science* 295: 496–499.

McCormack K, Tanouye MA, Iverson LE, Lin JW, Ramaswami M, McCormack T, Campanelli JT, Mathew MK, Rudy B (1991). A role for hydrophobic residues in the voltage-dependent gating of Shaker K^+ channels. *Proc Natl Acad Sci USA* 88:2931–35

Melman, Y.F., A. Krumerman, and T.V. McDonald (2002). A single transmembrane site in the KCNE-encoded proteins controls the specificity of KvLQT1 channel gating. *J Biol Chem* 277:25187–25194.

Melman, Y.F., S.Y. Um, A. Krumerman, A. Kagan, and T.V. McDonald (2004). KCNE1 binds to the KCNQ1 pore to regulate potassium channel activity. *Neuron* 42:927–937.

Morais-Cabral JH, Zhou Y & MacKinnon R (2001). Energetic optimization of ion conduction rate by the K^+ selectivity filter. *Nature* 414, 37-42.

Nimigean CM, Magleby KL (2000). Functional coupling of the beta(1) subunit to the large conductance Ca(2+)-activated K(+) channel in the absence of Ca(2+). Increased Ca(2+) sensitivity from a Ca(2+)-independent mechanism. *J Gen Physiol* 115:719-36.

Panaghie G, Tai KK, Abbott GW (2006). Interaction of KCNE subunits with the KCNQ1 K+ channel pore. *J Physiol* 570:455-67.

Panaghie G, Abbott GW (2007). The role of S4 charges in voltage-dependent and voltage-independent KCNQ1 potassium channel complexes. *J Gen Physiol* 129:121-33.

Park KH, Piron J, Dahimene S, Merot J, Baro I, Escande D, Loussouarn G (2005). Impaired KCNQ1-KCNE1 and phosphatidylinositol-4,5-bisphosphate interaction underlies the long QT syndrome. *Circ Res* 96:730-9.

Pathak M, Kurtz L, Tombola F, Isacoff E (2005). The cooperative voltage sensor motion that gates a potassium channel. *J Gen Physiol* 125:57–69

Peterson BZ, DeMaria CD, Adelman JP, Yue DT (1999). Calmodulin is the Ca2+ sensor for Ca2+ -dependent inactivation of L-type calcium channels. *Neuron* 22:549-58.

Potet F, Scott JD, Mohammad-Panah R, Escande D, and Baro I (2001). AKAP proteins anchor cAMP-dependent protein kinase to KvLQT1/IsK channel complex. *Am J Physiol Heart Circ Physiol* 280: H2038–H2045.

Prole DL, Yellen G (2006). Reversal of HCN channel voltage dependence via bridging of the S4-S5 linker and Post-S6. *J Gen Physiol* 128:273-82.

Pusch M, Magrassi R, Wollnik B, Conti F (1998). Activation and inactivation of homomeric KvLQT1 potassium channels. *Biophys J* 75:785-92.

Pusch M, Bertorello L, Conti F (2000). Gating and flickery block differentially affected by rubidium in homomeric KCNQ1 and heteromeric KCNQ1/KCNE1 potassium channels. *Biophys J* 78:211-26

Qian X, Magleby KL (2003). Beta1 subunits facilitate gating of BK channels by acting through the Ca^{2+}, but not the Mg^{2+}, activating mechanisms. *Proc Natl Acad Sci U S A* 100:10061-6.

Ramu Y, Xu Y, Lu Z (2006). Enzymatic activation of voltage-gated potassium channels. *Nature* 442:696-9.

Robbins J (2001). KCNQ potassium channels: physiology, pathophysiology, and pharmacology. *Pharmacol Ther* 90:1-19.

Rocheleau JM, Gage SD, Kobertz WR (2006). Secondary structure of a KCNE cytoplasmic domain. *J Gen Physiol* 128:721-9.

Romey G, Attali B, Chouabe C, Abitbol I, Guillemare E, Barhanin J, Lazdunski M (1997). Molecular mechanism and functional significance of the MinK control of the KvLQT1 channel activity. *J Biol Chem* 272:16713-6

Sands ZA, Sansom MS (2007). How does a voltage sensor interact with a lipid bilayer? Simulations of a potassium channel domain. Structure 15:235-44.

Sanguinetti MC, Curran ME, Zou A, Shen J, Spector PS, Atkinson DL, and Keating MT (1996). Coassembly of K(V)LQT1 and minK (IsK) proteins to form cardiac I(Ks) potassium channel. *Nature* 384: 80–83.

Sanguinetti MC, Xu QP (1999). Mutations of the S4-S5 linker alter activation properties of HERG potassium channels expressed in Xenopus oocytes. *J. Physiol.* 514:667–75.

Schmidt D, Jiang QX, MacKinnon R (2006). Phospholipids and the origin of cationic gating charges in voltage sensors. *Nature* 444:775-9.

Schmitt N, Schwarz M, Peretz A, Abitbol I, Attali B, Pongs O (2000). A recessive C-terminal Jervell and Lange-Nielsen mutation of the KCNQ1 channel impairs subunit assembly. *EMBO J* 19:332-40.

Schoppa NE, McCormack K, Tanouye MA, Sigworth FJ (1992). The size of gating charge in wild-type and mutant Shaker potassium channels. *Science* 255:1712-5.

Schroeder BC, Waldegger S, Fehr S, Bleich M, Warth R, Greger R, and Jentsch TJ (2000). A constitutively open potassium channel formed by KCNQ1 and KCNE3. *Nature* 403: 196–199.

Schwake M, Pusch M, Kharkovets T, and Jentsch TJ (2000). Surface expression and single channel properties of KCNQ2/KCNQ3, M-type K^+ channels involved in epilepsy. *J Biol Chem* 275: 13343–13348.

Seebohm G, Lerche C, Busch AE, Bachmann A (2001). Dependence of I(Ks) biophysical properties on the expression system. *Pflugers Arch* 442:891-5.

Seebohm G, Scherer CR, Busch AE, Lerche C (2001). Identification of specific pore residues mediating KCNQ1 inactivation. A novel mechanism for long QT syndrome. *J Biol Chem* 276:13600-5.

Seebohm G, Sanguinetti MC, Pusch M (2003). Tight coupling of rubidium conductance and inactivation in human KCNQ1 potassium channels. *J Physiol* 552:369-78.

Seebohm G, Westenskow P, Lang F, Sanguinetti MC (2005). Mutation of colocalized residues of the pore helix and transmembrane segments S5 and S6 disrupt deactivation and modify inactivation of KCNQ1 K+ channels. *J Physiol* 563:359-68.

Seoh SA, Sigg D, Papazian DM, Bezanilla F. 1996. Voltage-sensing residues in the S2 and S4 segments of the Shaker K+ channel. *Neuron* 16:1159-67.

Sesti F and Goldstein SA (1998). Single-channel characteristics of wild-type IKs channels and channels formed with two minK mutants that cause long QT syndrome. *J Gen Physiol* 112: 651–663.

Shalaby FY, Levesque PC, Yang WP, Little WA, Conder ML, Jenkins-West T, Blanar MA (1997). Dominant-negative KvLQT1 mutations underlie the LQT1 form of long QT syndrome. *Circulation* 96(6):1733-6.

Shamgar L, Ma L, Schmitt N, Haitin Y, Peretz A, Wiener R, Hirsch J, Pongs O, Attali B (2006). Calmodulin is essential for cardiac IKS channel gating and assembly: impaired function in long-QT mutations. *Circ Res* 98(8):1055-63.

Shin KS, Maertens C, Proenza C, Rothberg BS, Yellen G (2004). Inactivation in HCN channels results from reclosure of the activation gate: desensitization to voltage. Neuron 41:737-44.

Sigworth FJ (1994). Voltage gating of ion channels. *Q. Rev. Biophys.* 27:1–40

Smith-Maxwell, J.L. Ledwell and R.W. Aldrich (1998). Role of the S4 in Cooperativity of Voltage-dependent Potassium Channel Activation. *J. Gen. Physiol* 111:399–420

Soler-Llavina GJ, Chang TH, Swartz KJ (2006). Functional interactions at the interface between voltage-sensing and pore domains in the Shaker K(v) channel. *Neuron* 52:623-34.

Sukhareva M, Hackos DH, Swartz KJ (2003). Constitutive activation of the Shaker Kv channel. *J Gen Physiol* 122:541-56.

Sun Y, Olson R, Horning M, Armstrong N, Mayer M, Gouaux E (2002). Mechanism of glutamate receptor desensitization. *Nature* 417:245-53.

Schumacher MA, Rivard AF, Bachinger HP, Adelman JP (2001). Structure of the gating domain of a Ca2+-activated K+ channel complexed with Ca2+/calmodulin. *Nature* 410:1120-4.

Swartz KJ (2004). Towards a structural view of gating in potassium channels. *Nat Rev Neurosci* 5:905–16

Tai KK, Goldstein SA (1998). The conduction pore of a cardiac potassium channel. *Nature* 391:605-8.

Tapper, A.R., and A.L. George Jr (2000). MinK subdomains that mediate modulation of and association with KvLQT1. *J Gen Physiol* 116:379–390

Terrenoire C, Clancy CE, Cormier JW, Sampson KJ, and Kass RS (2005). Autonomic control of cardiac action potentials: role of potassium channel kinetics in response to sympathetic stimulation. *Circ Res* 96: e25–e34.

Tohse N (1990). Calcium-sensitive delayed rectifier potassium current in guinea pig ventricular cells. *Am J Physiol* 258:H1200-7.

Tristani-Firouzi M, Sanguinetti MC (1998). Voltage-dependent inactivation of the human K+ channel KvLQT1 is eliminated by association with minimal K+ channel (minK) subunits. *J Physiol* 510:37-45

Vallon V, Grahammer F, Richter K, Bleich M, Lang F, Barhanin J, Volkl H, and Warth R (2001). Role of KCNE1-dependent K^+ fluxes in mouse proximal tubule. *J Am Soc Nephrol* 12: 2003–2011.

Voets T, Droogmans G, Wissenbach U, Janssens A, Flockerzi V, Nilius B (2004). The principle of temperature-dependent gating in cold- and heat-sensitive TRP channels. *Nature* 430:748-54.

Webster SM, Del Camino D, Dekker JP, Yellen G (2004). Intracellular gate opening in Shaker K^+ channels defined by high-affinity metal bridges. *Nature* 428:864–68.

Wen, H., and Levitan, I. B. (2002). Calmodulin is an auxiliary subunit of KCNQ2/3 potassium channels. *J Neurosci* 22: 7991–8001.
Xia XM, Fakler B, Rivard A, Wayman G, Johnson-Pais T, Keen JE, Ishii T, Hirschberg B, Bond CT, Lutsenko S, Maylie, Adelman JP (1998) Mechanism of calcium gating in small-conductance calcium-activated potassium channels. *Nature* 395: 503-7

Yang Y and Sigworth FJ (1998). Single-channel properties of IKs potassium channels. *J Gen Physiol* 112: 665–678.

Yellen G (2002). The voltage-gated potassium channels and their relatives. *Nature* 419:35-42.

Yifrach O, MacKinnon R (2002). Energetics of pore opening in a voltage-gated K(+) channel. *Cell* 111:231-9.

Yus-Najera E, Santana-Castro I, Villarroel A (2002). The identification and characterization of a noncontinuous calmodulin-binding site in noninactivating voltage-dependent KCNQ potassium channels. *J Biol Chem* 277:28545-53.

Zagotta WN, Hoshi T, Aldrich RW (1994). Shaker potassium channel gating. III: Evaluation of kinetic models for activation. *J Gen Physiol* 103:321-62

Zei PC, Aldrich RW (1998). Voltage-dependent gating of single wild-type and S4 mutant KAT1 inward rectifier potassium channels. *J Gen Physiol* 112:679-713.

Zhang H, Craciun LC, Mirshahi T, Rohacs T, Lopes CM, Jin T, Logothetis DE (2003). PIP(2) activates KCNQ channels, and its hydrolysis underlies receptor-mediated inhibition of M currents. *Neuron* 37:963-75.

Zhou M, Morais-Cabral JH, Mann S, MacKinnon R (2001). Potassium channel receptor site for the inactivation gate and quaternary amine inhibitors. *Nature* 411:657–61

8 Appendix

8.1 Abbreviations

A	Ampere (electric current unit)
AKAP	A-kinase anchoring protein
BK	big conductance Ca2+ potatssium channel
C	electric capacitance
CPK	space-filling model developed by Corey_Pauling-Koltun
$[Ca^{2+}]$	Calcium concentration
CaM	Calmodulin
DMSO	dimethylsulphoxide
EGTA	(ethylene glycol-bis(2-aminoethyl-ether) -N,N,N',N'-tetracetic acid
Exp	exponential
F	Faraday constant
F_{ina} (%)	inactivation fraction
G_{Rb}/G_K	relative Rb^+ conductance compared to K^+
GV	conductance-voltage relationship
h	hour
HEPES	N-(2-hydroxyethyl)piperazine-N'-(2-ethanesulfonic acid)
I	electric current
I_{KS}	cardiac slowly activating delayed rectifier current
KcsA	potassium channel from Streptomyces lividans
Kv	voltage-activated potassium channel
Kir	inward rectifier potassium channel
LQT	Long QT syndrome
MthK	Methanobacter thermoautotropium potassium channel
nA	nanoampere
OR2	oocyte Ringer 2 solution
pA	picoampere
PIP2	Phosphatidylinositol (4,5)-bisphosphate
PCR	polymerase chain reaction
RT	room temperature
SK	small conductance voltage- and Ca^{2+}-gated K^+ channel
TOK	Two-Pore Rectifying K^+ channel
TM	transmembrane segment
Tricain	3-Aminobenzoic acid ethyl ester
$V_{1/2}$	half voltage of activation
(v /v)	volume /volume
W-7	calmodulin antagonist N-(6-Aminohexyl)-5-chloro-1-naphthalenesulfonamide hydrochloride
WT	wild-type
(w / v)	weight / volume
z	slope of voltage-dependent activation
ΔG_0	Gibb´s free energy
^oC	degree of Celsius
τ	tau, time constant
µA	macroampere

8.2 Voltage-dependent activation recordings for KCNQ1 mutant channels

Representative voltage-dependent activation current traces recorded from *Xenopus* oocytes expressing wild-type and the KCNQ1 mutant channels in 20 mM K^+ bath solutions in two-electrode voltage clamp. Depolarizations were from holding potential to the potential indicated in 20 mV increments. Holding potential was -80 mV, -100 mV or -120 mV, and tail potential was or -100 mV, -120 mV or -140 mV as indicated in the inset. Current traces in red are current responses to voltage steps to -20 mV.

KCNQ1 pore Trp mutants: R259W to L271W

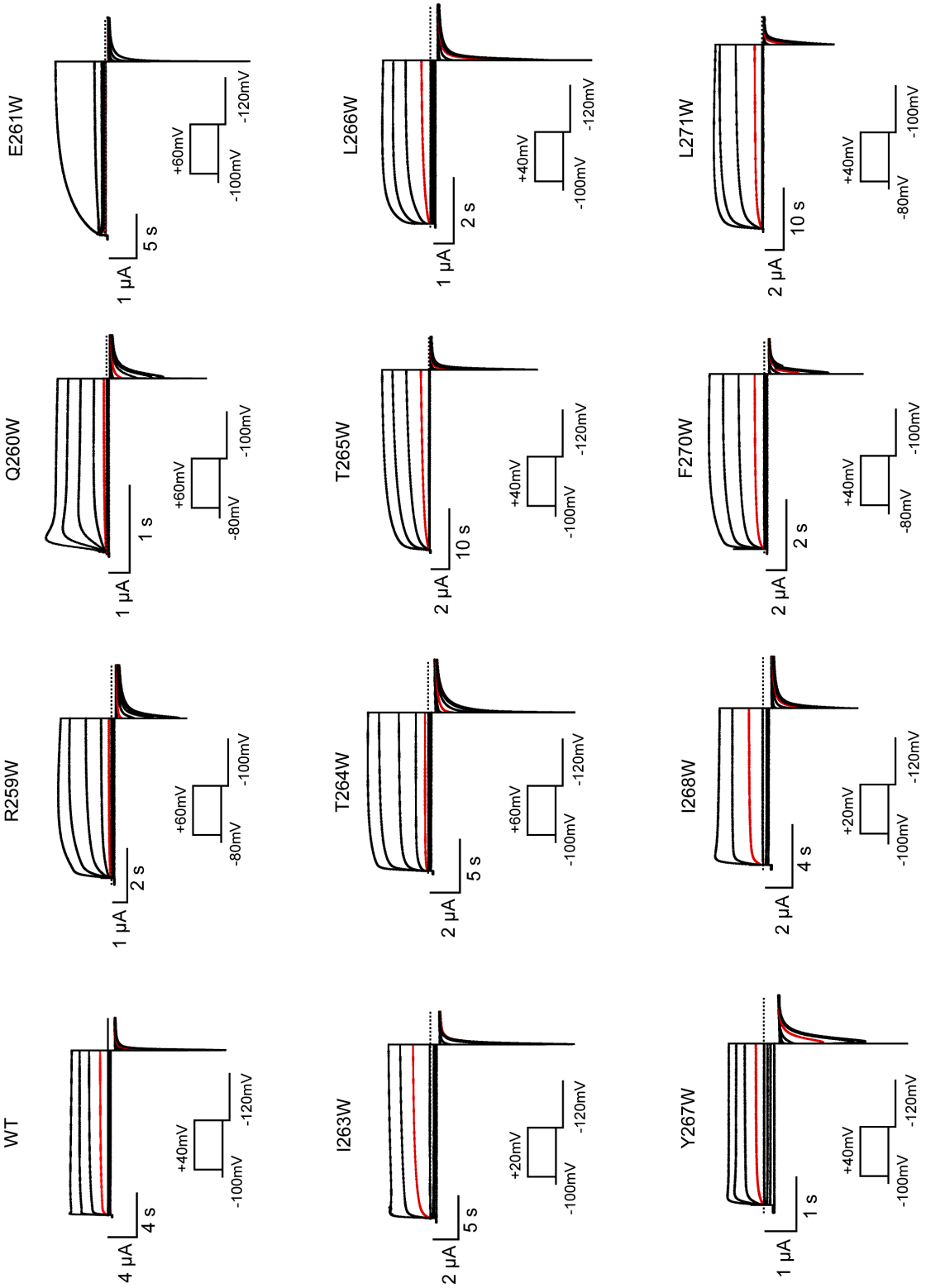

KCNQ1 pore Trp mutants: G272W to V294W

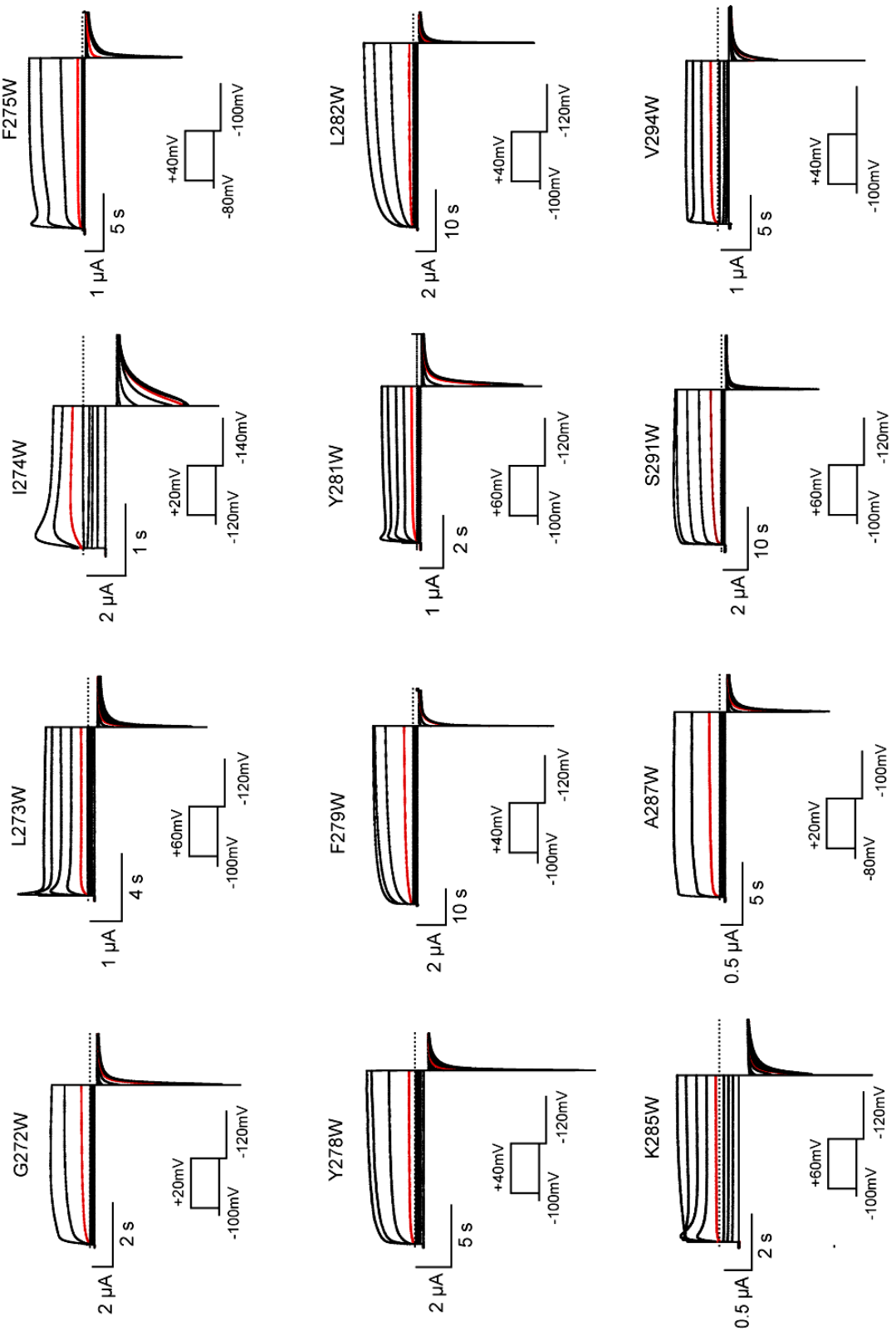

KCNQ1 pore Trp mutants: G297W to L353W

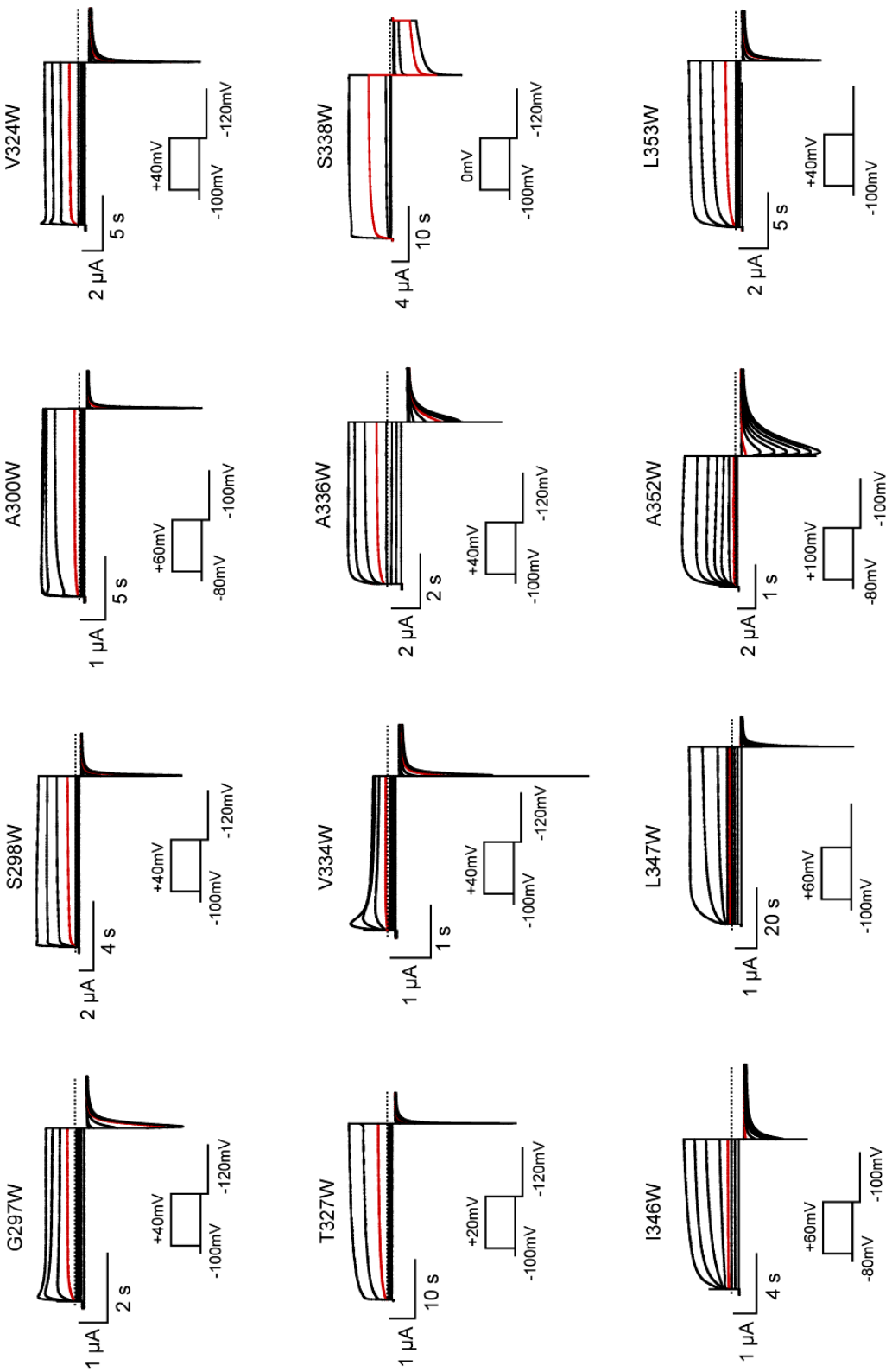

KCNQ1 pore Trp mutants: K354W to V355W

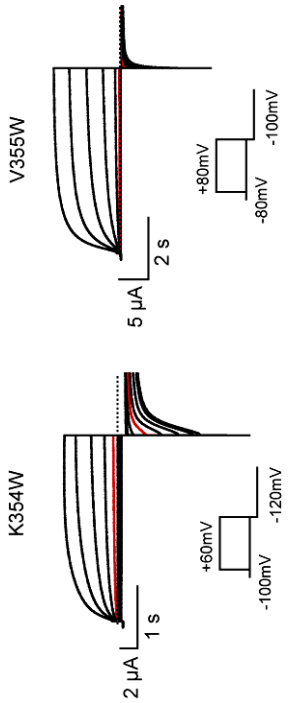

KCNQ1 S4-S5 linker mutants: G245W to L257W

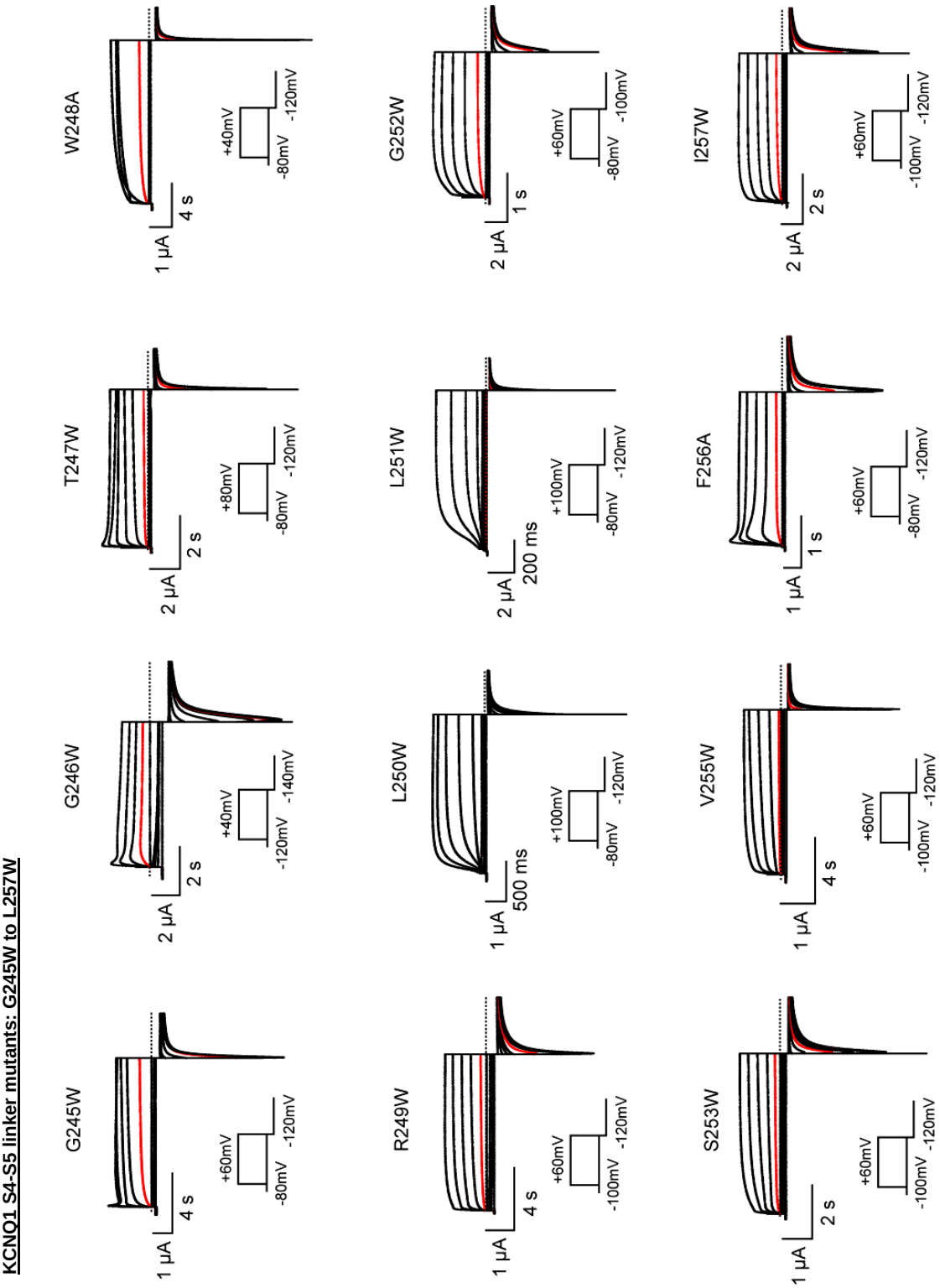

KCNQ1 S4-S5 linker mutants: H258W

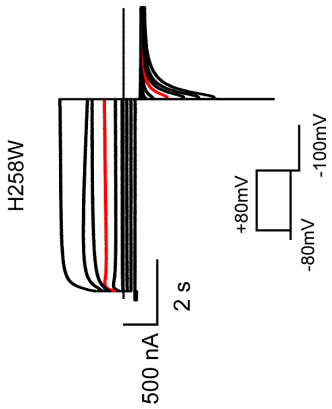

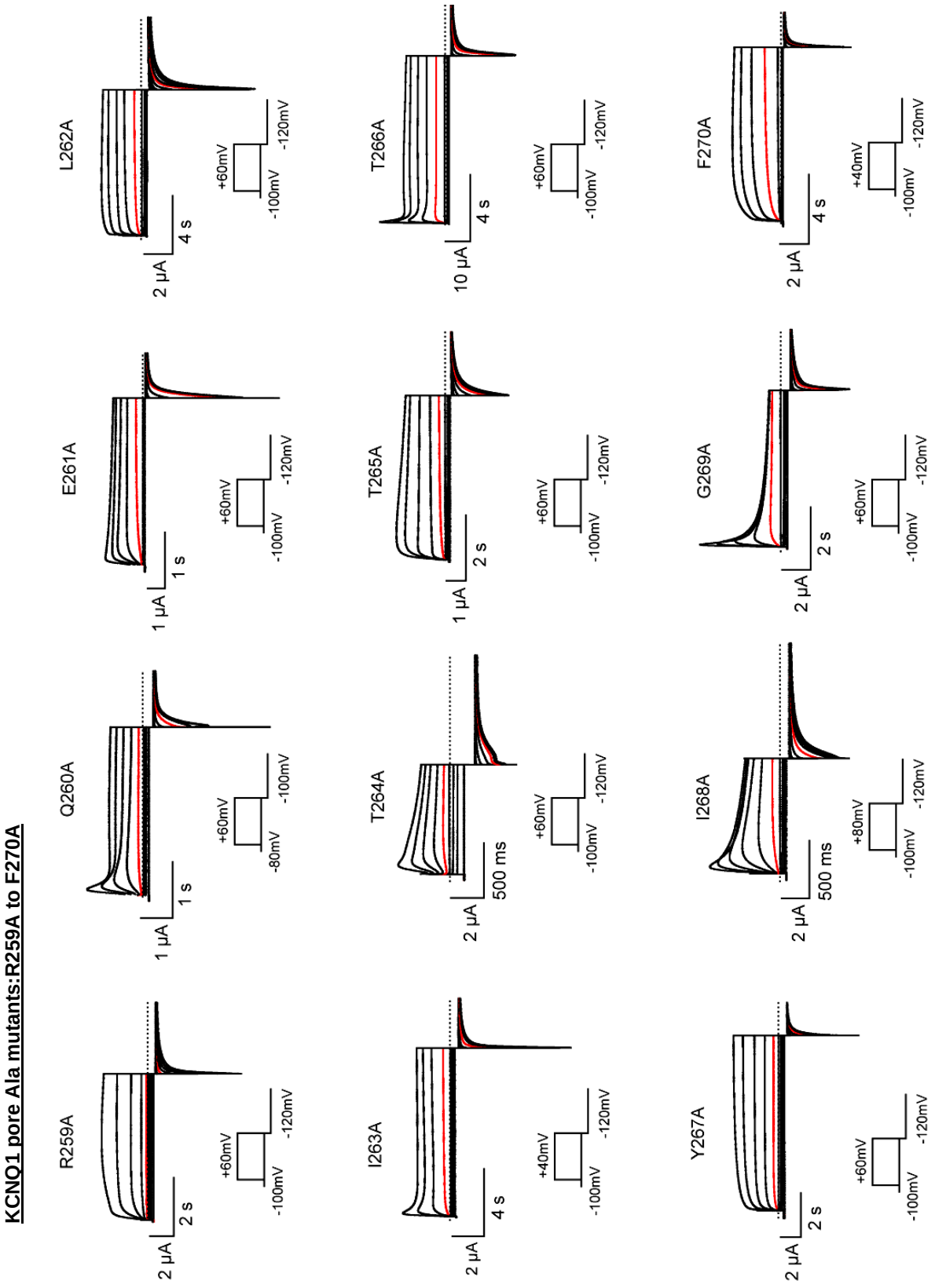
KCNQ1 pore Ala mutants:R259A to F270A
R259A
2 µA
2 s
+60mV
-100mV
-120mV
Q260A
1 µA
1 s
+60mV
-80mV
-100mV
E261A
1 µA
1 s
+60mV
-100mV
-120mV
L262A
2 µA
4 s
+60mV
-100mV
-120mV
I263A
2 µA
4 s
+40mV
-100mV
-120mV
T264A
2 µA
500 ms
+60mV
-100mV
-120mV
T265A
1 µA
2 s
+60mV
-100mV
-120mV
T266A
10 µA
4 s
+60mV
-100mV
-120mV
Y267A
2 µA
2 s
+60mV
-100mV
-120mV
I268A
2 µA
500 ms
+80mV
-100mV
-120mV
G269A
2 µA
2 s
+60mV
-100mV
-120mV
F270A
2 µA
4 s
+40mV
-100mV
-120mV

KCNQ1 pore Ala mutants: L271A to N289A

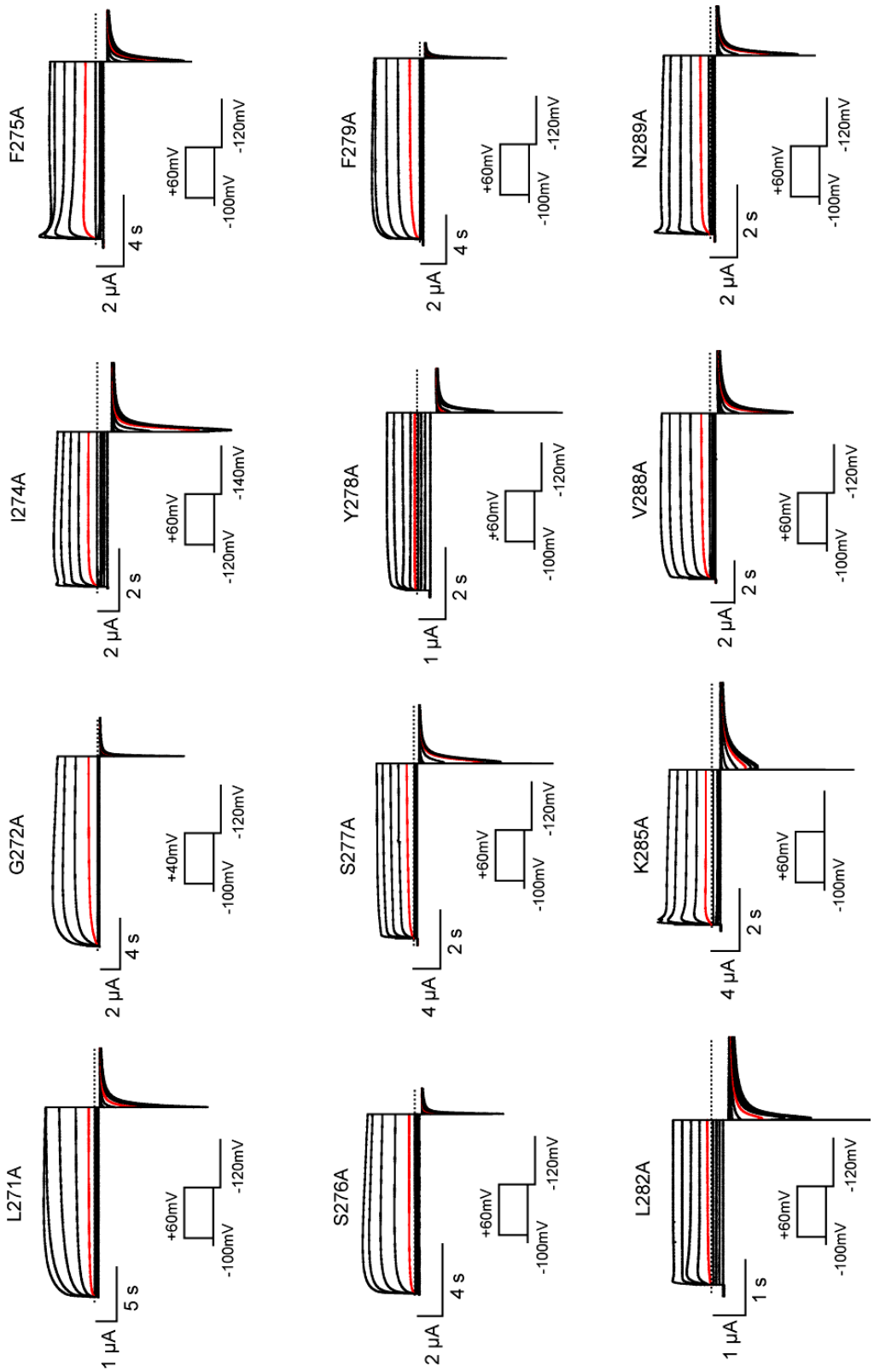

KCNQ1 pore Ala mutants: E290A to S330A

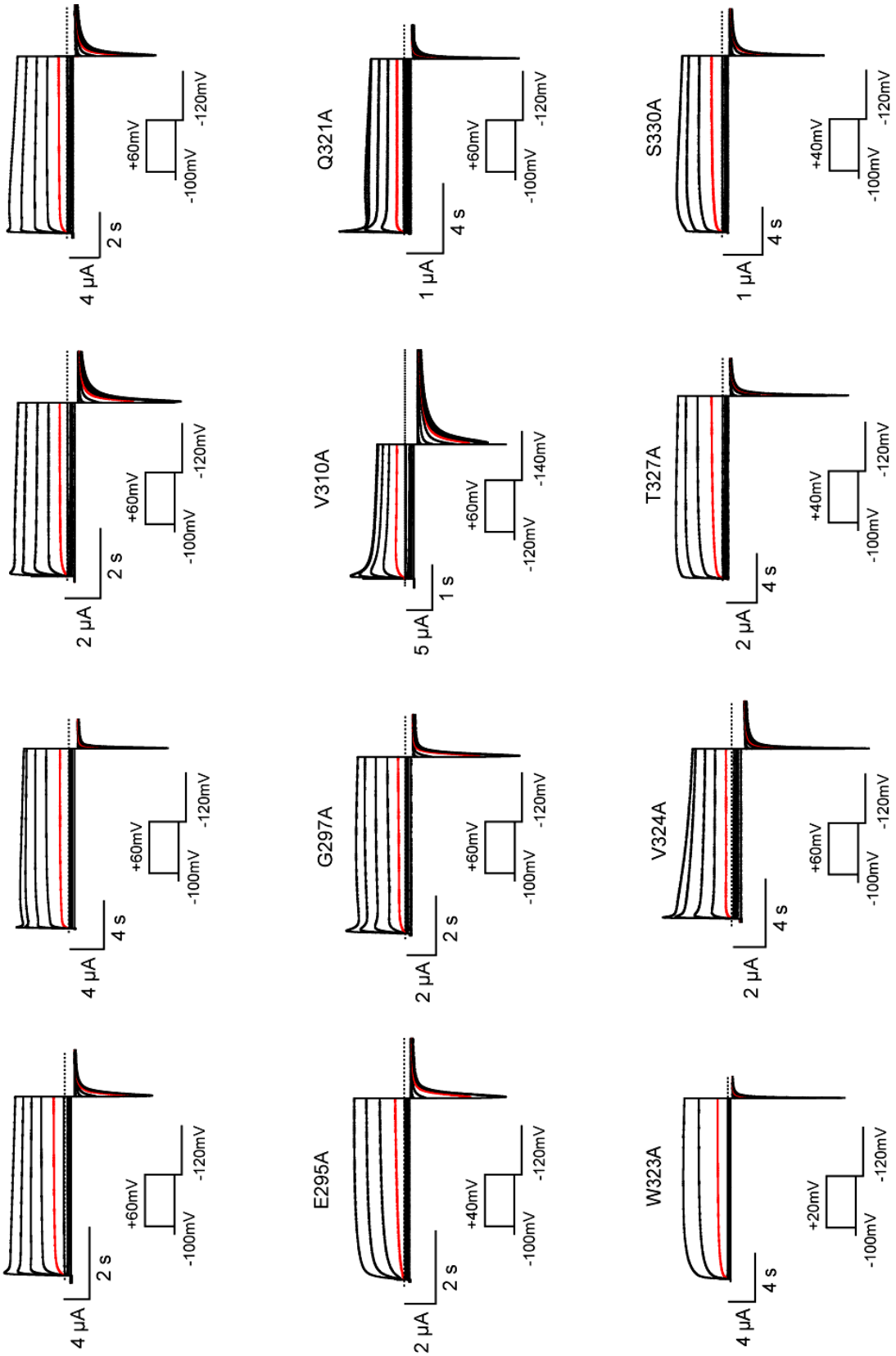

KCNQ1 pore Ala mutants: C331A to G348A

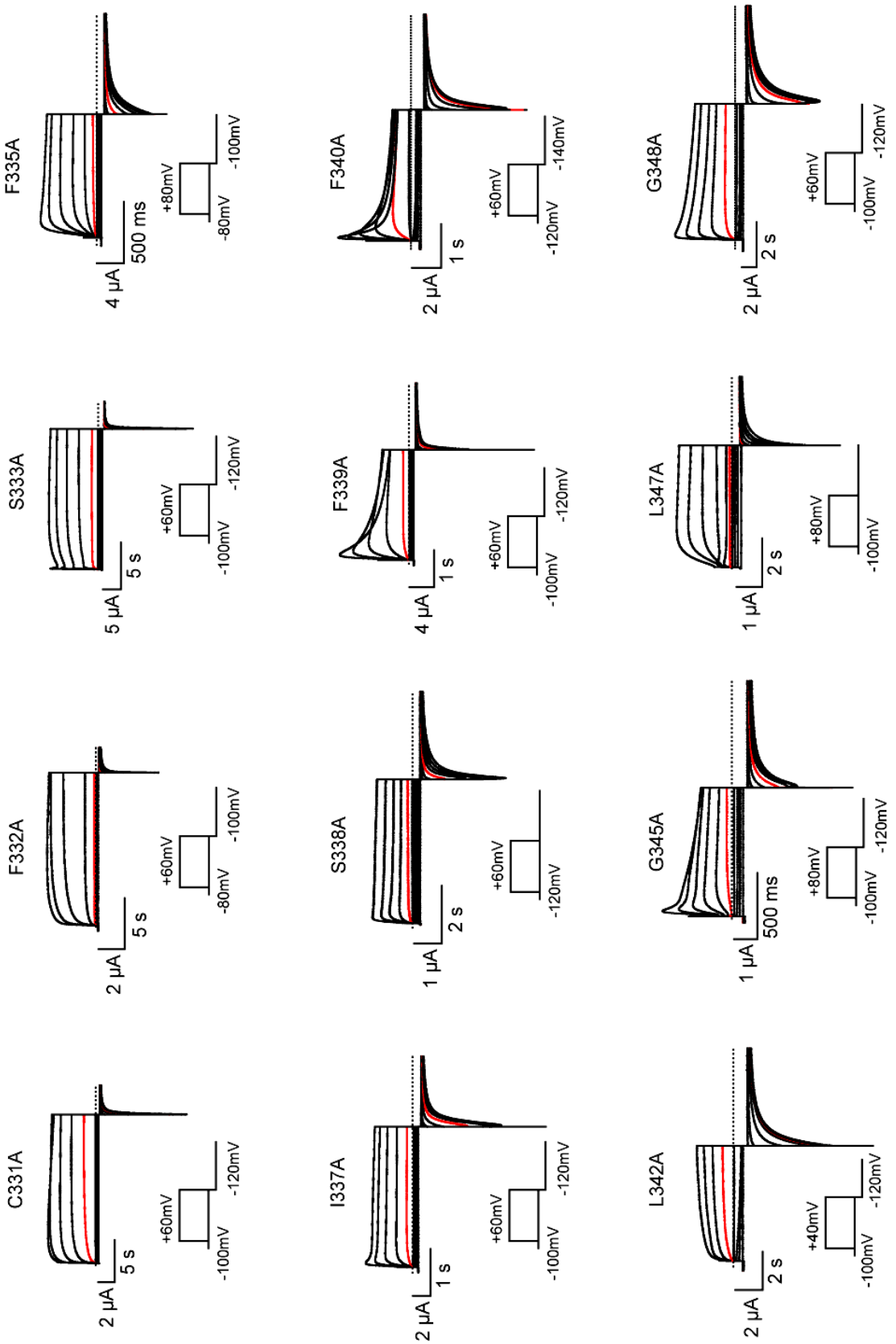

KCNQ1 pore Ala mutants: S349A to V355A

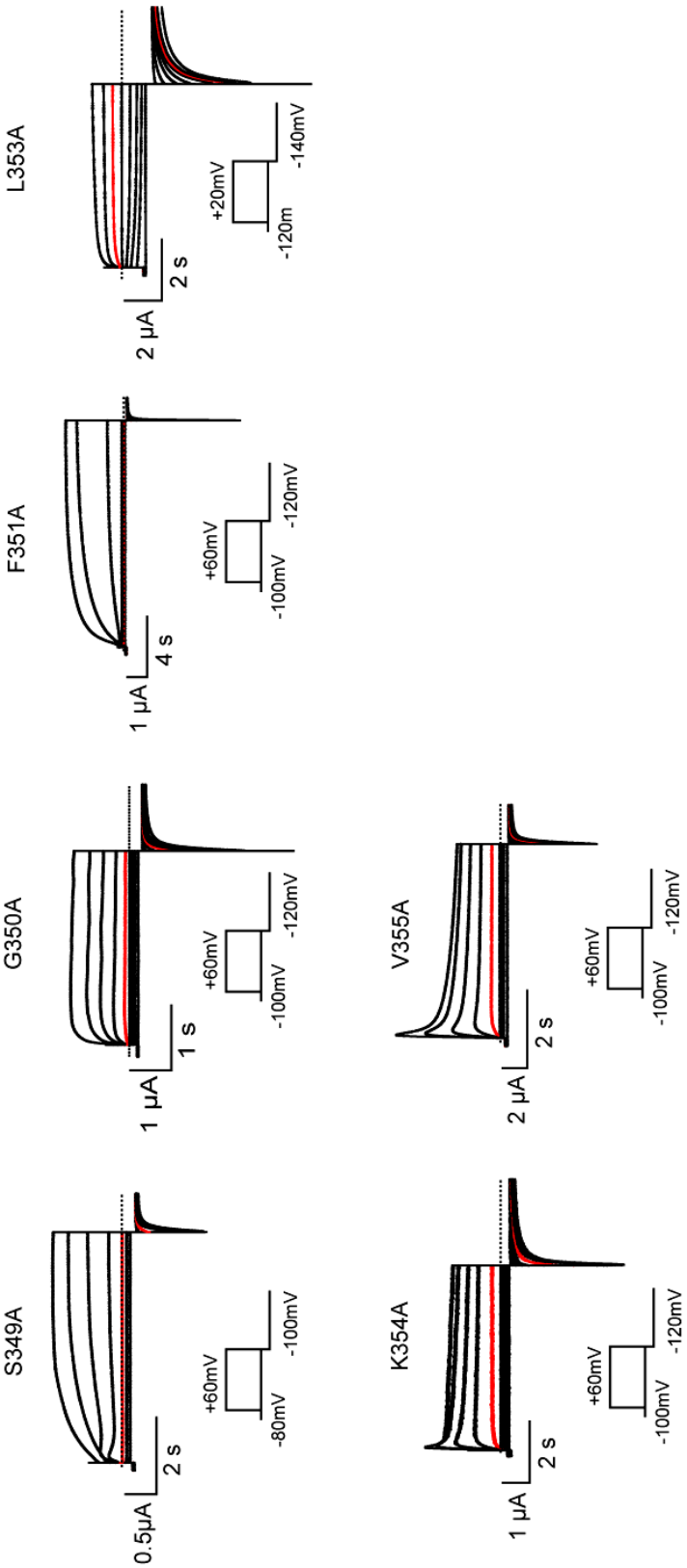

8.3 Currents recordings to determine G_{Rb}/G_K and inactivation properties for KCNQ1 mutant channels

Representative current traces for WT and KCNQ1 mutant channels recorded at -120 mV after 3-second channel activation to +40 mV. Currents recorded in 100 mM K^+ solutions (black traces) were supimposed on those recorded from the same oocyte bathed in 100 mM Rb^+ solutions (red traces). Dotted line indicates the zero-current level.

KCNQ1 pore Trp mutants: R259W to L271W

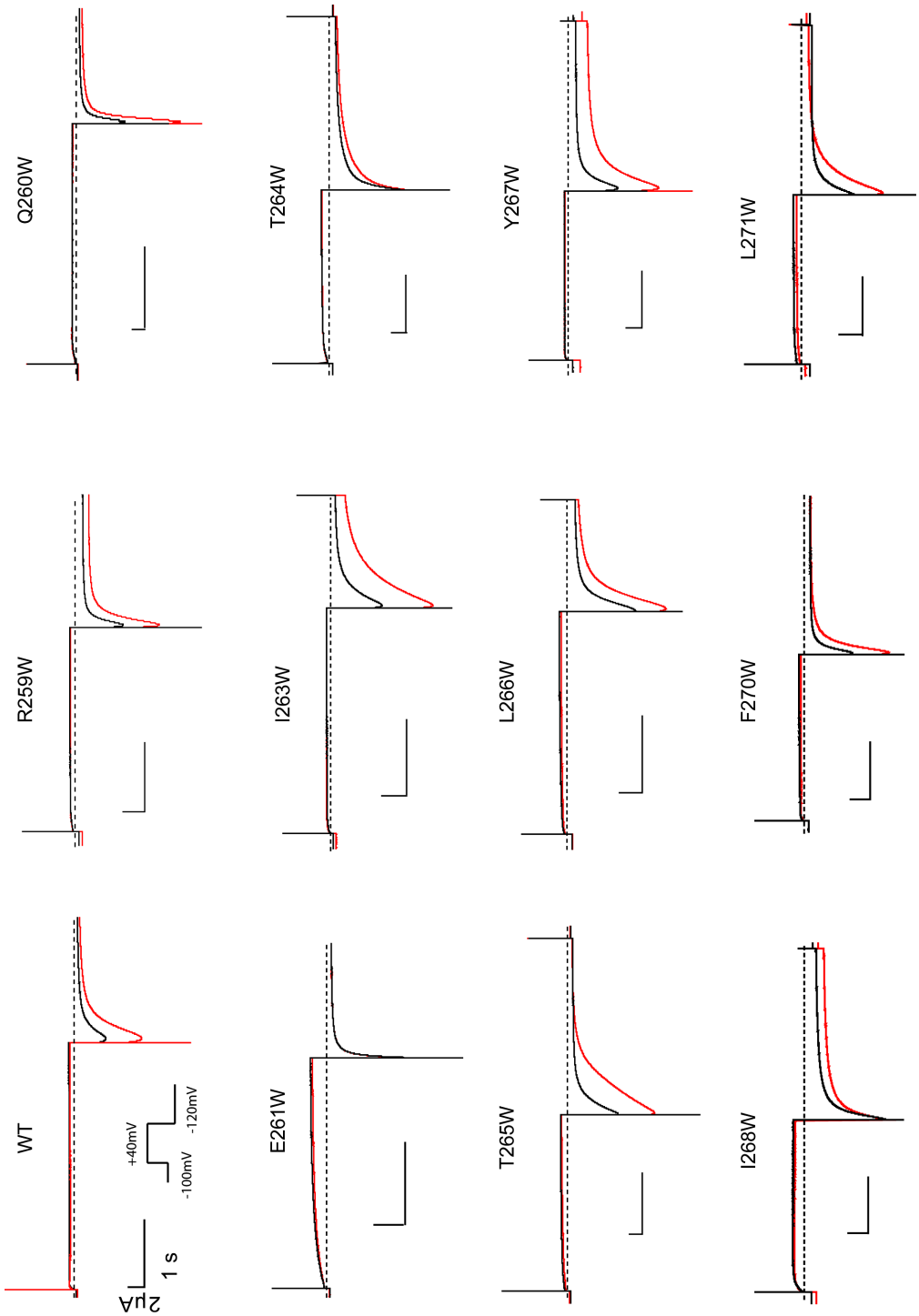

KCNQ1 pore Trp mutants: G272W to V294W

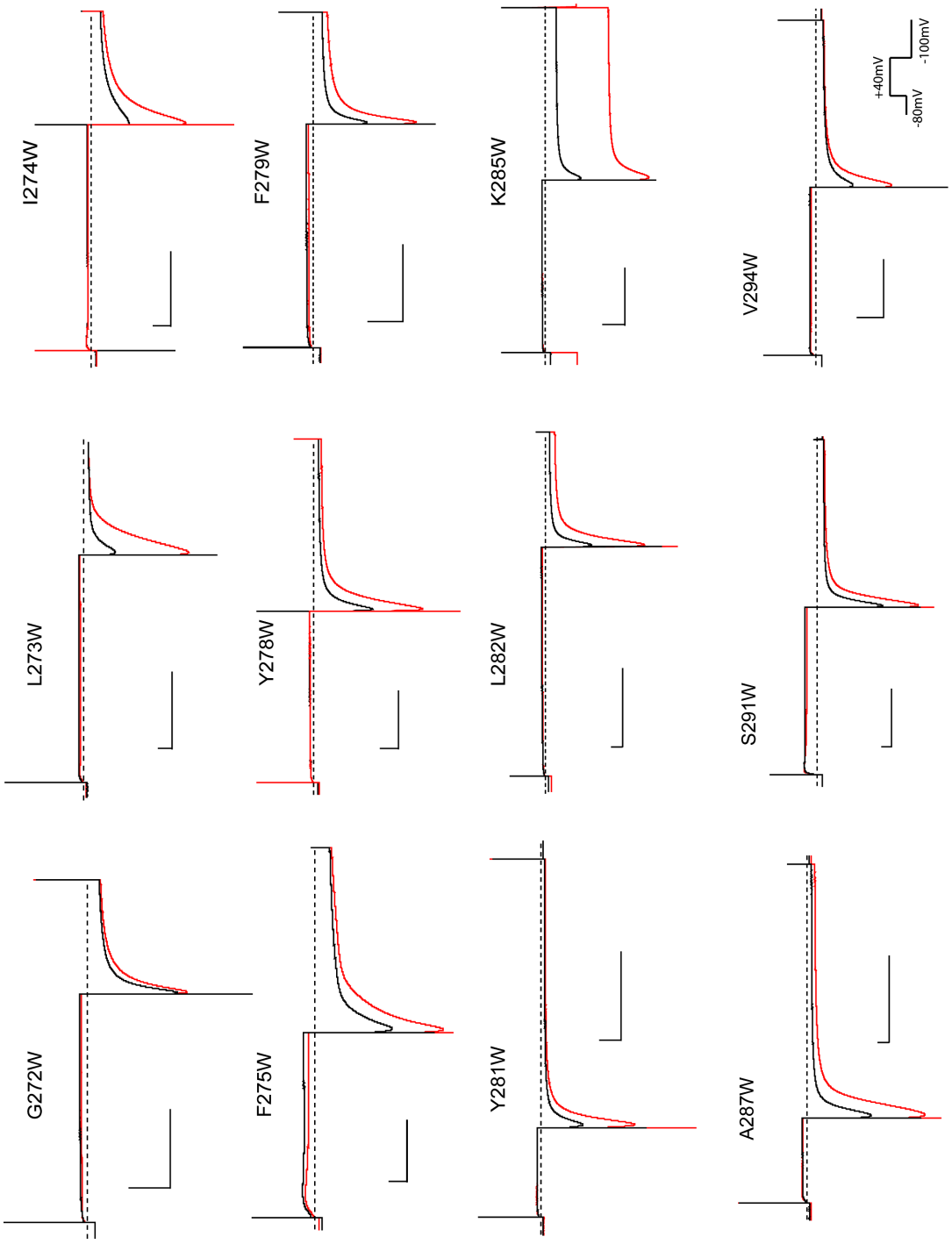

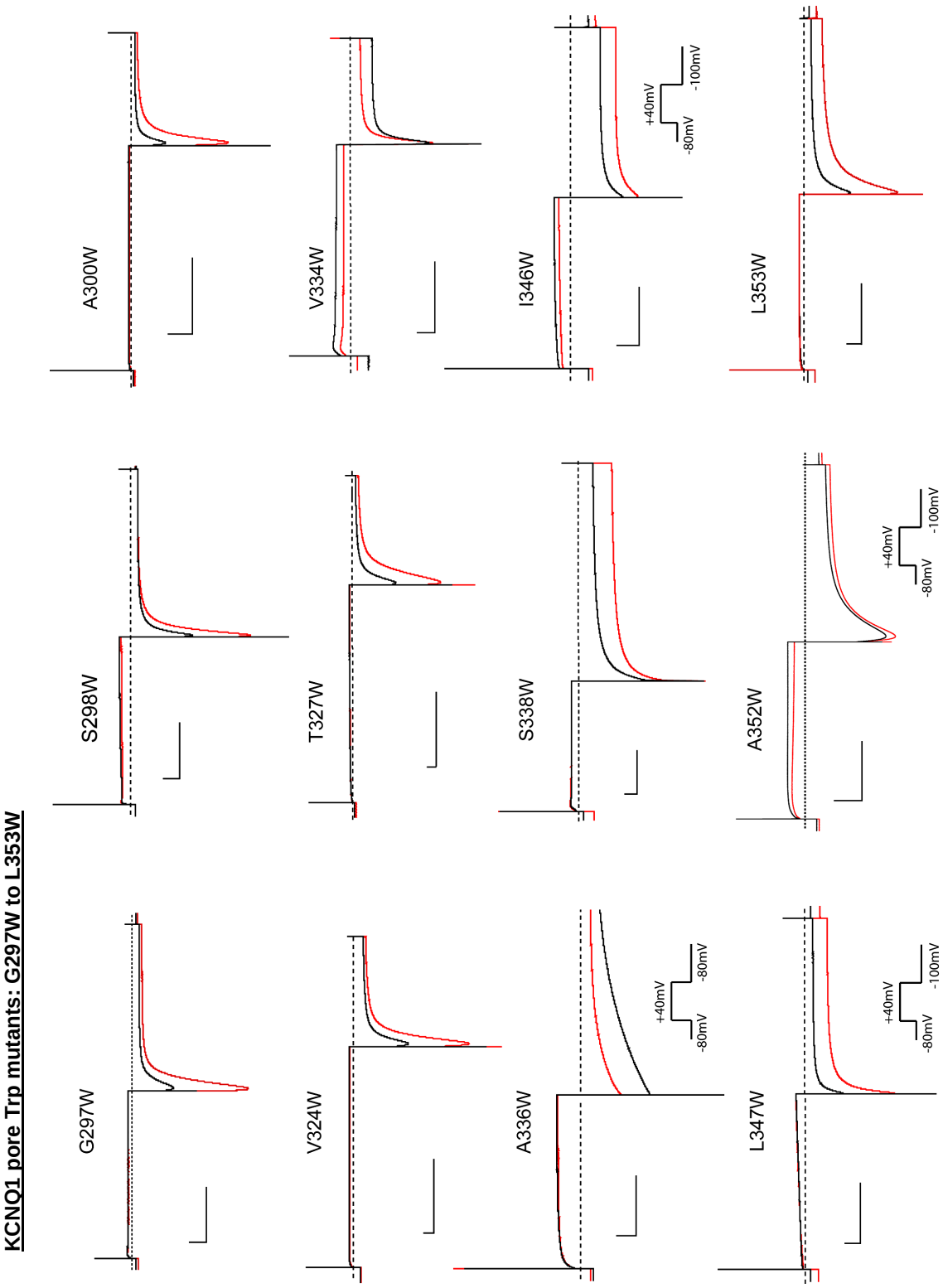
KCNQ1 pore Trp mutants: G297W to L353W
A300W
V334W
I346W
L353W
S298W
T327W
S338W
A352W
G297W
V324W
A336W
L347W
+40mV
-80mV
-100mV

KCNQ1 pore Trp mutants: K354W to V355W

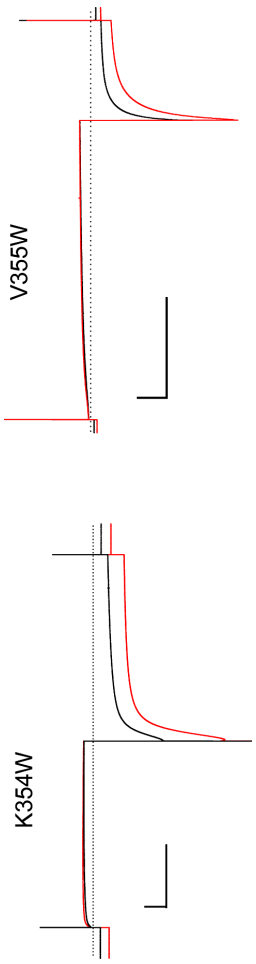

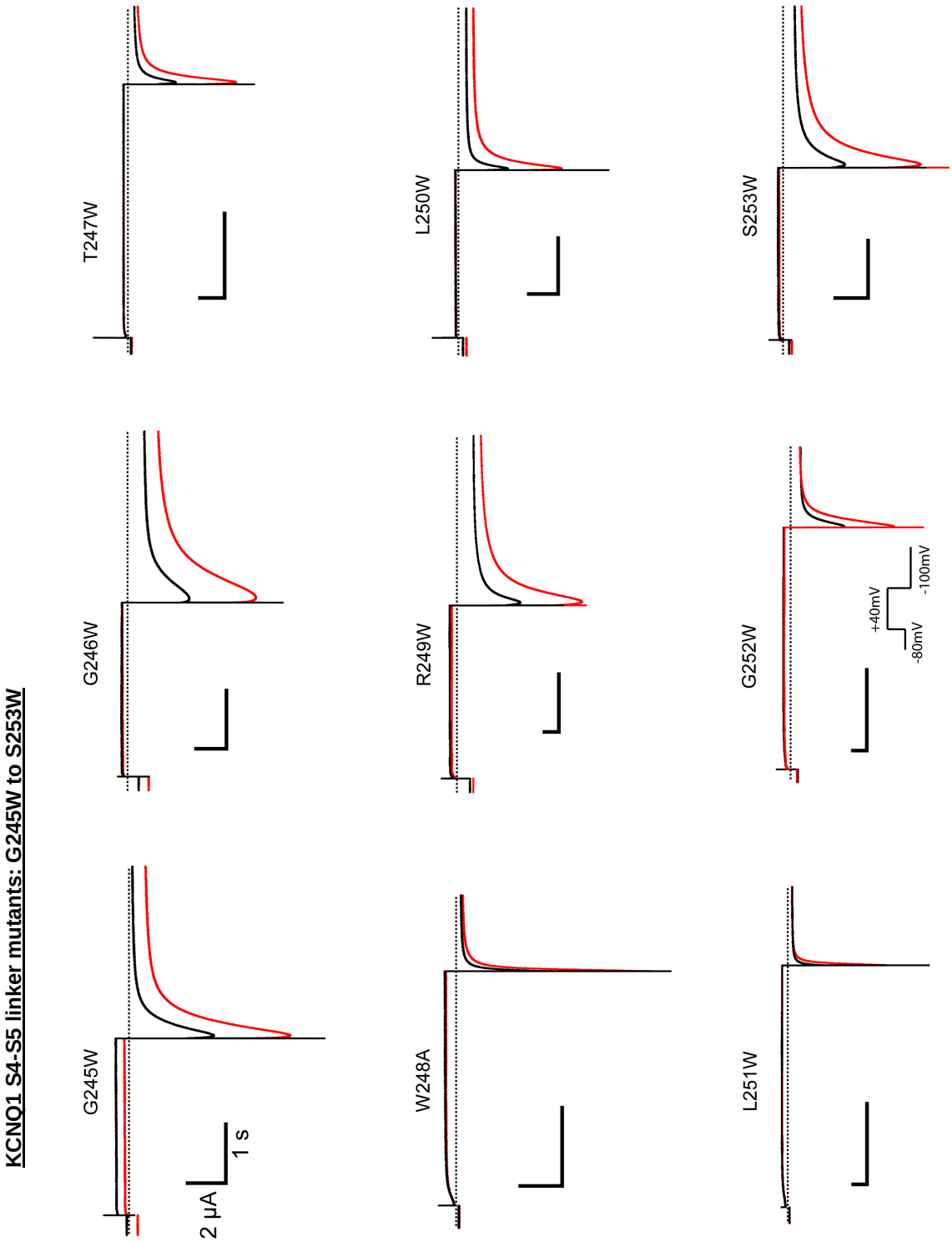
KCNQ1 S4-S5 linker mutants: G245W to S253W
G245W
G246W
T247W
W248A
R249W
L250W
L251W
G252W
S253W
2 µA
1 s
+40mV
-100mV
-80mV

KCNQ1 S4-S5 linker mutants: V255W to H258W

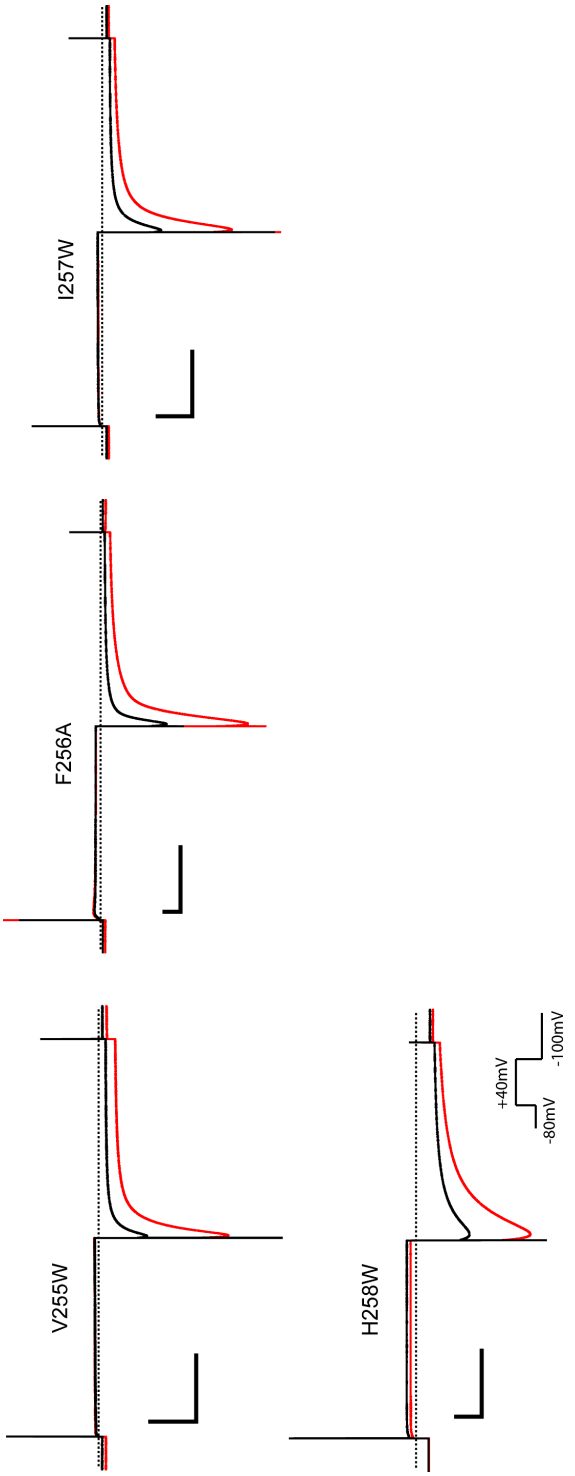

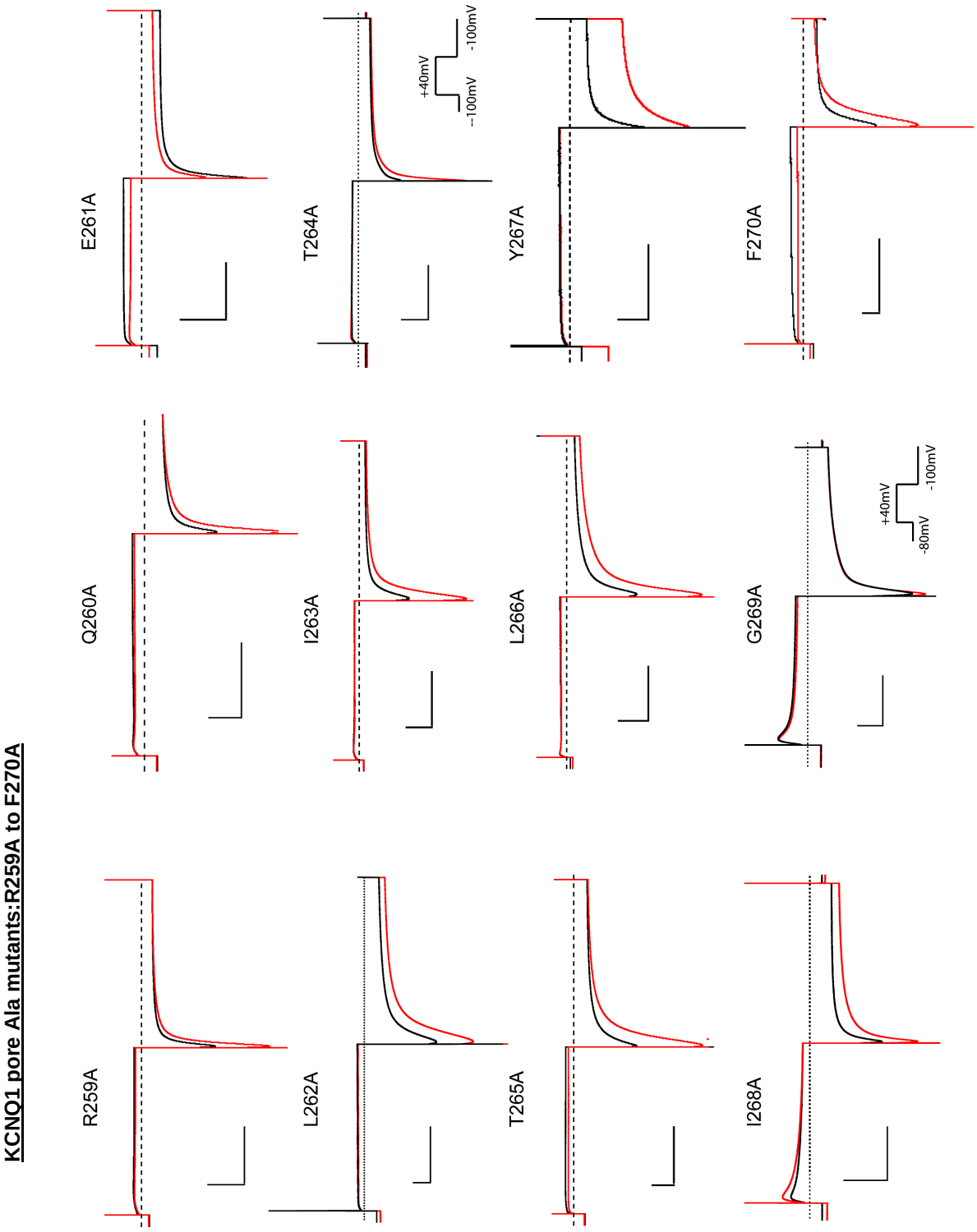
KCNQ1 pore Ala mutants:R259A to F270A
R259A
Q260A
E261A
L262A
I263A
T264A
+40mV
-100mV
--100mV
T265A
L266A
Y267A
I268A
G269A
+40mV
-100mV
-80mV
F270A

KCNQ1 pore Ala mutants: L271A to N289A

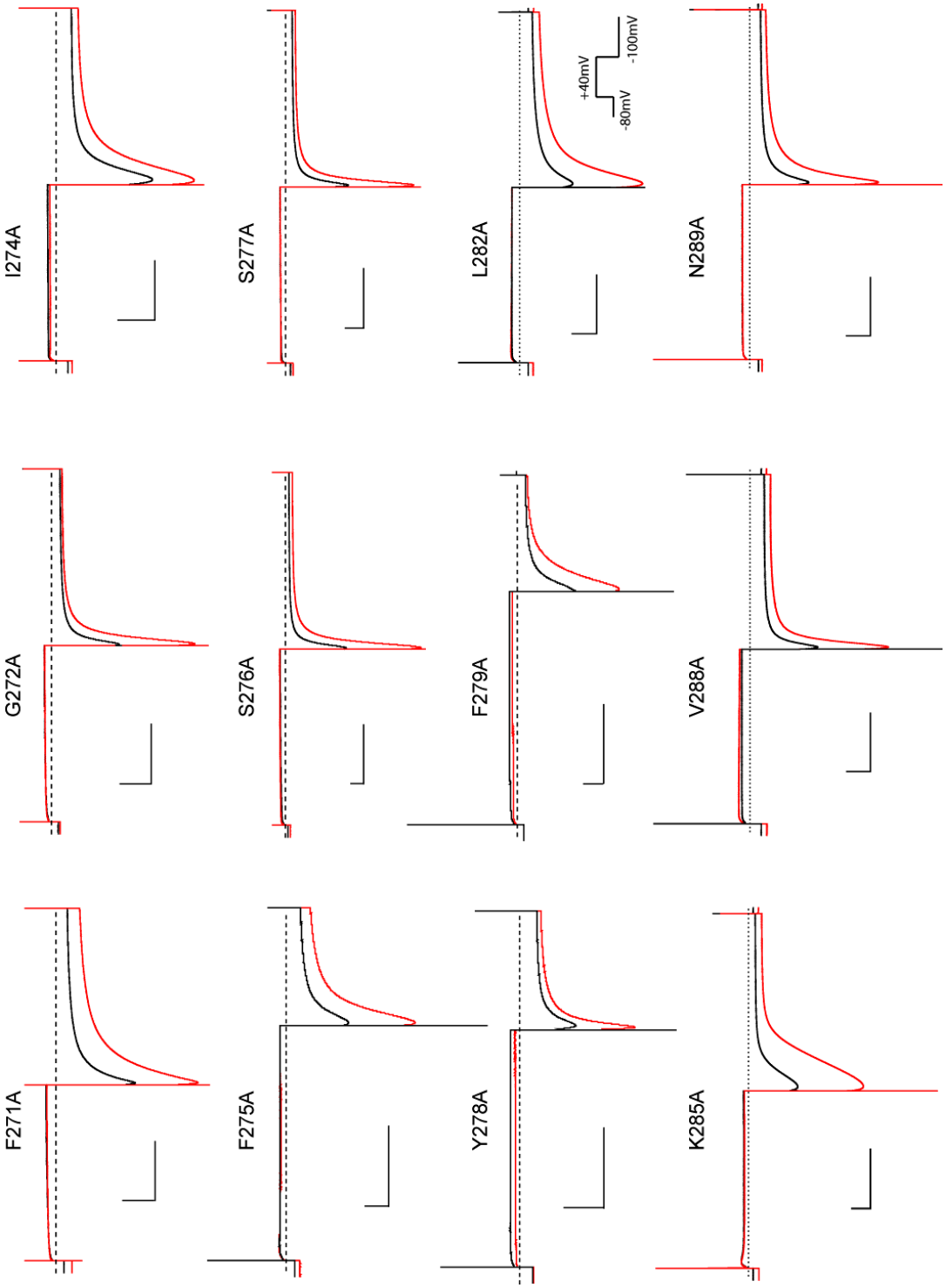

KCNQ1 pore Ala mutants: E290A to S330A

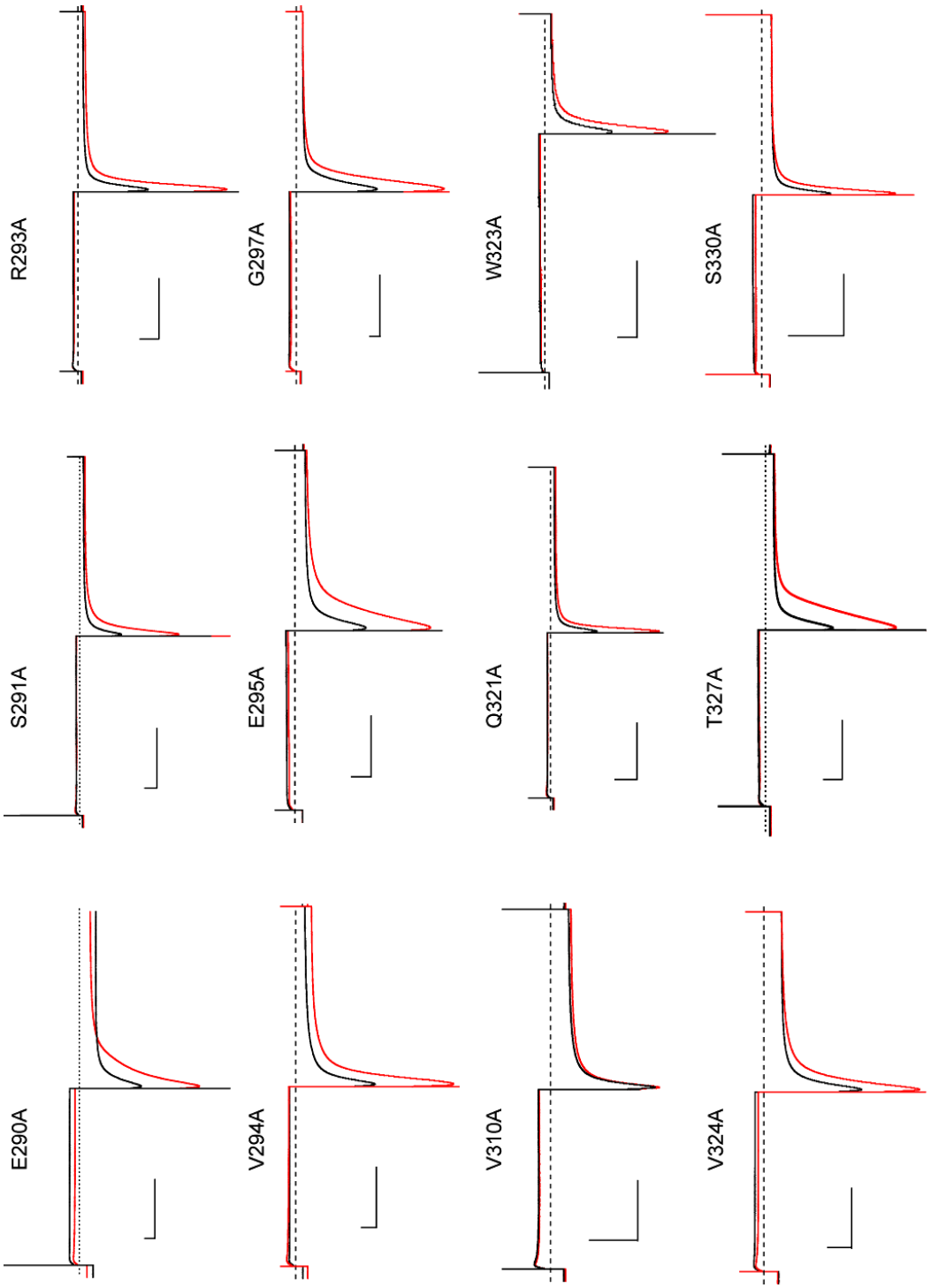

KCNQ1 pore Ala mutants: C331A to G348A

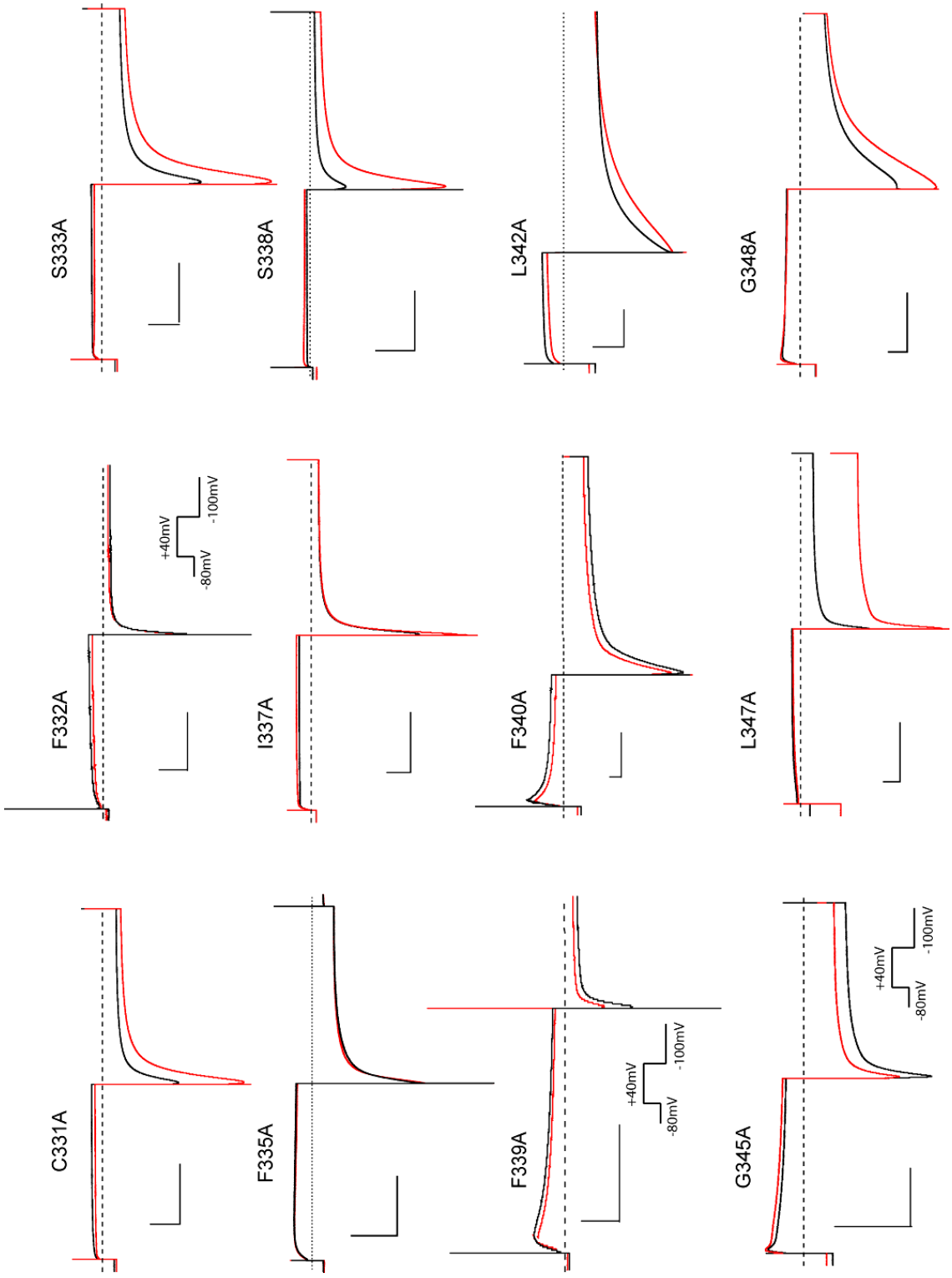

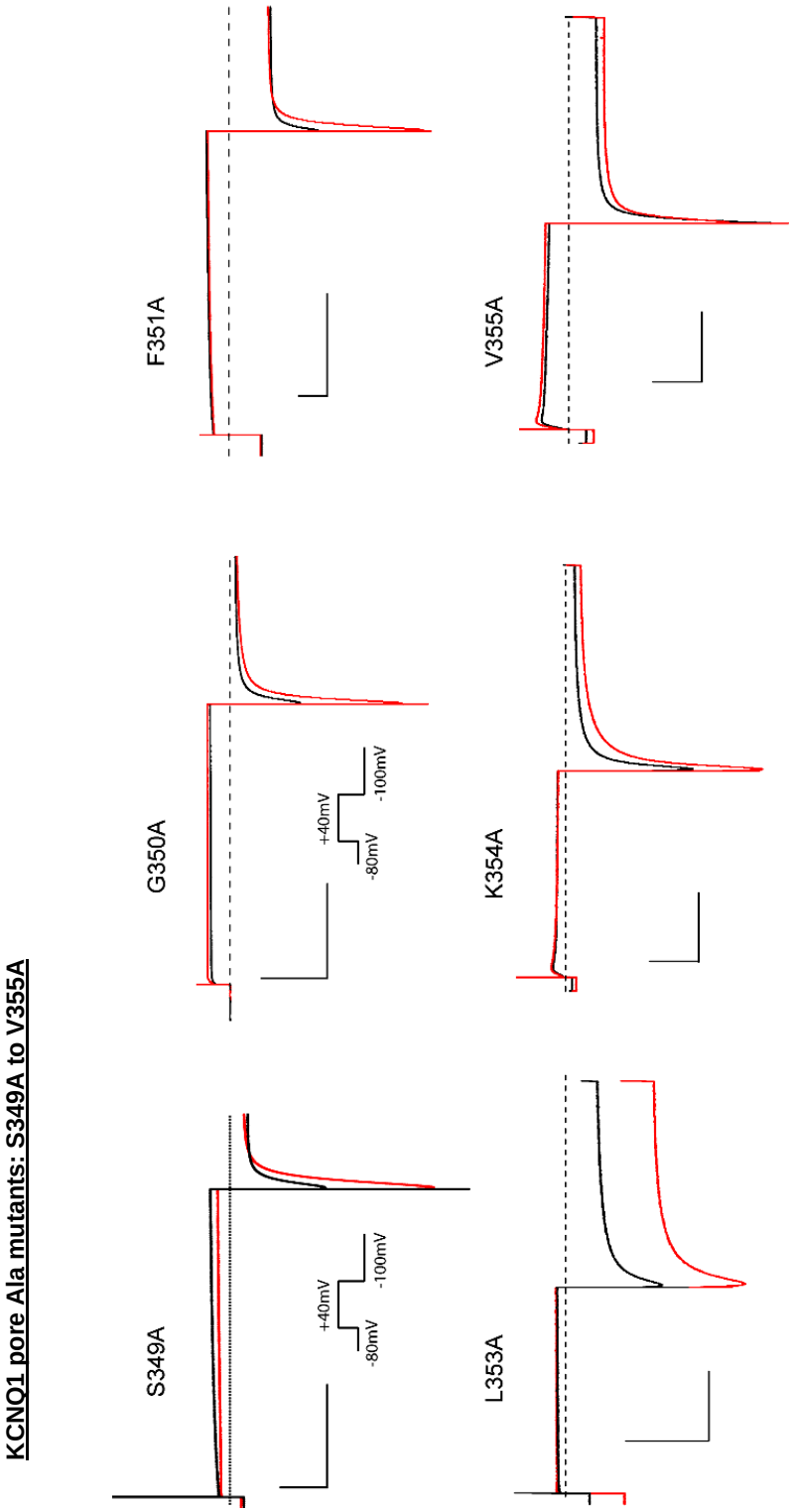
KCNQ1 pore Ala mutants: S349A to V355A
F351A
V355A
G350A
K354A
S349A
L353A
+40mV
-100mV
-80mV
+40mV
-100mV
-80mV

8.4 Voltage-dependent activation current recordings for KCNQ1 mutant channels coexpressed with KCNE1 (performed at 32℃)

Representative current recordings from the oocytes coexpressed of KCNQ1 mutant channels with KCNE1 in ND96 solutions from two electrode voltage clamp. Channels were activated by voltage steps from -80 mV to +80 mV or +100 mV in 20 mV increments. Holding potential was -80 mV and tail potential was -40 mV if not mentioned specifically. Current traces in red are current responses to voltage steps to +20 mV.

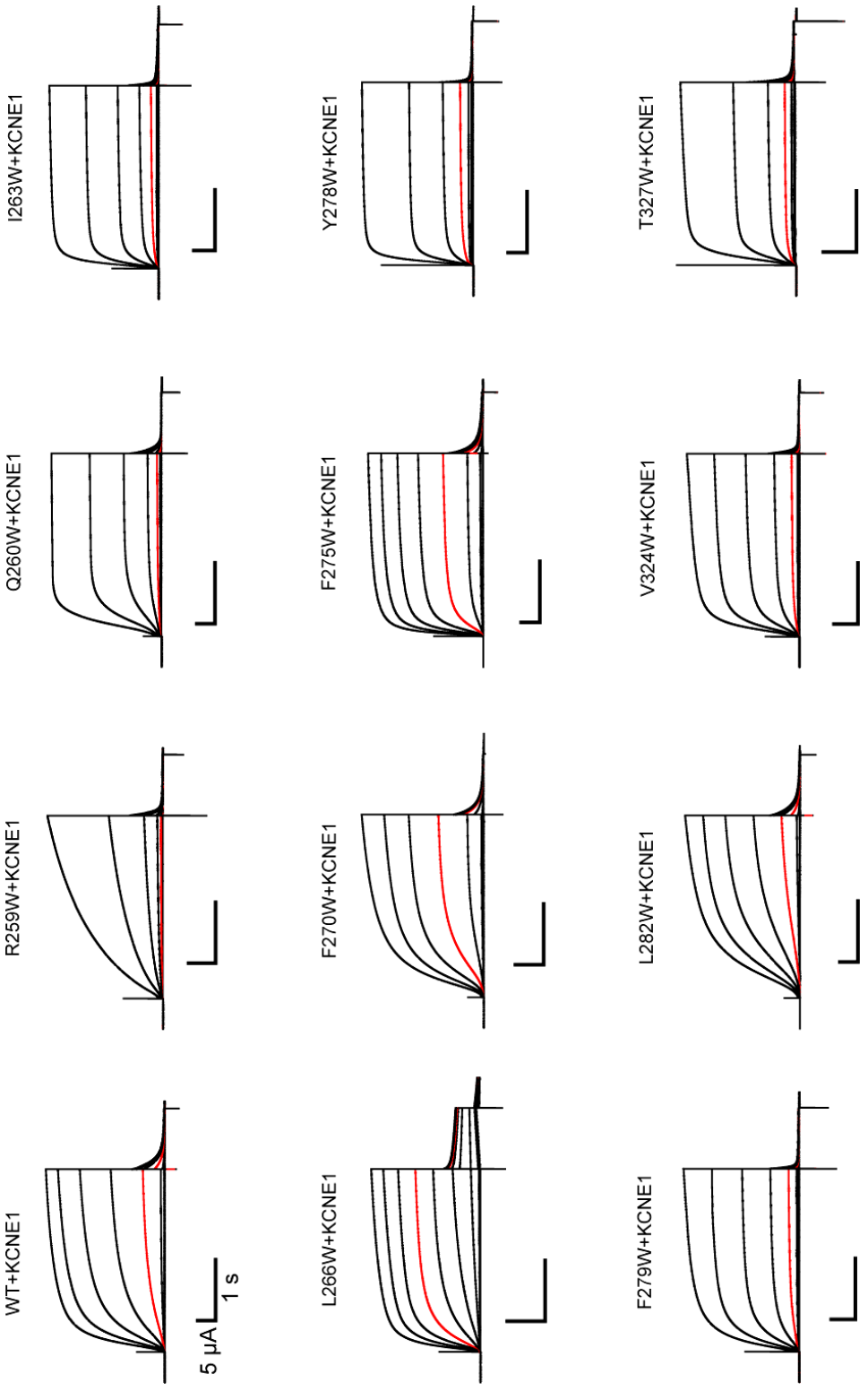
WT+KCNE1
R259W+KCNE1
Q260W+KCNE1
I263W+KCNE1
L266W+KCNE1
F270W+KCNE1
F275W+KCNE1
Y278W+KCNE1
F279W+KCNE1
L282W+KCNE1
V324W+KCNE1
T327W+KCNE1
5 µA
1 s

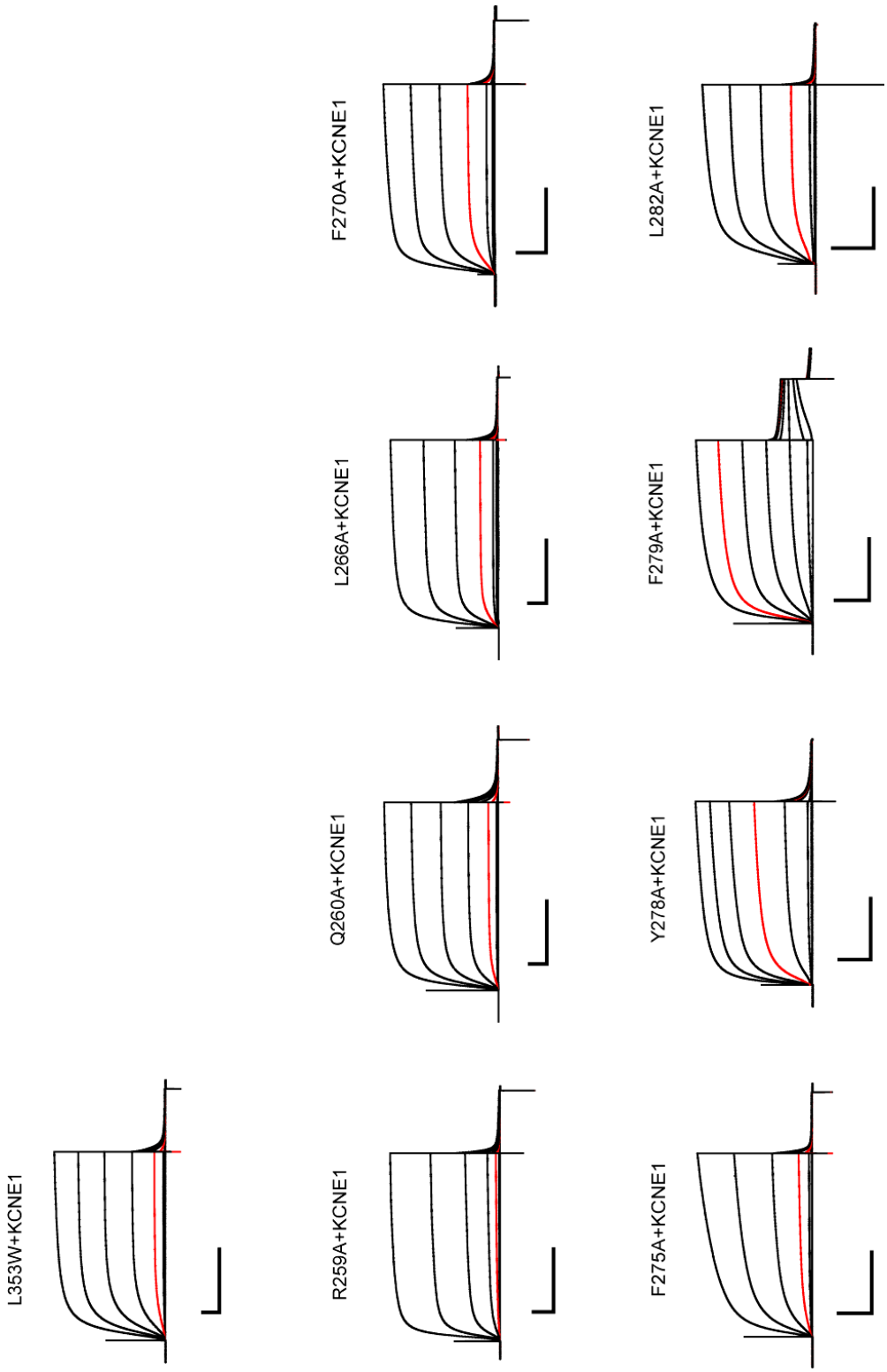
F270A+KCNE1
L282A+KCNE1
L266A+KCNE1
F279A+KCNE1
Q260A+KCNE1
Y278A+KCNE1
R259A+KCNE1
F275A+KCNE1
L353W+KCNE1

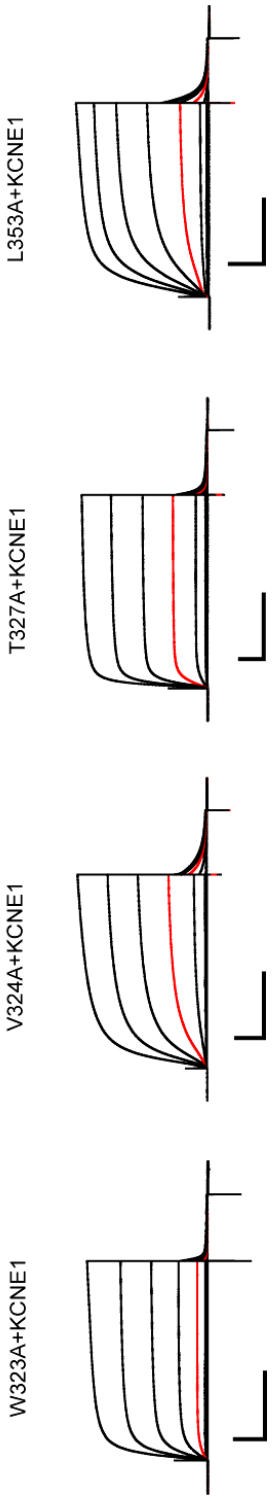
L353A+KCNE1
T327A+KCNE1
V324A+KCNE1
W323A+KCNE1

8.5 Curriculum Vitae

Personal data:

Name	Lijuan Ma
Birthday	29.01.1969
Place of birth	Hebei province, China
Nationality	China

Education and experience:

Oct. 2003 — Nov. 2007	Ph. D Biochemistry and Molecular Biology Zentrum für Molekulare Neurobiologie, University of Hamburg, Germany
Aug. 2000 — Jul. 2003.	Master of Science, Biochemistry and Molecular Biology Chinese Academy of Medical Sciences & Peking Union Medical College, China
Aug. 1991 — Aug. 2000	R&D genetic engineering drugs New drug R&D Institute, North China Pharmaceutical Group Cooperation, China
Sep. 1986 — Jul. 1991	Bachelor of Science, Molecular Biology University of Science and Technology, China

8.6 **Publications and conference presentations**

Publications**:**

1. Shamgar L, **Ma L**, Schmitt N, Haitin Y, Peretz A, Wiener R, Hirsch J, Pongs O, Attali B (2006). Calmodulin is essential for cardiac I_{KS} channel gating and assembly: impaired function in long-QT mutations. *Circ Res* 98:1055-63.

2. **Ma L**, Lin C, Teng S, Chai Y, Bahring R, Vardanyan V, Li L, Pongs O, Hui R (2003). Characterization of a novel Long QT syndrome mutation G52R-KCNE1 in a Chinese family. *Cardiovasc Res* 2003 59:612-9.

3. Teng S, **Ma L**, Zhen Y, Lin C, Bahring R, Vardanyan V, Pongs O, Hui R (2003). Novel gene hKCNE4 slows the activation of the KCNQ1 channel. *Biochem Biophys Res Commun* 303:808-13

4. Teng S, **Ma L**, Dong Y, Lin C, Ye J, Bahring R, Vardanyan V, Yang Y, Lin Z, Pongs O, Hui R (2004) . Clinical and electrophysiological characterization of a novel mutation R863X in HERG C-terminus associated with long QT syndrome. J Mol Med 82:189-96.

Conference presentations:

1. Title: A Novel Mutation R863X in HERG C-Terminus Caused Long QT Syndrome by Trafficking Deficiency (Poster). AHA Scientific Sessions 2003 (American Heart Association). Orlando, Florida, America. Nov 9 - 12, 2003.

2. Title: Gating of KCNQ1 by Ca^{2+} and voltage (Poster). Calcium 2006 Strasbourg, France. July 19-22, 2006.

8.7 Acknowledgments

It is a pleasure to thank the many people who made this thesis possible.
In the first place I would like to record my gratitude to Prof. Olaf Pongs for his supervision, advice, and guidance through out the work. Above all and the most needed, he provided me unflinching encouragement and support in various ways. His truly scientist intuition has made him as a constant oasis of ideas and passions in science, which exceptionally inspire and enrich my growth as a student, a researcher and a scientist want to be. I am indebted to him more than he knows.
I gratefully thank Prof. Uli Hahn for reviewing my thesis. I am happy to have such a supportive co-supervisor. I enjoyed his interest in my research as well as the fruitful discussion.
I am indebted to Prof. Jürgen R. Schwarz for proof-reading this manuscript and providing helpful suggestions for improving this manuscript.
Many thanks go particularly to my friends and colleagues for the great time I had in our group. I enjoyed the atmosphere, their friendship, and their support. It was a pleasure to work with all these people and to benefit from their knowledge. Special thanks go to Gegor, Sönke, Joanna and Phanindra for proof-reading this manuscript and helpful discussions.
Lastly, but most importantly, I own my great thanks to my family and my friends. Without their support and encouragement, life could not be easy. I am also thankful to my husband and my daughter both of whom had to suffer a lot during my project work.